FUNDAMENTAL CHEMISTRY ADVANCES TOWARD THE DEVELOPMENT OF DEGRADABLE POLYMER-BASED NANOPARTICLES FOR THE TREATMENT OF INFECTIOUS DISEASES

A Dissertation

by

GYU SEONG HEO

Submitted to the Office of Graduate and Professional Studies of
Texas A&M University
in partial fulfillment of the requirements for the degree of

DOCTOR OF PHILOSOPHY

Chair of Committee,	Karen L. Wooley
Committee Members,	François P. Gabbaï
	Christian Hilty
	Perla B. Balbuena
Head of Department,	François P. Gabbaï

May 2016

Major Subject: Chemistry

ABSTRACT

Microorganisms, including bacteria, viruses, fungi, or parasites, give rise to infectious diseases, which can spread between people, and can even transfer from animals or insects to humans. Infectious diseases are common, sometimes fatal, health issues. To date, the treatment of infectious diseases has largely relied on antibiotics. However, the therapeutic outcomes of current treatments need to be enhanced due to the emergence of drug-resistant microorganisms and the decline in the development of new antibiotics. Nanotechnology could help improve the efficacy of currently available antibiotics *via* changing the pharmacokinetics and biodistribution of drugs, which could enhance bioavailability, reduce side effects, help overcome physical and biological barriers for the efficient delivery to the site of infection, and so on. This dissertation aims to explore a novel treatment method to treat infectious diseases using degradable polymer-based nanoparticles.

In a first project, bacterial adhesin, $FimH_A$-targeted polymeric nanoparticles were developed for the delivery of antimicrobials to bacteria hiding inside the cells by mimicking the bacterial mode of cell invasion in order to treat and eradicate recurrent urinary tract infections. Amidation between carboxylic acids located in the shell of the poly(acrylic acid)-*block*-polystyrene-based polymeric nanoparticles and primary amine groups of lysine residues on $FimH_A$ was employed as the conjugation method. We prepared $FimH_A$-polymeric nanoparticle conjugates with varying amounts of adhesins on

the surface without free and/or physically-associated proteins under the improved coupling conditions.

In a second direction involving a series of projects, functional polycarbonates were developed in order to expand the pool of degradable polymers and their self-assembled nanostructures, which can be utilized as drug-delivery vehicles. Degradable polycarbonates were synthesized by metal-free organocatalytic ring-opening polymerization of cyclic carbonate monomers. Postpolymerization modifications were also employed to introduce new functionalities onto the same degradable polymer backbone. Water-soluble polycarbonate formed a hydrophilic shell domain of polymeric nanostructures, and reactive aldehyde- and vinyl ether-functionalized polycarbonates were synthesized and their potential for drug delivery systems were demonstrated.

In a third direction, advanced mechanistic understanding of organocatalytic ring-opening polymerization (ROP), which is widely used for syntheses of degradable polymers, was gained by specialized NMR spectroscopy studies. The collection of ^{13}C NMR data in real time during polymerization was enhanced *via* hyperpolarization of nuclear spins. The "living" characteristics of ring-opening polymerization enabled the observation of NMR resonances associated with an intermediate formed during ROP.

DEDICATION

To my father, Young Ryeol Heo, my mother, Meeja Lee,

my wife, Hye Lim Han,

our three children, Yunho (Jeremy), Yunjay (June), and Yuna (Janice),

and my advisor, Karen Lynn Wooley

ACKNOWLEDGEMENTS

I would like to express my deepest gratitude to my advisor, Dr. Karen L. Wooley, for her tremendous support, guidance, patience, generosity, as well as giving me an undeniable opportunity to work in the exceptional atmosphere. She has been and will be a prime example of a great scientist with a great personality in my mind.

I would like to thank my committee members, Dr. François P. Gabbaï, Dr. Christian Hilty, and Dr. Perla B. Balbuena for their invaluable advices.

I would also like to convey my sincere appreciation to all people, collaborators, past and present Wooley group members, and my dear friends, who have helped and supported me to complete my graduate studies at Texas A&M University. Without their guidance, discussion, contribution, as well as friendship, this dissertation would not be completed. Even though I do not mention their names, I will always keep them in my mind.

Lastly, and most importantly, I would like to express my special and sincere thanks and dedicate this dissertation to my family, father, mother, wife, and three children for their constant support, trust, devotion, sacrifice, and love not only during graduate studies, but also throughout my life.

NOMENCLATURE

AIBN	2,2'-Azobis(2-methylpropionitrile)
AFM	Atomic force microscopy
ATRP	Atom transfer radical polymerization
PAA	Poly(acrylic acid)
Bis-MPA	2,2-Bis(hydroxymethyl)propionic acid
CRP	Controlled radical polymerization
DBU	1,8-Diazabicyclo[5.4.0]undec-7-ene
DCC	*N,N'*-Dicyclohexylcarbodiimide
DCM	Dichloromethane
DIPEA	*N,N*-Diisopropylethylamine
DLS	Dynamic light scattering
DMAP	4-Dimethylaminopyridine
DMF	*N,N*-Dimethylformamide
DCM	Dichloromethane
DMSO	Dimethyl sulfoxide
DSC	Differential scanning calorimetry
EA	Ethyl acetate
ESI-MS	Electrospray ionization mass spectrometry
GPC	Gel-permeation chromatography

HBTU	*N,N,N′,N′*-Tetramethyl-*O*-(1*H*-benzotriazol-1-yl)uronium hexafluorophosphate
HOBt	Hydroxybenzotriazole
HPMA	*N*-(2-Hydroxypropyl)methacrylamide
IR	Infrared
MAC	5-Methyl-5-allyloxycarbonyl-1,3-dioxan-2-one
MBC	5-Methyl-5-benzyloxycarbonyl-1,3-dioxan-2-one
MMA	Methyl methacrylate
M_n	Number-average molecular weight
M_w/M_n	Dispersity
NMR	Nuclear magnetic resonance
PC	Polycarbonate
Pd/C	Palladium on carbon
PDI	Polydispersity index
PEG	Poly(ethylene glycol)
PEO	Poly(ethylene oxide)
PHPMA	Poly(*N*-(2-hydroxypropyl)methacrylamide)
PMAC	Poly(5-methyl-5-allyloxycarbonyl-1,3-dioxan-2-one)
PMBC	Poly(5-methyl-5-benzyloxycarbonyl-1,3-dioxan-2-one)
PMC	Poly(5-methyl-5-carboxyl-1,3-dioxan-2-one)
PMOC	Poly(5-methyl-5-oxoethyloxycarbonyl-1,3-dioxan-2-one)
PMPC	Poly(5-methyl-5-propyloxycarboxyl-1,3-dioxan-2-one)

PMHPAC	Poly(5-methyl-5-(2-hydroxypropyl)aminocarbonyl-1,3-dioxan-2-one)
PMMC	Poly(5-methyl-5-methyloxycarbonyl-1,3-dioxan-2-one)
RAFT	Reversible addition−fragmentation chain transfer
ROMP	Ring-opening metathesis polymerization
ROP	Ring-opening polymerization
T_d	Decomposition temperature
TEA	Triethylamine
TEM	Transmission electron microscopy
TFA	Trifluoroacetic acid
T_g	Glass transition temperature
TGA	Thermogravimetric analysis
$TMSCH_2N_2$	(Trimethylsilyl)diazomethane
UV	Ultraviolet

TABLE OF CONTENTS

LIST OF FIGURES

FIGURE Page

FIGURE Page

FIGURE Page

FIGURE Page

FIGURE Page

FIGURE Page

LIST OF SCHEMES

SCHEME Page

LIST OF TABLES

CHAPTER I

INTRODUCTION*

Proper medical diagnosis and therapy are essential for providing patients with proper care, but improper detection of the diseases, unsatisfactory therapeutic outcomes, and/or serious adverse reactions often result from inefficient diagnoses and conventional therapy. Advances in the design of various diagnostic and therapeutic agents and the recent trend of utilizing molecules for both therapeutic and diagnostic applications (*i.e.*, theranostics) still have not achieved complete control of the navigation and biodistribution of these molecules within the biological system during therapy. From small molecules to macromolecular drugs (*e.g.*, natural product-, protein-, and nucleic acid-based drugs, or synthetic, polymer-based conjugates, carriers, or other systems), the key challenges toward the use of existing therapeutic agents are typically the loss of activity *via* rapid clearance or degradation, inefficient delivery to the target sites, and/or inappropriate probing of the disease states.

The concept of nanotechnology was initiated early in 1959 by Richard Feynman during his legendary talk at Caltech, "There's Plenty of Room at the Bottom," where he introduced the possibility of manipulating materials at the atomic and molecular levels.[1] Nearly twenty years later, Norio Taniguchi at Tokyo University, coined the term

---

*Adapted with permission from "Polymeric Nanostructures for Imaging and Therapy" by Mahmoud Elsabahy, Gyu Seong Heo, Soon-Mi Lim, Guorong Sun, and Karen L. Wooley, *Chem. Rev.* **2015**, *115* (19), 10967-11011. Copyright © 2015 American Chemical Society.

"nanotechnology" in 1974, referring to the design of materials on the nanoscale.[2] Since the early 1990s, the use of nanomaterials of different compositions (organic and inorganic) and for various applications (from medical, to electronic, to manufacturing) has been greatly expanded, in particular over the last couple of decades.[3,4] In the medical field, nanotechnology now includes noninvasive systems for probing of disease, capable of carrying cargo for localized high-concentration delivery with reduction of off-target effects. The use of nanomaterials, in particular polymeric nanostructures, in nanomedicine has demonstrated both improved efficiency in delivery of diagnostic and therapeutic agents to the target sites, as well as the ability to fine-tune control of their navigation to target sites by incorporating several therapeutic/diagnostic/targeting moieties within specific compartments in the nanoparticles. Recent understanding of the nature of microenvironments within biological systems (*e.g.*, different pH, temperature, permeability, drainage, or overexpression of proteins, enzymes, or receptors) and the barriers toward the delivery of various moieties to their intra- or extracellular destinations has aided the design of nanomaterials that deftly evade various physiological barriers. Selective delivery to the site of the disease increases the therapeutic efficacy, imaging contrast, and accuracy, while reducing adverse reactions and the dose and cost of medications.

The remarkable advantage of polymeric nanostructures over other types of nanomaterials is the flexibility with which their structures can be modified to yield materials of various compositions, morphologies, sizes, and surface properties, with the possibility of hierarchical assembly of several nanomaterials of various components into

one construct that can be accommodated with a variety of therapeutic, diagnostic, and/or targeting moieties, within selective compartments of the nanodevices. Efficiency in diagnosis and treatment of diseases and patient quality-of-life and compliance can be vastly improved by grasping the molecular events associated with various diseases and combining advances in the design of therapeutic and diagnostic agents and nanomaterials together with innovative instruments utilized for monitoring these agents.

1.1. Capabilities and Challenges for Medical Therapy

Medical therapy, in particular the systems that target special events related to a disease, promises effective treatment of several diseases on the molecular level, for instance, *via* correcting genetic mutations or protein misfolding or *via* interfering with one or more of the pathway cascades involved in disease progression. Diseased tissues typically differ from healthy ones in several aspects, such as having different microenvironment (pH or temperature), permeability, or drainage, or overexpressing specific proteins, enzymes, or receptors. Exploitation of these differences allows selective delivery once the therapeutic molecules overcome biological barriers and reach the diseased tissues and molecular targets. The same principles apply to therapy as to imaging, where selective binding or release of the diagnostic agents to the diseased tissues can improve the imaging contrast and provide more efficient diagnosis and information on the disease status and progression. Theranostic agents are being developed currently *via* either utilizing a particular probe or drug that has therapeutic and diagnostic capabilities or labeling therapeutic agents with imaging probes, for both therapy and imaging. The use of a theranostic approach, in addition to providing simultaneous therapy

and imaging, reducing the frequency of administration, enhancing patient compliance, and decreasing the burden on patients and caregivers, can also provide useful information on the drug biodistribution and clearance.

Selective delivery to the site of the disease can increase the therapeutic and imaging efficacy, reduce adverse reactions, and reduce the cost. However, there are several challenges toward this efficient delivery (Figure 1.1). Several of these drugs have poor aqueous solubilities and, thus, cannot be solubilized, dispersed, or diluted in saline prior to injection, or solubilized in other aqueous solutions for administration *via* other routes of administration. Rapid degradation, enzymatic or hydrolytic, of some drugs, both *in vitro* during storage and *in vivo* after administration (extra- or intracellularly), hinders drugs from reaching their target sites in an intact form. Interaction between drugs and various biological environments (depending on the administration route and target site) may destabilize the drug, prevent their penetration to the target site, or redirect their distribution in the body. The detailed biological barriers (external, en route, internal) have been reviewed previously by our group (Figure 1.1) and others.[5-8]

The main barriers toward the delivery of therapeutic and diagnostic agents to their target sites are the external barriers (skin and mucosa that cover body surface) that prevent them from entering the body, blood, blood components, and extracellular matrices that hinder them from reaching the targeted cells or sites in the various organs, and cellular barriers (limited uptake, degradation in the endosomes/lysosomes or the cytoplasm, and low nuclear uptake, if the nucleus is the target site). These barriers also destabilize the therapeutic and diagnostic agents before they reach their target sites. The tightly packed

layers of the stratum corneum of the skin usually hinder penetration of various drugs, whereas the viscoelastic hydrogel of the mucus that covers various body surface areas hinders delivery to the underlying tissues *via* several mechanisms.[9,10] The mucus has various compositions (cells, bacteria, lipids, salts, proteins, macromolecules, and cellular debris), thicknesses, and pH's, depending on the physiological region and disease status; thus, mucus work to inhibit drug delivery *via* adhesiveness, steric hindrance, and mucociliary clearance. Additionally, drugs that reach the bloodstream are subjected to opsonization, degradation, immune response, nonspecific biodistribution, and renal, hepatic, and/or splenic clearance.[11] Even upon reaching the cellular surface, drugs are usually not at their final destination yet, and may not have the capability of entering cells, especially if they are hydrophilic macromolecules; after uptake, they may degrade within the endosomal/lysosomal compartments. When the target site is a subcellular organelle, such as mitochondria or the nucleus, yet another barrier is incorporated into the journey, as these organelles do not allow nonspecific uptake of various moieties.

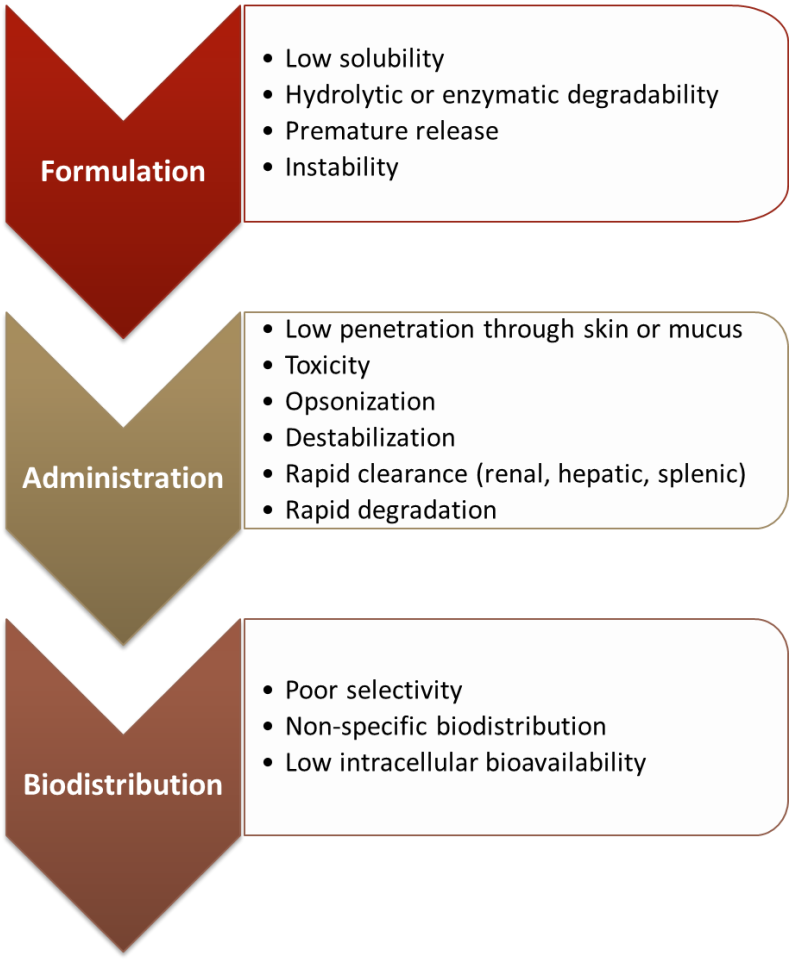

Figure 1.1. The main challenges towards the use of various therapeutics, diagnostics and theranostics, during formulation, administration and the resulting biodistribution, with no control over their characteristics and navigation within the biological system.

1.2. Infectious Diseases as Targets for Medical Therapy

Infectious diseases are usually caused by bacteria, viruses, parasites, or fungi. They typically spread from one organism to another and may become serious, difficult to treat, and life-threatening. More recently, the outbreaks of Ebola, influenza, salmonella, HIV, *etc*. have brought worldwide attention to zoonotic diseases that can be transmitted to humans by infected animals. Since the expansion of the global transport network,

infectious diseases have become more broadly transmissible,[12] increasing the urgency to develop efficient treatment methods. Although there are several therapeutics and diagnostics for management of infectious diseases have been tested with varying degrees of success, the poor bioavailability (due to rapid metabolism and excretion from the body or inactivation of drugs) and serious side effects of some of these agents, development of resistant microorganisms, and biological barriers that hinder the efficient delivery of therapeutic and diagnostic agents to the infection sites compromise the expected therapeutic outcomes.[13-15]

We have a keen interest in the treatment of urinary tract infections (UTIs) and pulmonary infectious diseases due to their prevalence, limited treatment strategies, and promise for direct routes of administration, which may avoid complications from systemic delivery and damage to the human microbiome, among other beneficial microflora.

UTIs include infections in the urethra, bladder, ureters, and kidneys, which constitute the urinary system. Although several uropathogens including bacteria, viruses and fungi can also cause UTIs, bacteria, especially uropathogenic *Escherichia coli* (UPEC), are the primary source of infections.[16] A high tendency of recurrence makes treatments of UTIs more challenging.

Examples of infectious diseases that affect the lung are pneumonia, tuberculosis, and chronic obstructive pulmonary diseases. Barriers toward the delivery of antimicrobials for the treatment of infectious diseases depend upon the type and site of infections and could include, but are not limited to, multidrug-resistant bacteria and need for high doses, which often results in toxicity, mucociliary clearance, steric hindrance of

drug uptake, presence of enzymes and macrophages in the mucus gel and tissues, and high viscosity of sputum, especially in the case of cystic fibrosis.[9,36,46-54] Mucus is a viscoelastic hydrogel secreted by the mucosal glands to protect regions that are not covered by the skin, with varying composition, thickness, and permeability depending on the region and disease status.[10] The use of physical or chemical methods to hydrolyze mucin and mucolytic agents enhances penetration of the drug in patients with lung disease by reducing the viscosity of mucus.[17-19]

1.3. Design of Polymer Nanostructures to Address Challenges in Medical Therapy

Polymeric nanostructures have the potential to improve the medical outcomes of various therapeutics and diagnostics by enhancing the accumulation of the embedded active species into the target sites of diseased tissues *via* passive and/or active targeting (Figure 1.2). They can also be utilized for combinational therapy/diagnosis. In passive targeting, nanoparticles accumulate in pathological sites with leaky vasculature (*e.g.*, tumor and inflammation sites) due to the "enhanced permeability and retention" (EPR) effect,[20] whereas active targeting is achieved by decorating the surface of nanoparticles with targeting ligands that bind to receptors overexpressed on the diseased tissues.

Active targeting features can also be incorporated into the nanostructures *via* incorporating stimuli-responsive components into the nanomaterials. Ideally, both targeting mechanisms aim to concentrate the nanomaterials, while containing the embedded drugs and/or diagnostic probes, at the diseased tissues and avoid accumulation or drug release at healthy tissues. No matter which targeting strategy is employed, a common characteristic of nanoparticulate materials is that loading drugs into nanoparticles redirects biodistribution by preventing small molecule drugs from passing through normal blood vasculature, renal tubules, and other pores <10 nm, thus eliminating rapid biological clearance and alleviating severe side effects systemically. Instead, nanomaterials selectively permeate and accumulate in pathological areas with leaky vasculature (pores >100 nm). Local routes of administration offer opportunities to further narrow the selective region of access of nanomaterials, for instance, exclusively to diseased skin, lungs, urinary tracts, *etc*.

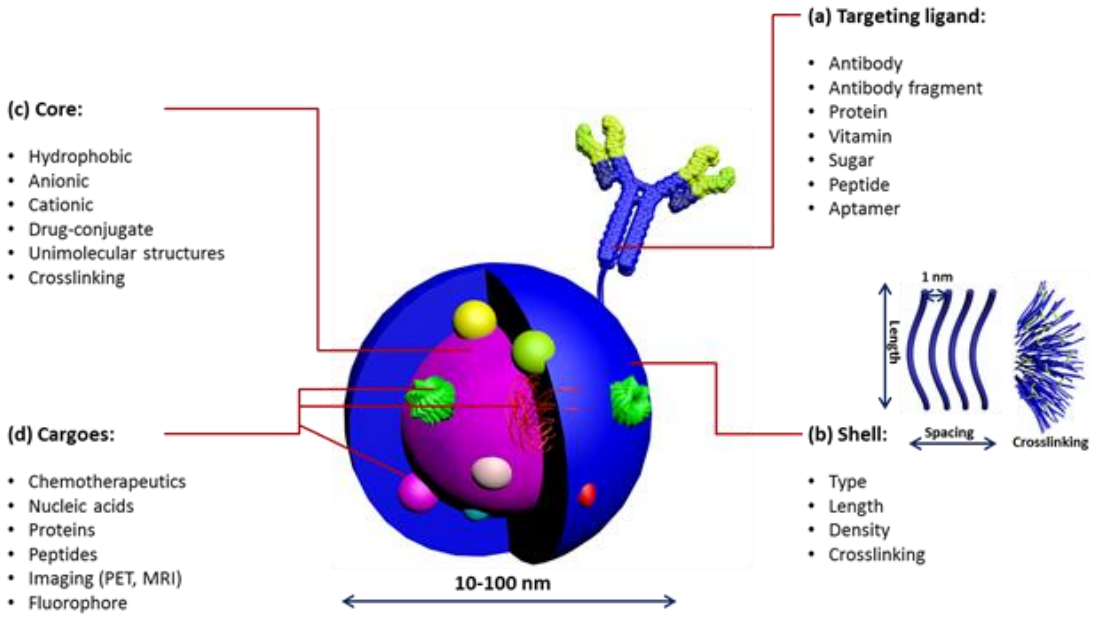

Figure 1.2. Compositional versatility of multifunctional nanoparticles for biomedical delivery applications, illustrated generically for a solid core–shell polymer nanoparticle scaffold. (a) Targeting: Clusters of targeting moieties are important for multivalent binding to receptors for enhanced cellular uptake; the use of various ligands (antibody, antibody fragment, peptide, *etc*.) depends on the therapeutic application and disease type. (b) Shell: The length, spacing, and cross-linking of the shell polymers are critical parameters that dictate the blood circulation time and stability of nanoparticles with ~1 nm spacing found to be efficient in preventing protein adsorption. (c) Core: The nature of the core dictates the type of drug to be encapsulated. Cross-linking and conjugation of drugs to the core-forming polymer are common strategies for enhancing the stability of nanoparticles and drug-encapsulation efficiency, respectively. (d) Cargo: A wide range of imaging agents and/or therapeutics can be packaged, ranging from small molecules to macromolecular cargoes. Reprinted with permission from refs [5,21]. Copyright 2012 and 2013 Royal Society of Chemistry.

Typically, nanoparticle-based carrier materials possess a core–shell morphology, for which the nature of the core-forming polymer dictates the type of therapeutics/diagnostics that can be incorporated into the nanomaterials, whereas the composition and structure of the shell-forming polymer components (*e.g.*, the polymer chain length, spacing, and incorporation of cross-linking moieties) control the stability of nanoparticles and their blood circulation time. Although there remain several challenges

toward the development of effective therapeutics, the ability to control their characteristics *via* chemical modifications of the building blocks is an exciting strategy to improve the utility of nanomaterials for biomedical applications. The building blocks can be modified to encapsulate hydrophobic drugs, nucleic acids, enzymes, hormones, small peptides, and other macromolecules. They can also be modified to respond to external or internal stimuli.

Multifunctional polymeric nanoparticles with precisely-controlled architecture of the individual polymer components and overall nanoparticle composition can be engineered *via* bottom-up control of the polymer chemistry and supramolecular assembly. The chemistry of polymer precursors can be modified for efficient encapsulation of various therapeutic molecules. For example, chemical modification with hydrophobic side chains or cationic functional groups can be utilized for incorporation of hydrophobic drugs and nucleic acids, respectively. These drugs also can be attached covalently onto polymers to afford drug–polymer conjugates, which consequently eliminate the diffusion-dominated premature release and provide further tunability of either hydrolytically- or enzymatically-induced controlled release. Diagnostic probes can also be included in these materials through orthogonal chemical modifications.

Hydrophilic polymer components/segments should be carefully selected to mask the hydrophobic domains of the nanoparticles and the embedded cargoes, as well as to allow for prolonged blood circulation time and low interaction with extracellular matrices and with the immune system components. Poly(ethylene glycol) (PEG), also known as poly(ethylene oxide) (PEO) or polyoxyethylene (POE), is the most commonly used

polymer to coat various types of nanomaterials and to impart stealth properties. Other polymers have also been investigated to form the corona of nanoparticles, such as poly(*N*-(2-hydroxypropyl)methacrylamide) (PHPMA), poly(acrylic acid) (PAA), poly(*N*-vinylpyrrolidone), poly(*N*-isopropylacrylamide), and poly(carboxybetaine) (PCB).[22-27] Although still controversial, it was reported that PCB can impart an antibiofouling effect better than PEG, possibly due to better hydration of the corona *via* the tighter electrostatic binding of water molecules than hydrogen bonding in the case of PEG, thus minimizing protein adsorption on the surface of nanoparticles.[25-27] Antibiofouling means lower competences for adsorbing proteins or other opsonins in the surrounding environment. As potential toxicities and immunogenicities of PEGylated therapeutics were previously reported,[28-30] alternative degradable PEG analogues are currently under investigation to improve the safety profiles of PEG-based therapeutics.[31] However, it is worth mentioning that safety, biocompatibility, and performance of nanomaterials depend on the overall nanoparticle composition and not only that of the shell.

The recently-developed controlled polymerization methodologies not only provide a powerful toolbox for incorporation of diverse functionalities into polymers but also enable precise rationalization of drug/targeting ligand/probes-to-polymer or unimer-to-unimer ratio, thus providing the possibility of predefined control over the size and shape of the formed nanoparticles. The size and morphology of polymer nanoparticles serve as critical characteristics for their *in vivo* fates, such as blood circulation time and organ biodistribution. While spherical nanostructures with hydrodynamic diameters (D_h's) ranging from tens to hundreds of nanometers have been extensively studied, recent

research activities on ultrasmall nanoparticles with D_h at the sub-10 nm scale revealed noticeable advantages of enabling effective renal excretion[32] and minimizing off-target accumulation,[33] which are attractive features for developing nanoparticulates for imaging applications. However, the decrease of nanoparticle size can enhance its permeability into both healthy and diseased tissues and can also result in rapid clearance from the blood and thus reduced accumulation in the targeted tissues, which deceases the benefits from nanoparticles in some therapeutic applications, such as in the case of cancer therapy. Regardless of the size of nanoparticles, imparting stability that prevents premature dissociation and release of the loaded therapeutic/diagnostic cargoes is crucial.

Premature disassembly of nanoparticles into the polymer constituents and/or breakdown into degradation products result in premature release of their loaded cargoes, and this is considered one of the main challenges for the effective delivery of nanoparticle-packaged therapeutics to their target sites. Not only might the drug release prematurely, but the free polymeric chains may also induce cyto/immunotoxicity. Stereocomplexation, noncovalent interactions, and cross-linking of one or more of the polymer's components are some of the most commonly utilized strategies to enhance the stability of nanomaterials.[34-36] Cross-linking can be performed within either the core or the corona of preformed micelles. Synthesis of unimolecular/hyperbranched structures that are not prone to dissociation upon dilution is another way to yield stable nanostructures. The relationship between chemical composition and cross-linking of different block copolymers and the relative copolymer block length on the size, core/shell dimensions, loading and release kinetics, and pH- and thermoresponsiveness of SCKs were previously

reviewed by our group and others.[37-40] The superior characteristics of the cross-linked nanomaterials over their non-cross-linked precursors include allowing unique processing opportunities, including overcoming complications of aggregation during lyophilization processes; biological advantages, including slower kinetics of release of therapeutic guests,[23,41] higher kinetic and blood stability,[42,43] longer pulmonary retention to provide for extended release,[41] and lower cyto/immunotoxicities; introducing of structural/functional factors that enable stimuli-responsive functions; and affording unusual nanoparticle properties and structures, including stabilization of nanocrystals and the formation of nanocages.

1.4. Scope of the Dissertation

This dissertation is focused on the development of targeted-polymeric nanoparticles for the treatment of infectious diseases and the synthesis of functional degradable polymers which can be used as a component of drug delivery vehicles. Furthermore, the ROP of lactide was investigated using hyperpolarized NMR, which will lead further research to improve catalytic activity by not only optimization of reaction conditions, but also modification of catalyst.

Chapter II is focused on the improvement of the conjugation conditions, which is crucial for the preparation of targeted polymeric nanostructures. Amidation between carboxylic acids located in the shell of the poly(acrylic acid)-*block*-polystyrene-based polymeric nanoparticles and primary amine groups of lysine residues on bacterial adhesin, $FimH_A$, was employed as the conjugation method. We found that free- and/or physically-

associated $FimH_A$ in the reaction mixture was difficult to remove by common purification methods, such as dialysis, centrifugal filtration, and column chromatography. Therefore, we aimed to obtain quantitative conjugation yields under improved amidation conditions, which would allow for avoiding demanding purification process. Amidation conditions were improved based on several aspects which could be overlooked, such as extents of shell cross-linking, half-lives and reactivity of coupling agents, impurities, *etc*.

Nanostructures employed in Chapter II were derived from non-degradable block copolymers to avoid potential *in situ* degradation during and after conjugation reactions, which could complicate analysis of results. In Chapter III, IV, and V, degradable polycarbonate-based macromolecular materials were developed in order to replace non-degradable components of polymeric nanostructures, which will allow for hydrolytic degradation and biological clearance of the nanomaterials. Functionalizable hydrophilic polycarbonate were designed and synthesized as a degradable alternative for widely used water soluble polymers, PHPMA and PEG in Chapter III. The resulting polymer was highly water-soluble and readily functionalizable by postpolymerization modifications with low cyto-/immunotoxicities, which are promising characteristics for a degradable alternative to PEG and PHPMA. In Chapter IV, aldehyde-functional polycarbonates were synthesized by ozonolysis and reductive work-up of allyl-functional polycarbonates. Resulting aldehyde moieties were readily functionalized with aminooxy compounds under mild conditions, which could be a promising conjugation strategy for the preparation of ligand-nanoparticle conjugates. In Chapter V, vinyl ether-functional polycarbonates were developed as a versatile template for multiple postpolymerization modification

chemistries including acetalization, thioacetalization, and thiol-ene reaction. Among them, the acetal moiety is a promising functionality for stimuli-responsive drug delivery systems due to its acid-labile characteristic. pH-dependent cleavage kinetics of an acetal linkage with a model drug compound demonstrated its potential for biomedical applications.

In Chapter VI, ring-opening polymerization, which is widely used polymerization to synthesize degradable polymers, such as polyesters, polycarbonates, polyphosphoesters, polypeptides, *etc.*, was investigated using a specialized NMR spectroscopy technique. Real-time NMR spectroscopy enhanced by hyperpolarization of nuclear spins enables to detect ^{13}C NMR signal of an intermediate formed during the polymerization. ^{13}C temporal correlation experiments and homonuclear selective saturation experiments verified that the observed ^{13}C NMR signal showed characteristics of intermediate species.

CHAPTER II

IMPROVEMENT OF THE CONJUGATION CONDITIONS FOR THE SYNTHESIS OF BACTERIAL ADHESIN-POLYMERIC NANOPARTICLE CONJUGATES FOR THE TREATMENT OF URINARY TRACT INFECTIONS

2.1. Introduction

Urinary tract infections (UTIs) are among the most common bacterial infections worldwide, the second most common infectious diseases after respiratory infections in the United States, and the most common hospital-acquired infection.[44-47] Socioeconomic burden of UTIs including direct (financial) and indirect (social) costs is estimated more than a few billion dollars in the United States and would be much higher since social impacts are immeasurable.[46,48] In addition, a high tendency of recurrence and emergence of antibiotic resistant bacteria make treatments more complicated. More frequent exposure of bacteria to antimicrobials promotes development of resistant strains as well as the suppression and alteration of normal microbiota for patients with recurring infections.[49,50] Therefore, there is an urgent need to develop more effective treatment methods in order to exclusively eradicate only UTI-causing pathogens from the human body and to prevent recurrent UTIs, while maintaining a healthy microbiome of commensal or mutualistic flora.

UTIs include infections in the urethra, bladder, ureters, and kidneys, which constitute the urinary system. Although several uropathogens including bacteria, viruses, and fungi can cause UTIs, bacteria, especially uropathogenic *Escherichia coli* (UPEC),

are the primary source of infections.[16] Attachment (adherence, adhesion) of uropathogens on the surfaces (epithelial cells) of each urinary system is a key initial step in the mechanisms of infection and colonization since it prevents bacteria from elimination from the urinary tract.[51] Adhesion of UPEC to urothelial cells are mediated by adhesive proteins (adhesins) at the tip of various pili, such as F1C pili, P pili, S pili, Type 1 pili, *etc*.[52] Among them, Type 1 pili are well-characterized and are known to be responsible for UPEC adherence, colonization, and invasion of urothelial cells in mouse model studies.[53,54] Tip adhesive domain of Type 1 pili ($FimH_A$) interact with mannosyl moieties on uroplakin and $\alpha_3\beta_1$ integrin on the surface of bladder epithelial cells, which leads to internalization of UPEC into these umbrella cells.[55-60] After internalization and escape from endocytic vesicles to cytoplasm, UPEC can develop intracellular bacterial communities (IBCs) and quiescent intracellular reservoirs (QIRs), which enable UPEC to evade both host defense system and antibiotic treatment. Notably, intraepithelial reservoirs might serve as a source of recurrent UTIs.[61-63] We hypothesized that bacterial adhesin-conjugated polymeric nanoparticles can deliver antimicrobials to reservoir bacteria hiding deep inside the cells by mimicking the bacterial mode of cell binding and internalization, thus treating and eradicating recurrent UTIs.

Our group reported the development of $FimH_A$-targeted polymeric nanoparticles and their $FimH_A$-specific adherence to the cultured bladder epithelial cells *in vitro*.[64] Amidation between carboxylic acids located in the shell of the shell cross-linked knedel-like nanoparticles (SCKs)[65,66] and primary amine groups of four lysine residues on $FimH_A$ variant was employed as the conjugation method. Although we observed several

internalized SCKs with the conjugates within the bladder epithelial cells, the majority was localized on the cell membranes/surfaces. In this study, we prepared adhesin-SCK conjugates with varying amounts of $FimH_A$ on the surface of the SCK nanoparticles without free- and/or physically-associated protein in order to improve the behavior of conjugates. First, we tried a few purification methods to remove unbound $FimH_A$ after conjugation, including dialysis, centrifugal filtration, and column chromatography, which turned out to be ineffective. Without a reliable purification method, we cannot increase the amount of $FimH_A$ in the reaction mixture as an approach to increasing $FimH_A$ density on the nanoparticle surface, which would have facilitated nanoparticles' binding and invasion into the bladder epithelial cells. As an alternative approach, therefore, we aimed to obtain *ca.* 100% conjugation yields under improved amidation conditions, which allows for the maximum density of targeting protein on the surface of nanoparticles with full covalent linkages. Conjugation conditions were improved by considering several aspects, such as extents of shell cross-linking, half-lives and reactivity of coupling agents, impurities, *etc*. Under the improved conditions, the equivalent ratios of protein to polymer chain were altered to compare the amount of $FimH_A$ added to aqueous solutions of the SCK nanoparticles *vs*. the conjugation efficiency, by which *ca*. 100% conjugation yield was achieved below 1:2 ratios of $FimH_A$: polymer. The amount of free protein was confirmed by SDS-PAGE with silver staining and Western blot. We prepared three conjugates to study cell internalization efficiency as a function of the amount of $FimH_A$ on the SCKs. However, resulting conjugates did not provide better cell attachment and internalization results *in vitro* compared to the previous report.

2.2. Results and Discussion

2.2.1. Challenge I: Purification of $FimH_A$-SCK conjugates to remove free $FimH_A$

First of all, we attempted to find an effective method of purification for $FimH_A$-SCK conjugates to remove free and/or non-covalently-attached proteins. Removal of free $FimH_A$ is critical to improve behaviors of $FimH_A$-SCK conjugates, since free targeting proteins could hinder the interaction of conjugates with the bladder epithelial cells by competitively binding to and reducing the number of available receptors. Also, a reliable purification method should allow for adjustment of the amount of $FimH_A$ on the surface of nanoparticles to observe the influence of adhesion density on binding and internalization of conjugates into the epithelial cells. $FimH_A$-SCK conjugates were first prepared under the same conditions to the previous report[64] with maximum amount of available $FimH_A$. The amount of added $FimH_A$ was determined by molar ratio of $FimH_A$ to polymer precursor (PAA-*b*-PS) of SCKs. For the purification trials, more than 3 equivalents (~3.4 equiv to single polymer chain) of $FimH_A$ were used for conjugation reaction, which is in excess based on previous experiments. Aliquots of the resulting reaction mixture were purified by three different methods: 1) column chromatography using Sephadex® G-50 (medium) with nanopure water as an eluent; 2) centrifugal filtration using Amicon® Ultra centrifugal filters (Millipore, 100 kDa MWCO, Ultracel®-100K) with 1X PBS or 1X PBS with 0.05% Tween 20; 3) dialysis against 1X PBS using dialysis tubings (Spectra/Por® Biotech Cellulose Ester (CE) dialysis membranes MWCO 100 kDa and 300 kDa). However, all three methods were unsuccessful in the removal of unbound proteins. Free $FimH_A$ and $FimH_A$-SCK conjugates passed through the Sephadex column

at similar rates. Extensive washing of reaction mixture using centrifugal filter unit with 1X PBS (final dilution factor = *ca*. $1/10^{10}$) did not work even though we selected a membrane with large enough molecular weight cut-off (MWCO = 100 kDa) compared to $FimH_A$ (*ca*. 17.7 kDa). Application of surfactant (0.05% Tween 20 in 1X PBS) to hinder the electrostatic interaction between the protein (pI = 8.55, positively charged in 1X PBS at pH 7.4) and the anionic SCKs did not improve the outcome either. After a few cycles of filtration, the color of FITC dye conjugated to the SCKs became fainter in the nanoparticle solution and was observed on the membrane of centrifugal filter unit, which indicated the undesirable adsorption of dye-labeled polymeric nanoparticles on the membrane. Dialysis against 1X PBS (final dilution factor = *ca*. $1/10^{14}$) did not yield more favorable results, even when we used dialysis tubing with larger MWCO (300 kDa). Incubation of reaction mixture in 1X PBS with 0.1% Tween 20 for 3 h before dialysis or centrifugal filtration[67] was also unsuccessful. After failures of the above purification attempts, we aimed to achieve *ca*. 100% conjugation yields, which would allow for the removal of only small molecular byproducts without the need of the problematic separation step. After improving conjugation conditions to ensure maximum yields, the amount of added $FimH_A$ was reduced until *ca*. 100% yield was achieved.

2.2.2. Challenge II: Precipitation during preparation

Precipitation of polymer and/or polymeric nanoparticles from solution was an occasional problem during the shell crosslinking reaction, dialysis, and/or centrifugal filtration for unknown reasons. One of our concerns about precipitation during shell-crosslinking reactions was whether inter-particle crosslinking reaction caused

precipitation. Size distributions measured by DLS showed little difference between normally prepared SCK solution and re-suspended SCK solution after precipitation occurred. This result indicated that reduced electrostatic repulsion during SCK formation might be attributed to precipitation problems. Since SCKs were prepared from poly(acrylic acid)-*block*-poly(styrene) (PAA-*b*-PS) for this study, formation of carboxylate salts in the shell domain would improve water solubility of SCKs as well as increase the repulsive force between the polymeric nanoparticles to prevent aggregation and precipitation. We found that precipitates were readily re-suspended under slightly basic conditions, which were prepared by dialysis against buffers (1X PBS (pH 7.4), phosphate buffer (pH 7.4), MES buffer (pH 6.0), *etc*) or by addition of $NaHCO_3$ solution. Based on these results, we used buffer solutions to provide a more reproducible environment compared to nanopure water in order to prevent pH gradient-induced aggregation of nanostructures. For the carbodiimide-involved reactions, usage of phosphate-containing buffers was avoided, since phosphate functionalities can also react with carbodiimide reagents and reduce coupling efficiency.[68] MES (4-morpholinoethanesulfonic acid) buffer (pH 6.0) is known to be a suitable reaction medium for water-soluble carbodiimide coupling reactions.[69,70] The slight acidity of MES buffer at pH 6 allows for the formation of sufficient carboxylate salts in the shell layer to stabilize PAA-*b*-PS-based polymeric nanoparticles in aqueous solution since pK_a of PAA is 4.5.[71] When shell crosslinking reactions were performed in MES buffer, well-defined SCKs ranging from 10% to 50% shell-crosslinking density were prepared without any precipitation problems (Figure 2.1). In addition, we compared two water-soluble

carbodiimide coupling reagents, EDC·HCl and EDC·MeI. This study revealed that EDC·HCl was better for SCK formation than EDC·MeI. More than 1 equivalent of EDC·HCl to the available acrylic acid units was applicable for SCK formation in nanopure water without precipitation problems, but 1 equivalent of EDC·MeI to the diamine cross-linker frequently caused precipitation under similar conditions. More detailed comparisons between two carbodiimides will be discussed in the later section.

Precipitates or floating debris are possible residual impurities inside the dialysis tubing created during the production process by the manufacturer. When nanopure water was added to the presoaked dialysis tubing and was transferred to a vial, some debris were observed even with the naked eye. Also, the DLS measurement of the solution showed multimodal size distributions. Although the amount of debris varied from batch to batch, careful washing of dialysis tubing is critical to avoid complications during characterization and potential interference for further experiments by undesirable impurities, which might be fragments of regenerated cellulose or other impurities during manufacturing process.

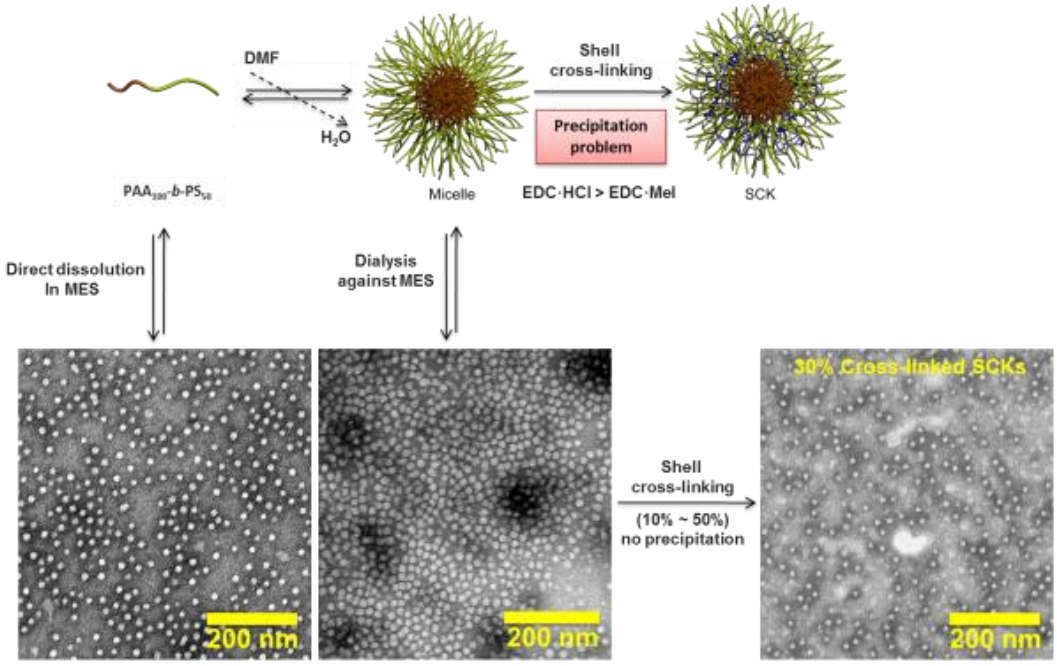

Figure 2.1. Preparation of SCKs.

2.2.3. Improvement of amidation conditions

Reliable and efficient conjugation chemistries are imperative to study behaviors of synthetic nanobiomaterials in the biological systems.[72] In this section, we will discuss a few critical aspects to improve the efficiency of amidation-based coupling chemistry. Our group previously reported the amidation of DOTA chelators to the SCKs prepared from PAA-*b*-PS.[72] We found that the coupling efficiency is influenced by physicochemical properties of polymeric nanoparticles including surface charge, permeability, extents of shell cross-linking, *etc*. as well as those of conjugated ligands. In this study, we investigated a few more factors to extend insights on conjugation chemistry.

Extents of shell cross-linking. We examined the influence of shell cross-linking percentage on the stability of the SCKs and the coupling efficiencies of $FimH_A$-SCK conjugates *via* sodium dodecyl sulfate polyacrylamide gel electrophoresis (SDS-PAGE) and Western blot to estimate the ratio of conjugated and unconjugated adhesin. $FimH_A$-conjugated SCKs with lower than 30% crosslinking showed smeared bands between 20 kDa and 100 kDa in Western blot results (Figure 2.2). It is hypothesized that those unidentified bands are originated from $FimH_A$-conjugated polymers that were disassembled from the SCK nanostructures under SDS-PAGE conditions, in which noncovalent interactions were interfered.[73] Smeared bands were not observed when 50%-crosslinked SCKs were used for conjugation. Therefore, more robust SCKs with 50% crosslinking were used for further studies to avoid disintegration of conjugates in extreme conditions, such as the environment inside the bladder. Higher extents of cross-linking will also reduce permeability of the shell domain,[74] which will promote the conjugation of adhesion onto the surface of SCKs. It is desirable for this study since binding sites of $FimH_A$ embedded within the shell domain might be inaccessible *via* steric hindrance.

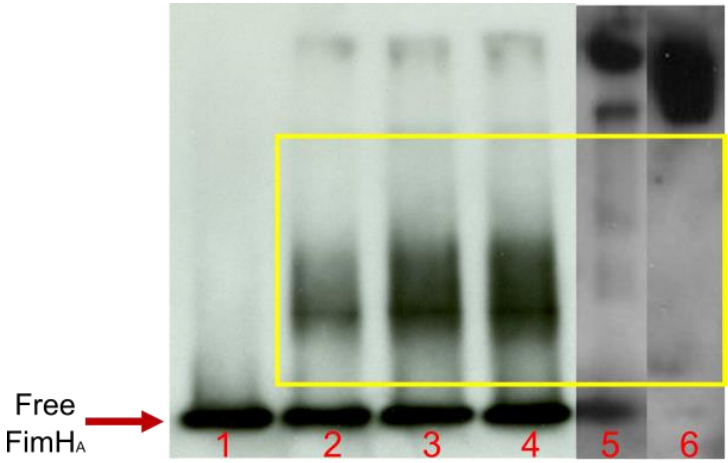

Figure 2.2. Western blot results of $FimH_A$-SCK conjugates with different extents of shell cross-linking. (1) $FimH_A$, (2) $FimH_A$-SCKs (10% cross-linked), $FimH_A$: PAA-*b*-PS = 1 : 4, (3) $FimH_A$-SCKs (10% cross-linked), $FimH_A$: PAA-*b*-PS = 1 : 3, (4) $FimH_A$-SCKs (10% cross-linked), $FimH_A$: PAA-*b*-PS = 1 : 2, (5) $FimH_A$-SCKs (20% cross-linked), $FimH_A$: PAA-*b*-PS = 1 : 1, (6) $FimH_A$-SCKs (50% cross-linked), $FimH_A$: PAA-*b*-PS = 1 : 1.

Unreacted amino groups after shell cross-linking reactions. After shell cross-linking reactions, there could be unreacted primary amines within the shell domain of SCKs. The residual amino groups would either be coordinated within the shell domain by electrostatic interaction or dangling on the surface of SCKs. Electrostatically-attached amino groups could further cross-link shell domain of SCKs during amidation of $FimH_A$ with SCKs. However, amine functionalities dangling on the SCKs could cause inter-SCK-coupling upon the addition of carbodiimide coupling reagent, which might lead to precipitation and/or multimodal size distributions in DLS. Our group recently reported that an addition of EDC·MeI to SCK solution caused inter-SCK cross-linking.[75] *In addition*, the $FimH_A$ variant used in the current experiments has four lysine residues, which could participate in inter-SCK conjugations. Therefore, further conjugation

reactions were performed under diluted concentrations (< 0.15 mg/mL, amount of PAA-*b*-PS in solution) in order to minimize inter-particle amidation reaction.[76] Another potential deteriorative effect of unreacted amino groups are their interaction with negatively-charged mannose binding pocket of $FimH_A$, which could interfere with essential hydrogen bonding interaction between $FimH_A$ and mannose.[77]

Half-lives and reactivity of coupling agents. Stabilities and reactivity of coupling agents are one of the most important aspects to improve conjugation efficiency. In this study, amidations were employed for both shell-crosslinking and adhesion conjugation reactions. In order to activate carboxylic acid functionalities within the shell of SCKs, water-soluble carbodiimides were used to form better electrophiles for primary amine groups of cross-linker or $FimH_A$. There have been a lot of studies and discussions about stability of carbodiimide coupling reagents in different conditions, including pH, buffer, and additives, *etc*.[78] Our group has been used either EDC·HCl or EDC·MeI for amidation reactions, such as shell crosslinking reactions, conjugation of dye or targeting ligand, *etc*. EDC·MeI is known to be more reactive than EDC·HCl since intramolecular cyclization of EDC·HCl is under equilibrium in solution, which might reduce the reactivity compared to non-cyclizable EDC·MeI.[68,79,80] However, EDC·MeI is less stable than EDC·HCl in aqueous solution. We examined and compared both water-soluble carbodiimides for shell cross-linking reactions. Applications of EDC·HCl did not cause any precipitation. However, cloudiness of micellar solution was often induced right after the addition of EDC·MeI during shell crosslinking process. When the excess amount of EDC was used in order to achieve higher cross-linking yields, excess EDC·MeI caused precipitation of

the micellar solutions. *O*-acylisourea intermediate derived from EDC·MeI and carboxylic acid functionality within the shell of micelles might decrease the solubility of polymeric nanostructures more than that derived from EDC·HCl might do. Therefore, slightly excess amount of EDC·MeI (2.3 equiv. to diamine cross-linker) had to be used to prevent precipitation. On the other hand, large excess of EDC·HCl (>1.0 equiv to carboxylic acids) was able to be applied without precipitation problems to activate all available carboxylic acid functionalities within the shell domain. So, EDC·HCl was selected for further reactions due to its longer half-life in aqueous solution and stability of nanoparticle solution during reactions. Since our conjugation experiments were performed under diluted conditions in order to prevent inter-particle crosslinking, longer half-life is desirable to increase conjugation yield and efficiency. In addition, use of EDC·HCl for SCK formation is more economical since buffer solutions were not required to prepare stable SCKs, while those were required when EDC·MeI was used.

Another key reagent is sulfonated *N*-hydroxysuccinimide (sulfo-NHS), which is often added to carbodiimide coupling reactions to enhance coupling efficiency. Reaction between carboxylic acid and carbodiimide reagent produces highly reactive *O*-acylisourea intermediate, which can readily react with primary amines. However, hydrolysis is a competing side reaction in aqueous solutions due to the high reactivity of the *O*-acylisourea intermediate. For conjugation of larger protein to polymeric nanoparticles under dilute conditions, there is a lower chance for nanoparticles to meet one of amino groups of proteins. Moreover, protein conjugations are usually conducted under slightly basic conditions to prevent protonation of primary amines, which accelerates hydrolysis

of the intermediate. Therefore, the unstable *O*-acylisourea intermediate was trapped by sulfo-NHS to form more stable activated ester in order to improve coupling efficiency. On the other hand, the shell cross-linking reactions were performed under slightly different conditions. Before adding carbodiimides, micelles and diamine cross-linkers were mixed, which promotes an attachment of cross-linkers to the micelles by electrostatic interactions between carboxylic acids and primary amines. Therefore, we were less concerned about hydrolysis since both functionalities are already in vicinity with excess amount of carbodiimides.

Another commonly used alternative to sulfo-NHS is sulfonated tetrafluorophenyl (sulfo-TFP), which is also included in the carbodiinmide coupling reaction to form activated ester by trapping unstable *O*-acylisourea intermediate.[81] Reactivity of TFP ester to primary amines is comparable to NHS ester. However, it is more resistant to hydrolysis under basic conditions.[82] The half-life of TFP ester is known to be at least two times longer than that of NHS ester at pH ~8.[70] In order to compare coupling efficiency between sulfo-NHS ester- and sulfo-TFP ester-mediated conjugations, $FimH_A$ conjugation reactions were conducted under the same conditions, except for swapping the two sulfonated reagents (Scheme 2.1). We did not perform conjugation reactions under more basic conditions to check relative stability and reactivity of each activated ester due to the potential stability issue of $FimH_A$. SDS-PAGE of resulting conjugates visualized by silver staining showed no free $FimH_A$, which indicated comparable conjugation yields (*ca.* 100%) under the similar conditions. Although either sulfo-NHS or sulfo-NHS will

provide similar conjugation results, sulfo-TFP was selected for further reactions since its higher stability could afford more consistent and reproducible outcomes.

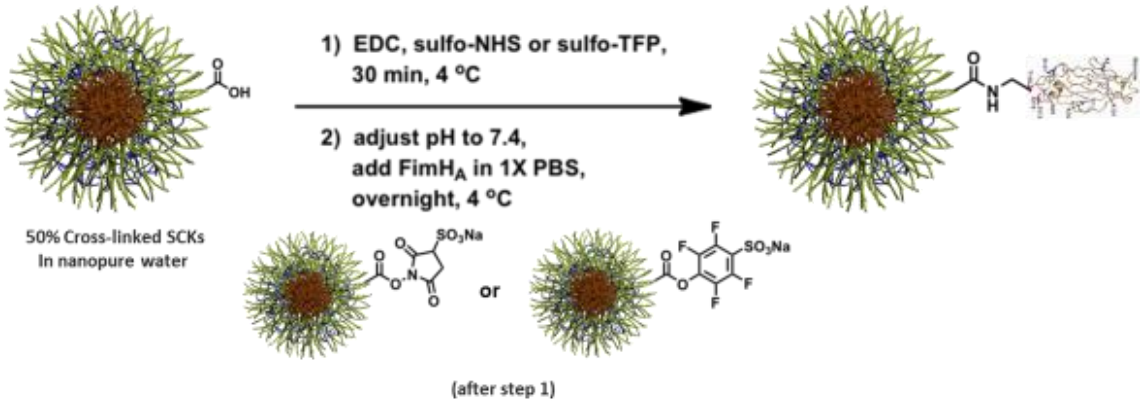

Scheme 2.1. Preparation of FimH$_A$-SCK conjugates *via* two different activate esters, sulfo-NHS ester and sulfo-TFP ester.

Trifluoroacetic acid (TFA). Carbodiimide coupling reagents, such as EDC, can react with the carboxylic acid functionality of residual TFA in PAA-*b*-PS after acidolysis of P*t*BA-*b*-PS, which could compromise coupling yields. Also, during shell cross-linking reactions, diamine cross-linker, 2,2′-(ethylenedioxy)bis(ethylamine) (EDDA) can form salts with TFA, which could reduce cross-linking efficiency. Above all, toxicity of residual TFA is undesirable for the materials intended for biomedical applications. After acidolysis of P*t*BA-*b*-PS in TFA, excess TFA was evaporated with gentle N_2 flow. Resulting solid was dissolved in nanopure water and dialyzed against nanopure water for at least 4 days with frequent changes of water (2 to 3 times per day). After lyophilization, ^{19}F NMR showed weak resonances, which indicated residual TFA or TFA salts. Since

free TFA is easier to remove than TFA salts, it is more preferable to purify it at this stage. However, we decided not to do further purification of polymer since excess EDC could mitigate influence of residual TFA for the conjugation experiments. Reactions of polymeric nanoparticles with proper coupling reagents in suitable aqueous solutions allow the use of excess coupling reagents without concern for nanoparticle destabilization by alteration of functionalities on the surface of nanostructures. If residual TFA is determined to be problematic, it can be removed by several methods, such as anion exchange, stirring with basic resins, dialysis against basic or acidic solutions, *etc*. Reliable purification and characterization methods are critical to achieve reproducible results.

2.2.4. Preparation of $FimH_A$-targeted SCKs under the improved conjugation conditions

The bacterial adhesion-conjugates were synthesized under deliberately-selected conditions based on experiments and literature search to ensure maximum conjugation efficiency. First, the stoichiometry of protein to polymer chain was altered until quantitative conjugation yield was achieved in order to exclude troublesome removal process of free protein. The amount of free protein in the crude reaction mixtures was confirmed by SDS-PAGE with silver staining and Western blot. As a result, free $FimH_A$ was not detected when the amount of added adhesin was less than ratio of one $FimH_A$ to two polymer chains.

Every conjugate would have different ratios of ligand to nanoparticle for optimum function. Also, optimum ratios need to be carefully characterized for their translation to clinical application.[83] Hence, we prepared three conjugates with different ratios of ligand to polymer chain, 1 to 3, 1 to 6, and 1 to 9 in order to study cell internalization efficiency as a function of the amount of $FimH_A$ on the SCKs (Figure 2.3). SDS-PAGE results with silver staining and Western blot results showed strong bands of $FimH_A$-SCK conjugates in the sample wells and the stacking gels, which were detected at the same positions with FITC signals on the SCKs. Also, there were very weak free $FimH_A$ bands. Both results indicated that covalently-conjugated $FimH_A$-SCKs were prepared under the improved amidation conditions. Dynamic light scattering (DLS) results showed distinct increase of hydrodynamic diameters after $FimH_A$ conjugations [D_h (DLS, number) of SCKs = 16 ± 5 nm, D_h (DLS, number) = 80 ± 22 nm of $FimH_A$-SCKs when $FimH_A$: polymer = 1 : 3]. However, diameters measured by TEM showed little difference.

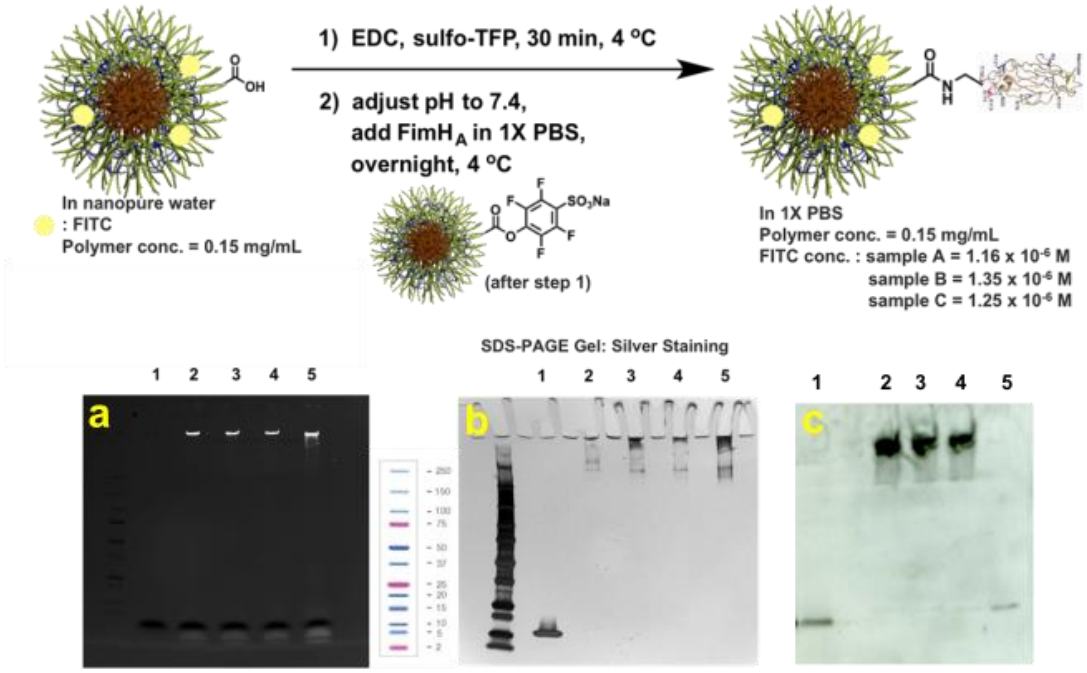

Figure 2.3. Schematic representation of FimH$_A$ conjugation to the shell of SCK nanoparticles *via* amidation coupling chemistry. a) SDS-PAGE visualized with UV, b) SDS-PAGE stained with silver stain, c) Western blot, (Lane 1) Free FimH$_A$, (Lane 2) FimH$_A$-SCKs (FimH$_A$: PAA-*b*-PS = 1 : 3), (Lane 3) FimH$_A$-SCKs (FimH$_A$: PAA-*b*-PS = 1 : 6), (Lane 4) FimH$_A$-SCKs (FimH$_A$: PAA-*b*-PS = 1 : 9), (Lane 5) FITC-SCKs, Note) Each SCKs is comprised of *ca*. 100 poly(acrylic acid)-*b*-polystyrene block copolymer chains, and each block copolymer contains *ca*. 100 acrylic acid residues, although only a single carboxylic acid and amide functionality is included to illustrate the coupling reaction between synthetic nanoparticle and protein.

Mannose-BSA ELISA results showed growth of signal with increasing FimH$_A$ concentrations, which indicated FimH$_A$ of the resulting conjugates are either in a favorable orientation or completely conjugated to SCKs with few free FimH$_A$ (Figure 2.4). When resulting reaction mixtures contained free and/or physically-associated FimH$_A$, mannose-BSA ELISA results showed no FimH$_A$ signal in the undiluted samples and higher signals in more diluted samples. Those results suggested that physically-associated FimH$_A$ has limited extent of conjugation into the shell or is in an unfavorable orientation, which did not allow for binding to mannose. Higher FimH$_A$ signal in the diluted conditions implied

that unconjugated $FimH_A$ was dissociated from the SCKs and was bound to mannose. The results in Figure 2.4 were promising for cell binding and internalization experiments *in vitro*.

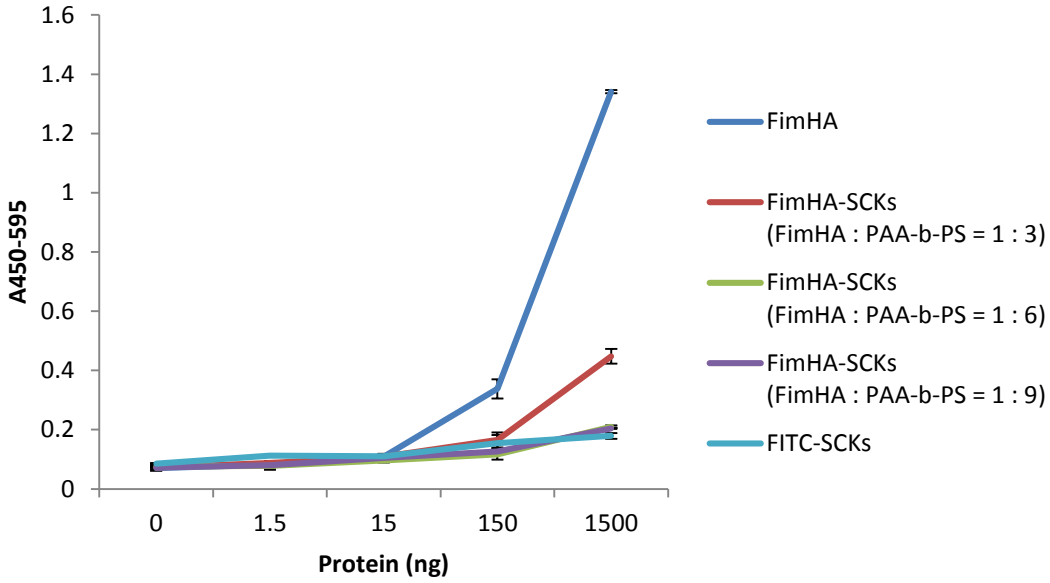

Figure 2.4. Results of mannose-BSA ELISA.

2.3. Experimental Section

2.3.1. Materials

PAA_{100}-*b*-PS_{50} (M_n^{NMR} = 13000 Da) and P*t*BA_{100}-*b*-PS_{50} ($M_n^{GPC\ THF}$ = 17800 Da, PDI = 1.08, M_n^{NMR} = 18800 Da, as a precursor to PAA_{100}-*b*-PS_{50}) were synthesized as reported using RAFT polymerization.[84] Sodium 2,3,5,6-tetrafluoro-4-hydroxybenzenesulfonate was purchased from TCI America. *N*-hydroxysulfosuccinimide sodium salt, 1-[3-(dimethylamino)propyl]-3-ethylcarbodiimide methiodide (EDC·MeI)

and 4-morpholineethanesulfonic acid (MES) monohydrate were obtained from Sigma-Aldrich. 1-(3-Dimethylaminopropyl)-3-ethylcarbodiimide hydrochloride (EDC·HCl) was purchased from Alfa Aesar. 5-((5-aminopentyl)thioureidyl)fluorescein, dihydrobromide salt (5-FITC cadaverine) was purchased from Invitrogen, Carlsbad, CA. Dimethylformamide (DMF) was purified by passage through solvent purification systm (JC Meyer Solvent Systems) and used as pure solvent. Spectra/Por membrane tubes were purchased from Spectrum Laboratory Inc. (Rancho Dominguez, CA). Amicon® ultra centrifugal filter devices (100 kDa MWCO) were purchased from Millipore (Bedford, MA). All other solvents and chemicals were obtained from Sigma-Aldrich, TCI America, or Fisher Scientific and used as received.

2.3.2. Characterization

Dynamic light scattering (DLS) measurements were conducted using Delsa Nano C (Beckman Coulter, Inc., Fullerton, CA) equipped with a laser diode operating at 658 nm. Size measurements were made in nanopure water ($n = 1.3329$, $\eta = 0.890$ cP at 25 ± 1 °C). Scattered light was detected at 165° angle and analyzed using a log correlator over 70 accumulations for a 3.0 mL sample in a glass sizing cell (4.0 mL capacity). The samples in a glass sizing cell were equilibrated for 30 minutes before measurements were made. The photomultiplier aperture and the attenuator were automatically adjusted to obtain a photon counting rate of *ca*. 10 kcps. The calculations of the particle size distributions and distribution averages were performed using CONTIN particle size distribution analysis routines. Transmission electron microscopy (TEM) images were collected on a JEOL 1200EX operating at 100 kV and micrographs were recorded at

calibrated magnifications using a SIA-15C CCD camera. The samples as aqueous solutions (5 μL) were deposited onto formvar/carbon-coated copper grids. After 5 min, the excess sample was wicked off using filter paper and the grids were allowed to air-dry for 2 min. Following that, the grids were negatively stained with 5 μL of a 1% phosphotungstic acid (PTA) or 1% uranyl acetate (UA) aqueous solution. After 1 min (for PTA staining) or 15 sec (for UA staining), the excess stain was wicked off using filter paper. The sample grids were left to dry under ambient conditions overnight before analyses.

2.3.3. Preparation of micelles

1) Nanoprecipitation (solvent displacement method): PAA_{100}-*b*-PS_{50} block copolymer precursor (*ca*. 15.5 mg) was dissolved in DMF (15.5 mL) and allowed to stir overnight at room temperature. To this solution, an equal volume of nanopure water (15.5 mL) was added dropwise *via* a syringe pump (10 mL/h). The resulting mixture was allowed to stir overnight at room temperature and dialyzed against nanopure water for 4 days in presoaked dialysis tubing (MWCO *ca*. 6 – 8 kDa) to afford a micelle solution (final volume = *ca*. 56.9 mL) with a final polymer concentration of *ca*. 0.27 mg/mL. D_{av} (TEM) = 17 ± 2 nm, D_h (DLS, number) = 14 ± 4 nm, D_h (DLS, volume) = 21 ± 14 nm, D_h (DLS, intensity) = 160 ± 160 nm. *2) Direct dissolution method*: PAA_{100}-*b*-PS_{50} block copolymer precursor (*ca*. 12.8 mg) was directly dissolved in 42.6 mL of 0.1 M MES buffer (0.5 M NaCl, pH 6.0). The final polymer concentration was *ca*. 0.30 mg/mL D_{av} (TEM) = 18 ± 2 nm, D_h (DLS, number) = 14 ± 4 nm, D_h (DLS, volume) = 20 ± 11 nm, D_h (DLS, intensity) = 54 ± 36 nm.

2.3.4. Representative procedure for the preparation of SCKs

A solution of 2,2′-(ethylenedioxy)bis(ethylamine) (EDDA) in nanopure water (*ca*. 10 mg/mL, 1.0 eq, nominal 10, 20, 30, 40, and 50% crosslinking) was added dropwise to the micelle solution (4.5 mg, 0.30 mg/mL polymer concentration, in nanopure water or 0.1 M MES buffer, 0.5 M NaCl, pH 6.0). After 30 min, 1-(3-dimethylaminopropyl)-3-ethylcarbodiimide hydrochloride (EDC·HCl) in nanopure water (*ca*. 10 mg/mL, 1.0 eq. to the available acrylic acids) or 1-[3-(dimethylamino)propyl]-3-ethylcarbodiimide methiodide (EDC·MeI) (*ca*. 10 mg/mL, 2.5 eq to EDDA) was added dropwise to this solution, and the resulting mixture was allowed to stir overnight before dialysis against nanopure water for 4 days in presoaked dialysis tubing (MWCO *ca*. 6 – 8 kDa) to afford SCK solutions with a final polymer concentration of *ca*. 0.21 mg/mL. SCKs (50% cross-linked): D_{av} (TEM) = 17 ± 2 nm, D_h (DLS, number) = 16 ± 5 nm; D_h (DLS, volume) = 24 ± 16 nm; D_h (DLS, intensity) = 140 ± 140 nm.

2.3.5. Preparation of 5-FITC cadaverine-labeled SCKs

A solution of EDC·HCl in nanopure water (4.7 mg, 10 mg/mL, 1 eq. relative to the acrylic acids, 24 μmol) and sulfo-NHS in nanopure water (5.3 mg, 10 mg/mL, 1 eq. relative to the acrylic acids, 24 μmol) were added dropwise to a solution of SCK (15 mL, 0.21 mg/mL polymer concentration) in nanopure water. After stirring for 30 min at room temperature, a solution of 5-FITC cadaverine in nanopure water (1.6 mg, 1 mg/mL, 0.1 eq. to the acrylic acids, 2.4 μmol) was added dropwise. The reaction was allowed to proceed overnight at room temperature before being transferred to presoaked dialysis tubing (MWCO *ca*. 6 – 8 kDa), then dialyzed against nanopure water for 4 days to remove

impurities, yielding a 5-FITC cadaverine-labeled SCK solution with a final concentration of *ca*. 0.20 mg/mL. D_{av} (TEM) = 15 ± 2 nm, D_h (DLS, number) = 82 ± 23 nm; D_h (DLS, volume) = 110 ± 50 nm; D_h (DLS, intensity) = 220 ± 120 nm.

2.3.6. Conjugation of $FimH_A$ to 5-FITC cadaverine-labeled SCKs

Solutions of sulfo-TFP (0.93 mg, 10 mg/mL, 3.46 μmol, 1.0 eq.) and EDC·HCl (0.66 mg, 10 mg/mL, 3.46 μmol, 1.0 eq.) in nanopure water was added to the solution of 5-FITC cadaverine-labeled SCKs (3.0 mL, 0.15 mg/mL polymer concentration) in nanopure water at 4 °C (in a cold room). After stirring for 30 min, the pH of solution was adjusted to *ca*. 7.4 by dropwise addition of sodium phosphate solution, followed by the addition of $FimH_A$ in 1X PBS (0.50 mg/mL, 0.20 mg when $FimH_A$: polymer = 1 : 3, 0.10 mg when $FimH_A$: polymer = 1 : 6, 0.065 mg when $FimH_A$: polymer = 1 : 9). The reaction was allowed to proceed at 4 °C overnight. The reaction mixture was purified by washing using a centrifugal filtration device (MWCO 100 kDa) with 1X PBS (pH 7.4) or dialysis against 1X PBS (pH 7.4), and the final volume was reconstituted to 3.0 mL with 1X PBS to yield $FimH_A$-conjugated, 5-FITC cadaverine-labeled SCKs (final polymer concentration = *ca*. 0.15 mg/mL). When $FimH_A$: polymer = 1 : 3, D_{av} (TEM) = 17 ± 2 nm, D_h (DLS, number) = 80 ± 22 nm; D_h (DLS, volume) = 120 ± 82 nm; D_h (DLS, intensity) = 880 ± 900 nm. When $FimH_A$: polymer = 1 : 6, D_{av} (TEM) = 17 ± 2 nm, D_h (DLS, number) = 76 ± 19 nm; D_h (DLS, volume) = 110 ± 88 nm; D_h (DLS, intensity) = 2400 ± 2800 nm. When $FimH_A$: polymer = 1 : 9, D_{av} (TEM) = 17 ± 2 nm, D_h (DLS, number) = 87 ± 19 nm; D_h (DLS, volume) = 100 ± 73 nm; D_h (DLS, intensity) = 980 ± 1060 nm.

2.4. Conclusions

The amidation-based conjugation conditions of $FimH_A$ to SCKs were improved in consideration of a few factors that might be overlooked, including extents of shell cross-linking, half-lives and reactivity of coupling agents, impurities, *etc*. Under these improved conditions, the equivalent ratios of protein to polymer chain were altered to compare the amount of $FimH_A$ added to aqueous solutions of the SCK nanoparticles *vs*. the conjugation efficiency, by which *ca*. 100% conjugation yield was achieved below 1:2 ratios of $FimH_A$: polymer. The amount of free protein was confirmed by SDS-PAGE with silver staining and Western blot. We prepared three conjugates to study cell internalization efficiency as a function of the amount of $FimH_A$ on the SCKs. However, resulting conjugates did not provide better cell attachment and internalization results *in vitro* compared to the previous report. One potential problem with this synthetic strategy is difficulty in ensuring favorable orientation of protein on SCKs since native $FimH_A$ has four lysine residues which can participate in the amidation-based conjugation to the SCKs. Therefore, we are planning to evaluate a few $FimH_A$ variants that have less lysine residues and/or an additional lysine tail with or without a flexible linker in order to improve the orientation of conjugated-$FimH_A$. In addition, it would be more important to investigate the influence of nanoparticle size and shape on cell adherence and internalization. Polyvalent interactions between Type 1 pili of UPEC and mannose receptors on the surface of epithelial cells are believed to be critical for cell binding and internalization of UPEC. Since mannose moieties for $FimH_A$ are arrayed on the surface of bladder epithelial cells

at intervals of *ca*. 16 nm, cylindrical nanostructures could enhance cell internalization efficiency *via* binding to multiple receptors.

CHAPTER III

FUNCTIONALIZABLE HYDROPHILIC POLYCARBONATE, POLY(5-METHYL-5-(2-HYDROXYPROPYL)AMINOCARBONYL-1,3-DIOXAN-2-ONE), DESIGNED AS A DEGRADABLE ALTERNATIVE FOR PHPMA AND PEG*

3.1. Introduction

Hydrophilic, water-soluble polymers have been employed in a wide range of products, including, pharmaceuticals, foods, adhesives, coatings, paints, textiles, *etc*.[85] Among these applications, hydrophilic polymers are one of the essential components of nanomedicines in order to enhance water solubility and stability of materials, such as drugs and drug carriers. Up to now, poly(ethylene glycol) (PEG), also known as poly(ethylene oxide) (PEO), has been the most widely used water-soluble polymer in the biomedical field, especially for drug delivery systems, due to its high hydrophilicity, biocompatibility, commercial availability, and stealth character in its ability to reduce opsonization and clearance of nanoparticles upon *in vivo* administration, which improve biodistribution and pharmacokinetics of nanocarriers.[86-88] However, its potential drawbacks have been gradually reported: nonbiodegradability along with undesirable degradation under mechanical, thermal, and chemical stress, accumulation in the body, PEG-induced

---

*Reprinted with permission from "Functionalizable Hydrophilic Polycarbonate, Poly(5-methyl-5-(2-hydroxypropyl)aminocarbonyl-1,3-dioxan-2-one), Designed as a Degradable Alternative for PHPMA and PEG" by Sangho Cho, Gyu Seong Heo, Sarosh Khan, Amelia M. Gonzalez, Mahmoud Elsabahy, and Karen L. Wooley, *Macromolecules* **2015**, *48*(24), 8797-8805.

hypersensitivity by the immune system, rapid clearance after repeated injection, *etc*.[88,89] Moreover, the polyether backbone of PEG limits the functionalizable sites to the chain ends, which is an inherent structural limitation. Such drawbacks of PEG have encouraged the exploration of PEG analogues that contain degradable[90] and/or side chain reactive functionalities[91,92] within repeat units along the backbone, and the development of other water-soluble polymers for biomedical applications.[87-89] Although several natural and synthetic hydrophilic polymers have been reported,[85,88,93] such as polyglycerol, polyvinylpyrrolidone (PVP), poly(vinyl alcohol) (PVA), poly(acrylic acid) (PAA), polyacrylamide, polyoxazolines, polyphosphates, poly(amino acid)s, *etc.*, few have achieved similar levels of success as PEG. Of the alternatives, poly(*N*-(2-hydroxypropyl)methacrylamide) (PHPMA) is a hydrophilic polymer that can be modified with several functionalities *via* pendant secondary hydroxyl groups and shows minimal toxicity.[94,95] Well-defined PHPMA can be prepared by controlled radical polymerizations;[96] however, the low toxicity and biocompatibility of PHPMA can be affected negatively by residual copper from atom transfer radical polymerization (ATRP) or the presence of a thiocarbonyl-based chain end group from reversible addition−fragmentation chain transfer (RAFT) polymerization, which require careful removal of the copper catalyst or RAFT end groups before their applications.[97,98] Furthermore, the lack of biodegradability could limit the use of PHPMA conjugates.[95]

As an alternative to a nondegradable backbone, metal-free organocatalytic ring-opening polymerization (ROP) of bis-MPA-derived cyclic carbonate monomers has been reported to lead to degradable analogues to polymethacrylate-based polymers with precise

control over size, dispersity, and functionalities incorporated.[99,100] In addition, biocompatibility, biodegradability, and low *in vivo* toxicity of aliphatic polycarbonates (PCs) make them an excellent candidate for biomedical applications.[101,102] We, therefore, hypothesized that the incorporation of *N*-(2-hydroxypropyl) amide functionalities on the bis-MPA-based PC backbone would afford a degradable and water-soluble polymer that has comparable properties to PHPMA. To confirm this hypothesis, we introduced *N*-(2-hydroxypropyl) amide functionalities *via* amidation of carboxylic acid-functional PCs as postpolymerization modification, since controlled ROP of acidic monomers, which contain carboxylic acid, amide, or other acidic functionalities, is challenging with common organobase catalysts.[103] While this work was in progress, Engler, Yang, Hedrick, and co-workers reported the synthesis of hydrophilic PCs by amidation of pentafluorophenyl ester-functional PC with various alkanolamines.[104] In this case, the activated ester-functional PC was synthesized by acid-catalyzed ROP of corresponding monomer (MTC−OC_6F_5)[105] and, following amidation with amino alcohols, yielded corresponding amide-functional PCs, including our PHPMA analogue. They demonstrated that their PCs were water-soluble and of low toxicity *in vitro*, and, moreover, the PCs exhibited the capability to resist aggregation in serum, which is a characteristic of stealth polymers. Here, we report complementary results, which include an alternative synthetic route of polycarbonate-based PHPMA analogue, poly(5-methyl-5-(2-hydroxypropyl)aminocarbonyl-1,3-dioxan-2-one) (PMHPAC), which requires three simple steps: metal-free organobase-catalyzed ROP of benzyl ester-functionalized cyclic carbonate monomers, removal of the benzyl esters by catalytic hydrogenolysis, and

subsequent amidation of the resulting carboxylic acid-functional PCs with the corresponding amine. This synthetic method also allows the introduction of pendant functionalities onto the degradable PC backbone through amide linkages. The resulting polymer was highly soluble in water and showed minimal cyto-/immuno-toxicities. In addition, the pendant hydroxyl groups were readily functionalizable. Furthermore, amphiphilic block copolymers were synthesized to demonstrate synthetic versatility and formation of nanostructures in aqueous solution for biomedical applications. Our results suggest that PMHPAC could be utilized as an alternative hydrophilic polymer in clinical nanomedicines.

3.2. Results and Discussion

Although a similar final polymer structure to PMHPAC was reported recently,[104] this current work extends to an alternate synthetic strategy, postpolymerization modification of the reactive hydroxyl side chain moieties, and full characterization of the polymer compositions, structures and properties, including evaluation of immunotoxicity and demonstration of degradability.

3.2.1. Synthesis of the polycarbonate-based PHPMA analogue, PMHPAC

The preparation of the PMHPAC relied upon construction of a PC containing one reactive side chain carboxylic acid functionality at each repeat unit. Benzyl ester-functional PCs [poly(5-methyl-5-benzyloxycarbonyl-1,3-dioxan-2-one), PMBC, 1] were synthesized by organobase-catalyzed ROP of the functionalized cyclic carbonate monomer, 5-methyl-5-benzyloxycarbonyl-1,3-dioxan-2-one (MBC) by a previously reported procedure with a slight modification (Scheme 3.1 and Figure 3.1, 3.2).[99,106,107]

The benzyl ester groups of the PMBCs were removed by Pd/C-catalyzed hydrogenolysis yielding PCs with carboxylic acid functionalities, [poly(5-methyl-5-carboxyl-1,3-dioxan-2-one), PMC, 2] (Scheme 3.2).[108] The selective cleavage of the benzyl ester groups without reduction of the polycarbonate backbone was confirmed by ^{1}H and ^{13}C NMR spectroscopy (Figure 3.3), IR spectroscopy (Figure 3.4), and GPC analysis (Figure 3.5), before and after hydrogenolysis. ^{1}H NMR spectra showed the disappearance of the benzylic protons (labeled as a and c in Figure 3.2) and the appearance of a carboxylic acid proton (labeled as a in Figure 3.3), as well as intact proton resonances of the polycarbonate backbone (labeled as b in Figure 3.3). Comparing the C=O stretching vibration bands of 1 and 2 (Figure 3.4), the ν(C=O) at ~1740 cm^{-1} of the carbonates remained after hydrogenolysis with a new peak at ~1710 cm^{-1} for the carbonyl stretch along with a broad OH absorbance resulting from the carboxylic acids. By ^{13}C NMR spectroscopy, maintenance of the carbonate carbonyl resonance at *ca*. 154 ppm was observed, while the ester carbonyl resonance at 172.0 ppm was replaced by the carboxylic acid carbonyl resonance at 173.6 ppm. In order to confirm that the degree of polymerization and dispersity were maintained upon transformation of 1 to 2, the carboxylic acid

functionalities of 2 were protected by methylation using (trimethylsilyl)diazomethane ($TMSCH_2N_2$) under mild conditions,[109] to allow for GPC analyses. The GPC profiles of 1 showed similar peak shape and PDI (1.09) with those (1.09) of methylated PMC, [poly(5-methyl-5-methyloxycarbonyl-1,3-dioxan-2-one), PMMC, 3], which indicates the minimal influence of hydrogenolysis on the polycarbonate backbone (Figure 3.5). As expected, the benzyl carbonate chain-end group was also eliminated by hydrogenolysis, which was verified by monitoring the aromatic proton resonances. Although remaining toluene interfered with the accurate interpretation immediately following hydrogenolysis, there were no aromatic proton signals remaining after the next stage of amidation and purification (Figures 3.6, 3.3, and 3.7). Should retention of the α-chain end be of interest, it would be necessary to use an alternate initiator, which would contain functionalities that are tolerable for catalytic hydrogenation.

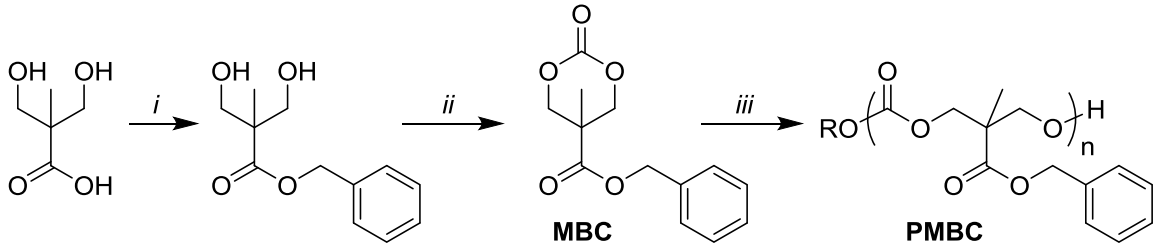

Scheme 3.1. Synthesis and ring-opening polymerization (ROP) of 5-methyl-5-benzyloxycarbonyl-1,3-dioxan-2-one, MBC. *Conditions*: (i) benzyl bromide, TEA, THF, 70 °C, overnight; (ii) ethyl chloroformate, TEA, THF, 0 °C to RT, overnight; (iii) ROH, DBU, DCM, 29 °C in the glovebox.

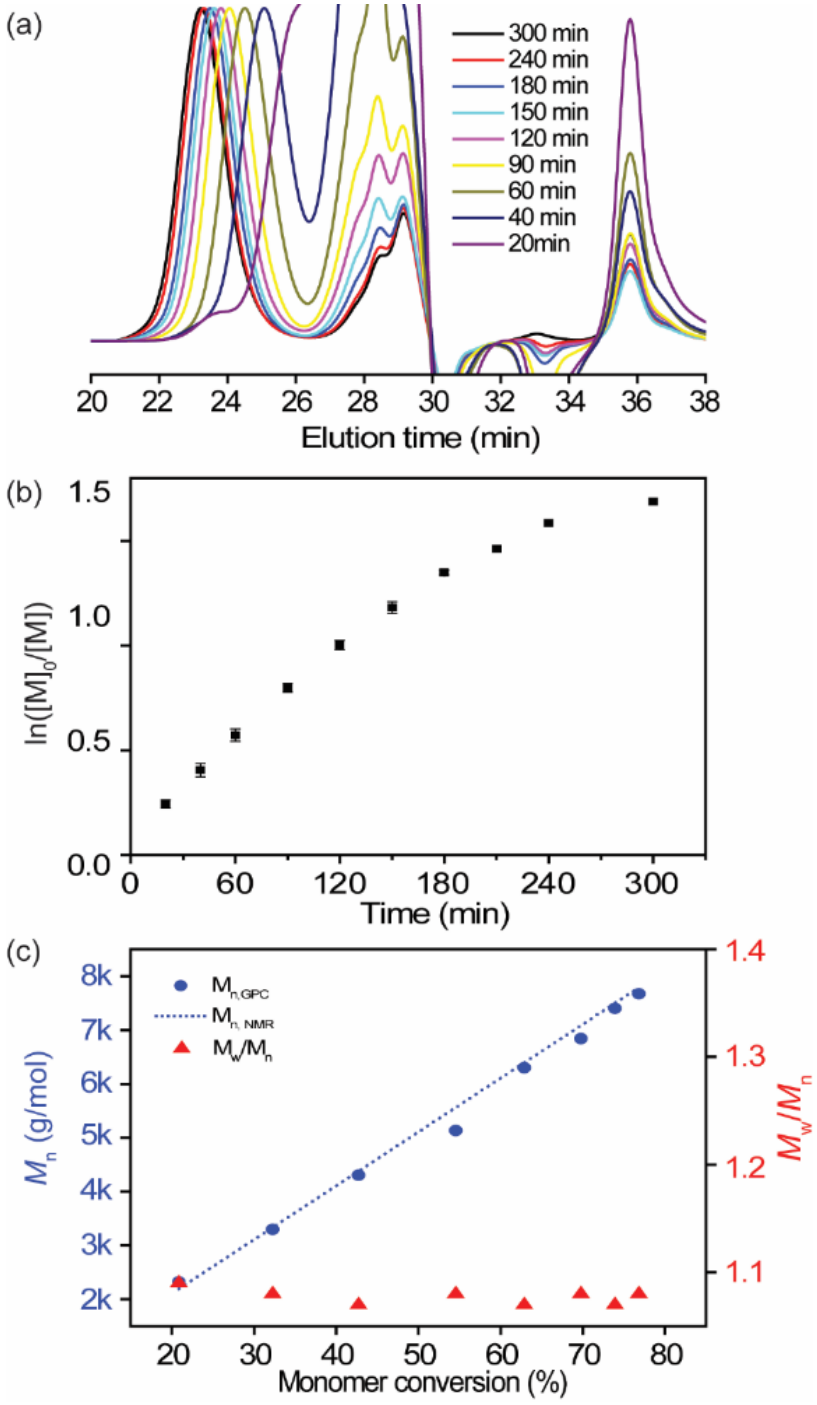

Figure 3.1. (a) GPC profiles (THF as an eluent, 1 mL/min) as a function of polymerization time, for the ROP of MBC; (b) Plot of $\ln([M]_0/[M])$ against time, obtained from ^{1}H NMR spectroscopy data; (c) Plot of number-average molecular weight (M_n) and polydipersity (M_w/M_n) against % monomer conversion in the ROP of MBC. *Conditions*: $[MBC]_0$ = 0.5 M in DCM at 29 °C in the glovebox, [MBC] : [BnOH] : [DBU] = 40 : 1 : 1.

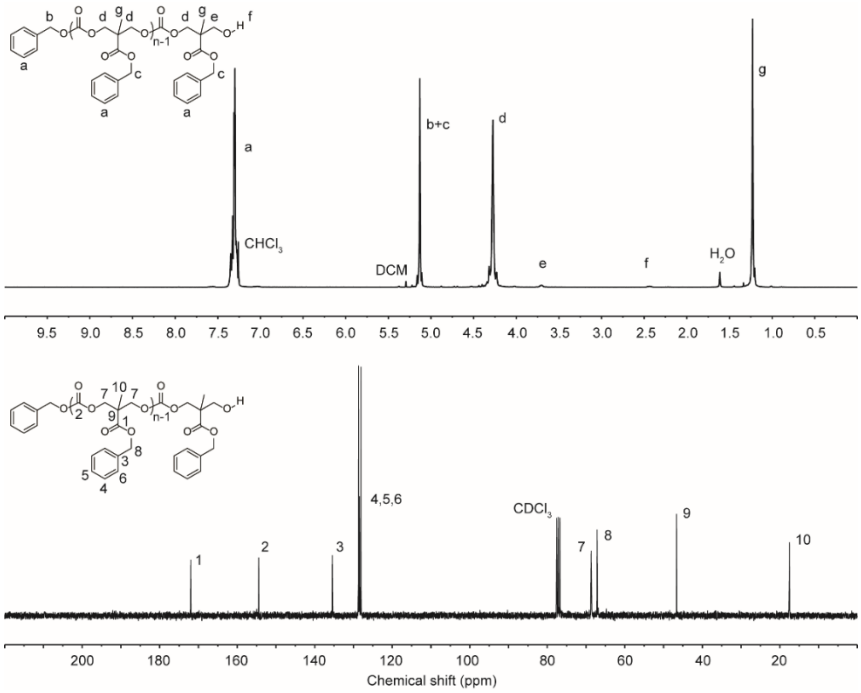

Figure 3.2. ^{1}H and ^{13}C NMR spectra ($CDCl_3$) of $PMBC_{27}$ (**1**) initiated from benzyl alcohol using DBU. *Conditions*: $[MAC]_0$ = 0.5 M in DCM at 29 °C in the glovebox, $[MBC]_0$: [BnOH] : [DBU] = 40 : 1 : 1.

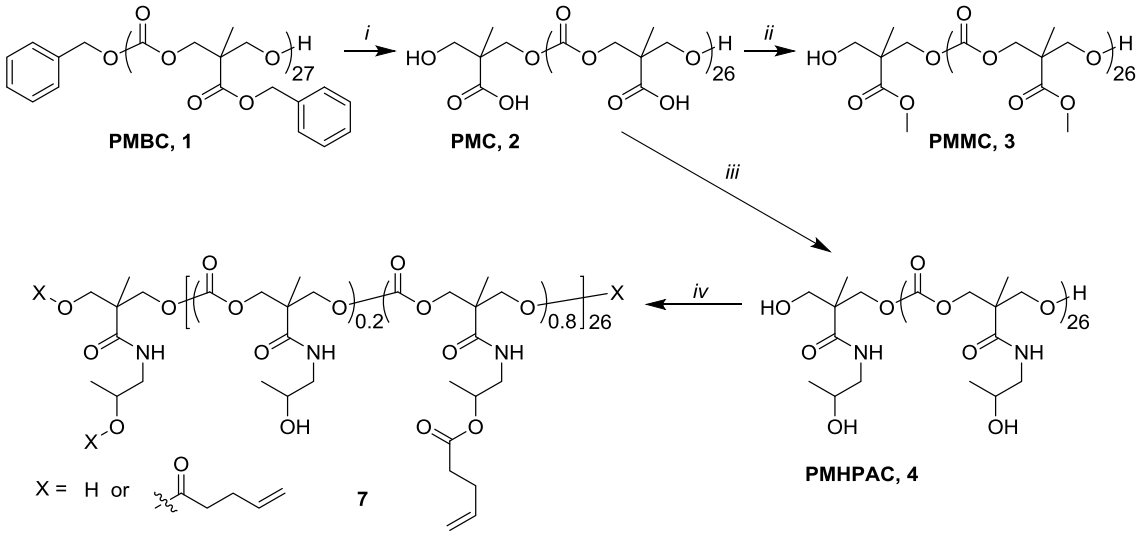

Scheme 3.2. Synthesis of hydrophilic polycarbonate, PMHPAC, and its functionalization. *Conditions*: (i) Pd/C, H_2, ethyl acetate, RT, overnight; (ii) $TMSCHN_2$; toluene:methanol (3:2), RT, 30 min; (iii) HOBt/HBTU, 1-amino-2-propanol, DIPEA, DMSO, RT, overnight; (iv) 4-pentenoic acid, DCC, DMAP, DMSO, RT, 24 h. $0 \leq a \leq 1$.

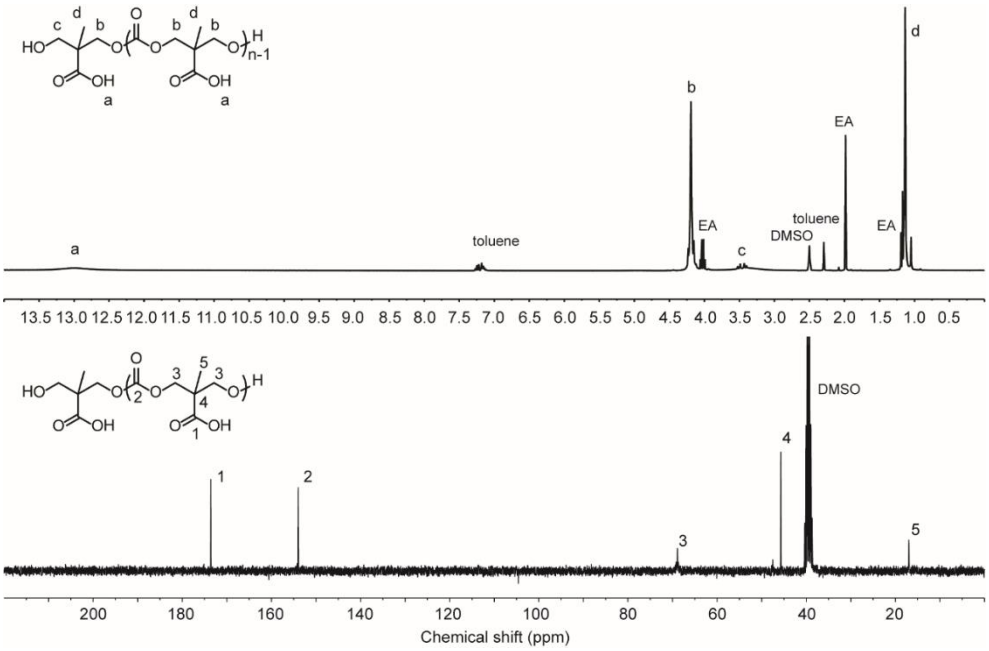

Figure 3.3. ^{1}H and ^{13}C NMR spectra (DMSO-d_6) of PMC_{27} (**2**). EA = ethyl acetate.

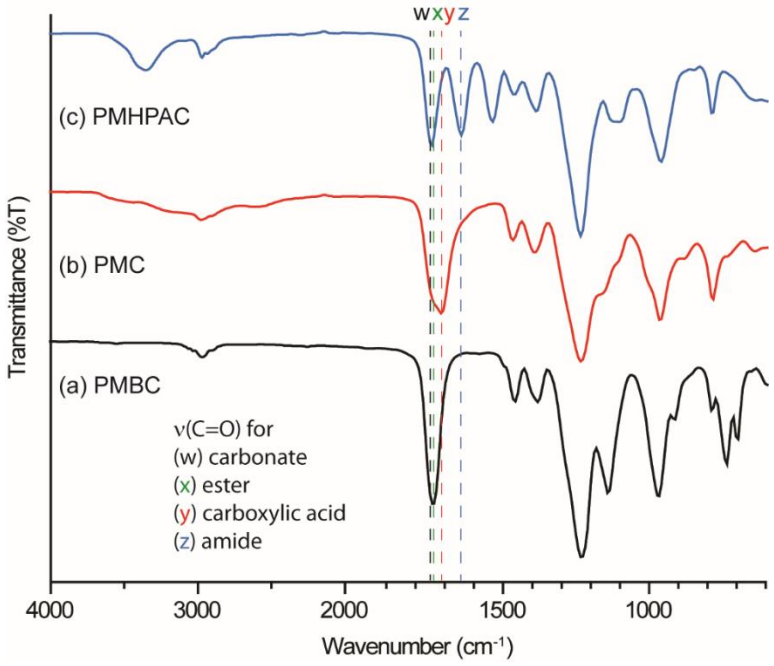

Figure 3.4. FTIR spectra of (a) $PMBC_{27}$ (**1**), (b) PMC_{27} (**2**), and (c) $PMHPAC_{27}$ (**4**).

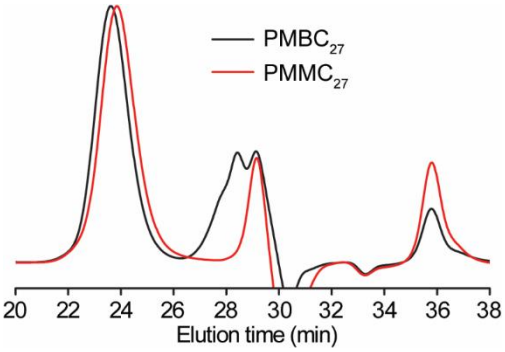

Figure 3.5. GPC profiles (THF as eluent, 1 mL/min) of before (PMBC, **1**) and after hydrogenolysis, followed by methylation (PMMC, **3**). The carboxylic acids of intermediate PMC (**2**) after hydrogenolysis of **1** were converted to methyl esters (PMMC, **3**) using $TMSCH_2N_2$ for GPC analysis.

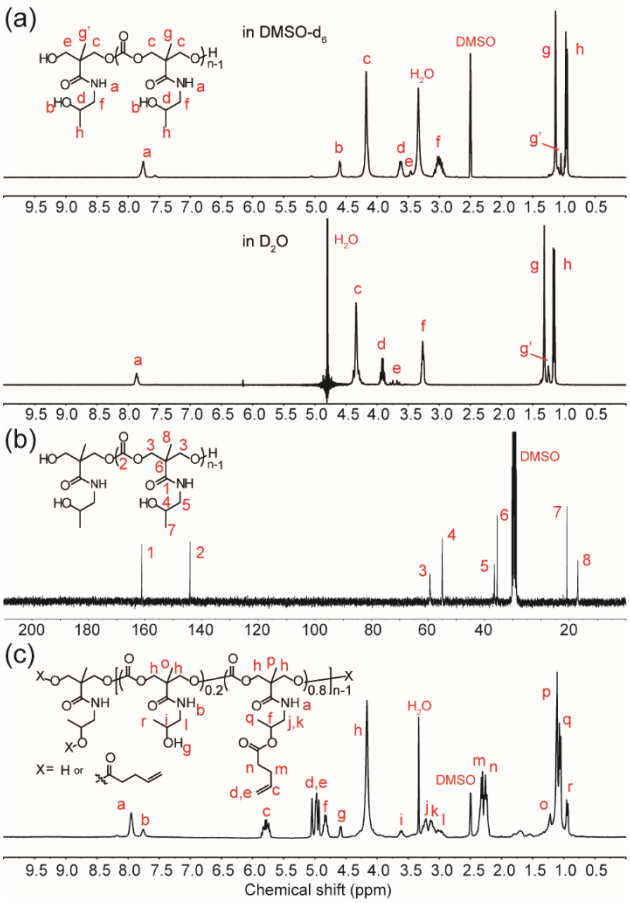

Figure 3.6. (a) ^{1}H NMR spectra of $PMHPAC_{27}$ (4) in DMSO-d_6 and D_2O. (b) ^{13}C spectrum of $PMHPAC_{27}$ (4) in DMSO-d_6. (c) ^{1}H NMR spectra of functionalized $PMHPAC_{27}$ with 4-pentenoic acid, 7, in DMSO-d_6.

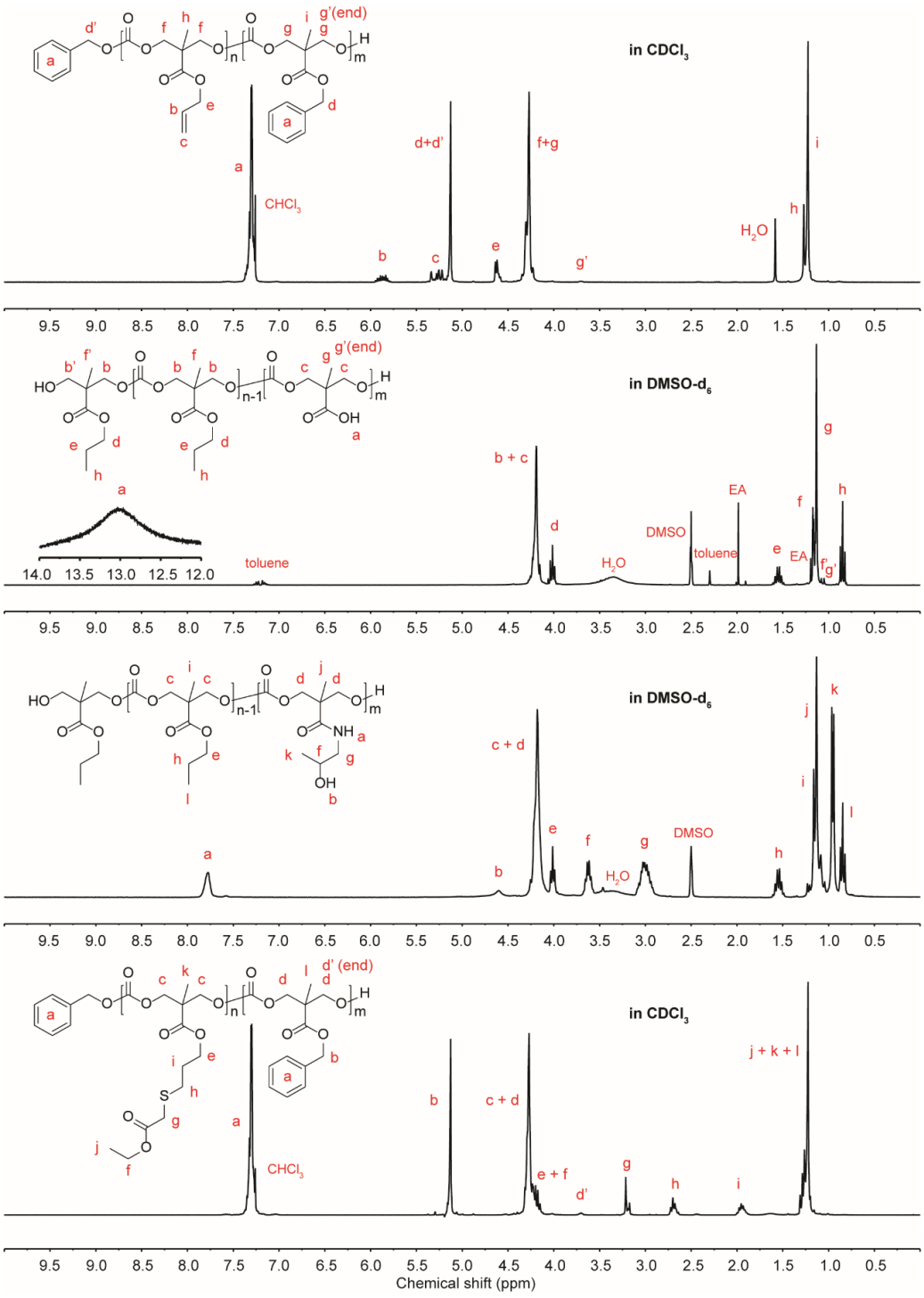

Figure 3.7. ^{1}H NMR spectra of $PMAC_{20}$-*b*-$PMBC_{70}$ (**8**), $PMPC_{20}$-*b*-$PMBC_{70}$ (**9**), $PMPC_{20}$-*b*-$PMHPAC_{70}$ (**10**) and **11**. EA = ethyl acetate.

Pendant 2-hydroxypropyl amide groups were introduced *via* amidation between the carboxylic acids of PMC and 1-amino-2-propanol using HBTU/HOBt, yielding poly(5-methyl-5-(2-hydroxypropyl)aminocarbonyl-1,3-dioxan-2-one (PMHPAC, 4) (Scheme 3.2). The proton resonances of the resulting amide (a) at 7.75 ppm, hydroxyl (b) at 4.60 ppm, methine (d) at 3.62 ppm, methylene (f) at 3.0 ppm, and methyl (h) at 0.96 ppm were observed by ^{1}H NMR spectroscopy, and the integral ratio of each signal indicated quantitative grafting density (Figure 3.6a). The amino group in 1-amino-2-propanol reacts selectively with the carboxylic acid on the PC backbone since the amino group is more nucleophilic than is the hydroxyl group,[110] as supported by ^{1}H NMR spectroscopy with no sign of esterification or cross-linking reactions. To further confirm the chemoselective coupling and intactness of the polycarbonate backbone during the amidation reaction, GPC analyses were performed. The GPC profile of PMHPAC shows slightly broadened molecular weight distribution, with a peak shift to longer retention time (Figure 3.8). Although a broadening of dispersity might be attributed to degradation, transesterification, or transamidation of the PC backbone, ^{13}C NMR spectroscopy observed only two carbonyl resonances—the carbonate signal maintained at 154.1 ppm and an amide carbonyl signal at 171.2 ppm (Figure 3.6b). In addition, PCs having different amide functionalities, as control polymers, were synthesized by coupling the carboxylic acids of PMC with two other amines, allylamine (5) and ethylamine (6) (Scheme 3.3). The GPC profiles of 5 and 6 showed almost no change of retention time compared to that of the precursor polymer, PMBC, with minimal increase of polydispersity (Figure 3.8). These results suggest that minimal transesterification or degradation of the polymer

backbone occurred during the amidation reactions, and the amide functionality itself did not contribute to the broadening of dispersity. Rather, the pendant hydroxyl groups of PMHPAC along the polycarbonate backbone were assumed to undergo interaction with the stationary phase of the GPC columns, and lead to changes in peak shape and position for PMHPAC, 4. The resulting PMHPAC is highly soluble in water (>300 mg/mL), highlighting that the structural similarity with PHPMA provides for similar water solubilities (Table 3.1).

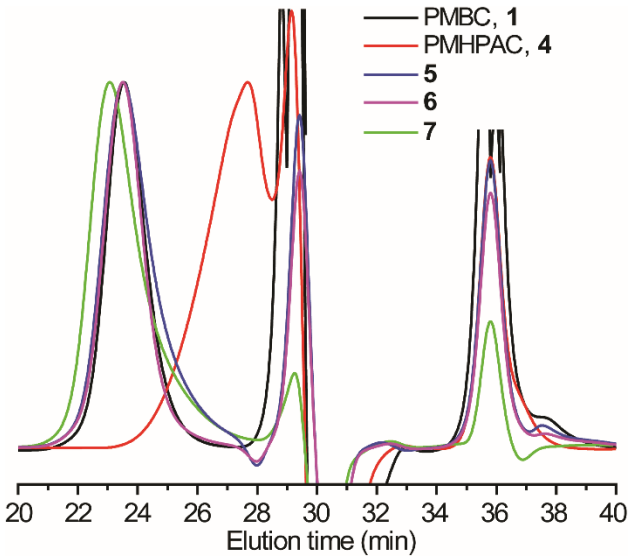

Figure 3.8. GPC profiles (DMF as an eluent, 1 mL/min) of PMBC and polycarbonates having amide functionalities.

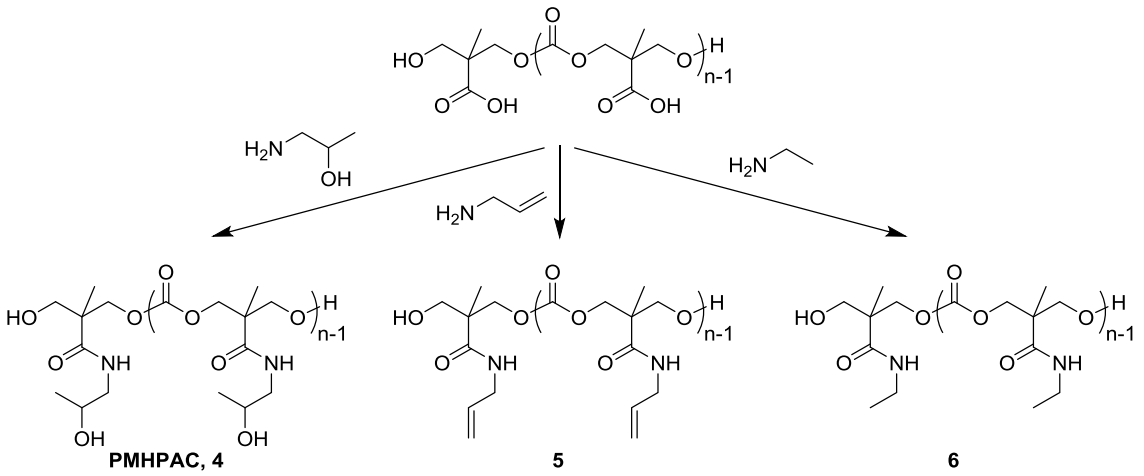

Scheme 3.3. Synthesis of polycarbonates having different amide functionalities by amidations between carboxylic acids of PMC and amines. *Conditions*: amines, HOBt/HBTU, DIPEA, DMSO, RT, overnight.

Table 3.1. Comparison of the physicochemical properties of PMHPAC, PEG, PHPMA, and their block copolymers.

		M_n (kDa)	T_g (°C)	T_d[b] (°C)	S[c] (g/mL)	Degradability
4	**PMHPAC$_{27}$**	5.8	59.5	182	>0.3	Full[d]
12	**PEG$_{135}$**	6.0	−12.5	320	>1	None
13	**PHPMA$_{40}$**	6.1	157.0	220	>0.3	None
10	**PMPC$_{20}$-*b*-PMHPAC$_{70}$**	4.0−15.2[a]	−13.2, 65.6	180	n/a	Full
14	**PEG$_{226}$-*b*-PMAC$_{19}$**	10.0−4.0[a]	−18.5	200	n/a	Partial
15	**PMMA$_{28}$-*b*-PHPMA$_{90}$**	3.2−12.9[a]	105.5, 162.0	250	n/a	None

[a]Molecular weight of block copolymers, A-*b*-B, are expressed as [M_n of A block]− [M_n of B block]. [b]Initial decomposition temperature. [c]Solubility in water. [d]See Supporting Information for details.

3.2.2. Functionalization of PMHPAC

In contrast to PEG, which is only functionalizable at the chain end, and similar to PHPMA, PMHPAC can be readily functionalized along the polymer backbone *via* pendant secondary hydroxyl groups. The availability of pendant hydroxyl groups for further functionalization was demonstrated by esterification with a model compound, 4-pentenoic acid using *N,N'*-dicyclohexylcarbodiimide (DCC) as a coupling agent and 4-dimethylaminopyridine (DMAP) as a catalyst (Scheme 3.2). The formation of ester bonds was confirmed by a shift of the methine peak from 3.62 ppm in PMHPAC (d) to 4.82 ppm in 7 (f), as well as the appearance of peaks at 5.87−4.92 and 2.40−2.20 from the 4-pentenoate group (Figure 3.6c). Consumption of the hydroxyl groups of PMHPAC was further confirmed by GPC, which demonstrated that the pentenoic acid-functionalized PMHPAC (7, Figure 3.8) had a narrow molecular weight distribution and retention time that was similar to those of 1, 3, 5, and 6, each of which lacked the hydroxyl groups of PMHPAC (4). This result supported our assumption that the pendant hydroxyl functionalities of 4 are ascribed to the lengthened retention time and broadened distribution of the GPC profile.

3.2.3. Synthesis of PMHPAC-based amphiphilic block copolymer

An amphiphilic block copolymer containing PMHPAC as a hydrophilic segment was synthesized to demonstrate synthetic versatility and formation of nanostructures in aqueous solution. Diblock copolymer, PMAC-*b*-PMBC (8), was synthesized by one-pot sequential ROPs of MAC (5-methyl-5-allyloxycarbonyl-1,3-dioxan-2-one) and MBC. Subsequent hydrogenolysis and amidation afforded the amphiphilic diblock copolymer, 10 (Scheme 3.4). The conditions for catalytic hydrogenolysis of PMAC-*b*-PMBC not only removed the benzyl ester groups but also resulted in hydrogenation of the allyl functionalities to propyl groups yielding poly(5-methyl-5-propyloxycarboxyl-1,3-dioxan-2-one) (PMPC)-*b*-PMC, 9, as expected, which was verified by ^{1}H NMR spectroscopy (Figure 3.7). In order to utilize the allyl functionalities of 8, various thiol compounds can be conjugated *via* thiol−ene "click" reaction before the hydrogenolysis procedure. A model compound, 2-mercaptoacetate was successfully incorporated onto the PMAC block through thioether linkages (11), and was selected for its ability to allow for further introduction of new functionalities onto the polymer block segment or into the core of micelles or other supramolecular assemblies. Other cyclic monomers for ROP such as cyclic carbonates, lactide, and ε-caprolactone, *etc*., could also be polymerized with MBC to increase the diversity of PMHPAC-based macromolecular structures.

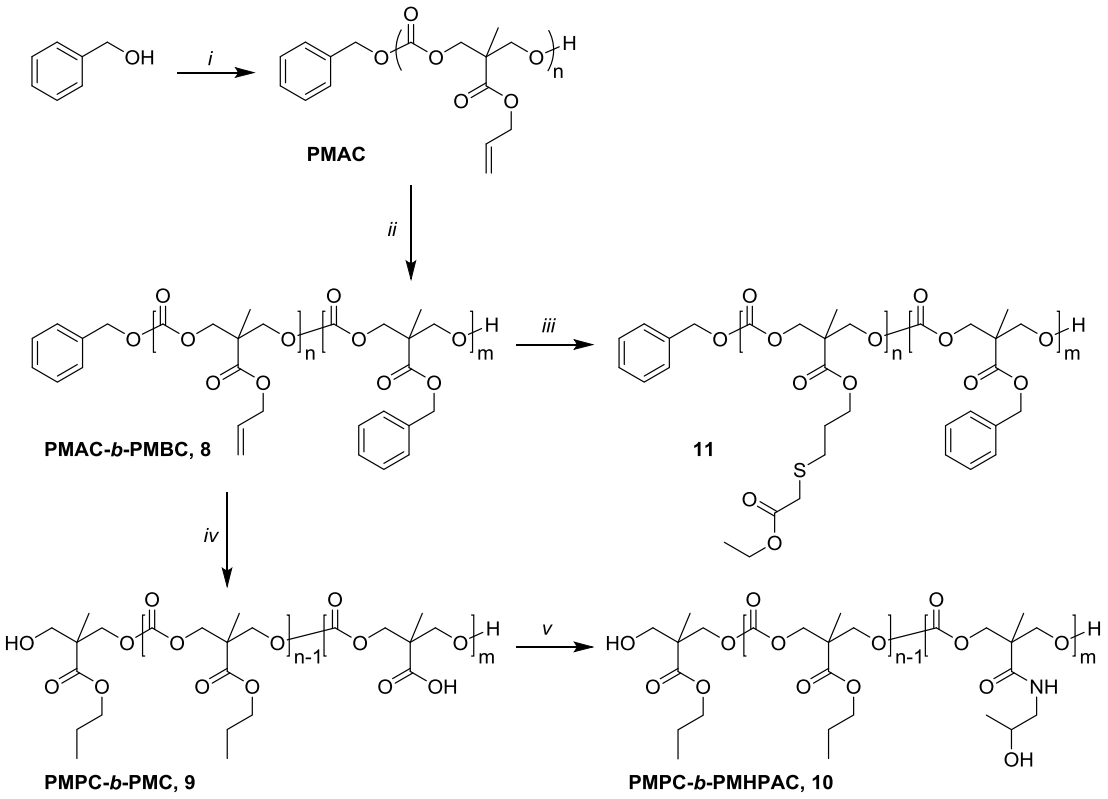

Scheme 3.4. Synthesis of amphiphilic block copolymer, PMPC-*b*-PMHPAC (**10**). *Conditions*: (i) MAC, DBU, DCM; (ii) MBC, DCM, 29 °C in the glovebox; (iii) DMPA, ethyl 2-mercaptoacetate, DMF, UV 365 nm, 2 h; (iv) Pd/C, H_2, ethyl acetate, RT, overnight; (v) 1-amino-2-propanol, HOBt/HBTU, DIPEA, DMSO, RT, overnight.

3.2.4. Polymer toxicity

The cytotoxicities of PMHPAC, PHPMA, and PEG homopolymers, as well as, micelles assembled from the corresponding block copolymers, were tested against RAW 264.7 mouse macrophages and OVCAR-3 cells as a function of concentration (Figures 3.9 and 3.10). Minimal cytotoxicity was observed for all polymers over the concentrations tested (5 to 3000 μg/mL after 24 h incubation), except for PHPMA (13) above 1 mg/mL. PHPMA showed higher toxicity, as compared to the polycarbonate-based analogue,

PMHPAC (4), and PEG. In addition, immunotoxicity studies performed for PMHPAC (4), PEG and PHPMA homopolymers demonstrated minimal immunotoxicity, with only a slight induction of the expression of G-CSF and TNF-α of the 23 measured cytokines, as compared to the control untreated cells. Low cyto-/immuno-toxicities are partial indicators for the biocompatibility of these highly hydrophilic polymers for potential biomedical applications Our group has recently established numerical descriptive values (*i.e.*, immunotoxicity indices) to compare the induction of cytokines by various types of nanoparticles, which provides a useful strategy for direct comparisons between immunotoxicities of nanoparticles.[111] The immunotoxicity indices calculated for the polymers tested in the current study were found to be low (< 4 for each), which highlights the high biocompatibility of the tested polymers.

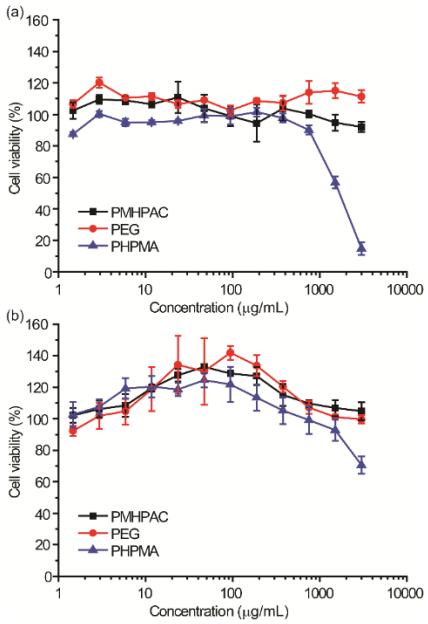

Figure 3.9. Cytotoxicity of PMHPAC (**4**), PEG (**12**), and PHPMA (**13**) in (a) RAW 264.7 mouse macrophages and (b) OVCAR-3 cells.

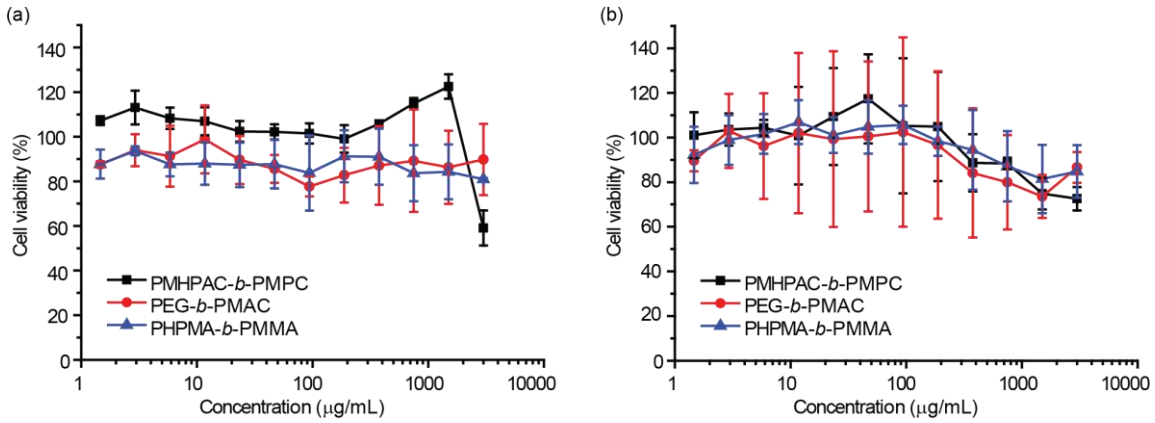

Figure 3.10. Cytotoxicity of PMHPAC-*b*-PMPC (10), PEG-*b*-PMAC (14), and PHPMA-*b*-PMMA (15) incubated with (a) RAW 264.7 mouse macrophages and (b) OVCAR-3 cells.

3.2.5. Comparison of physicochemical properties of PMHPAC, PHPMA, and PEG

The properties of PMHPAC and its block copolymer were compared with those of PHPMA, PEG, and their corresponding block polymers (Table 3.1). Homopolymers having similar molecular weights (M_n = ~6000 Da) were synthesized or purchased for direct comparison. Similar to PEG and PHPMA, which are known for their high water solubility, PMHPAC was highly water-soluble at the tested concentration (~300 mg/mL) and more concentrated solution could possibly be prepared; limited in this study by the

amount of material available. Glass transition temperature (T_g) values of the homopolymers varied, as measured by differential scanning calorimetry (DSC). The higher T_g values for PMHPAC (59.5 °C) and PHPMA (157 °C) compared to PEG (−12.5 °C) can be ascribed to inter- and intramolecular hydrogen bonding. The thermal stabilities of the homopolymers were also compared, using thermogravimetric analysis (TGA). As expected, the degradable polycarbonate-based PMHPAC showed lower initial decomposition temperature (T_d) compared to nondegradable PHPMA and PEG.

In addition, although PMHPAC was observed to be stable under neutral aqueous conditions, its, theoretical, ability to undergo hydrolytic degradation was verified under challenging, highly basic conditions to facilitate accelerated, base-promoted hydrolysis. After incubation of PMHPAC in 0.1 M NaOD/D_2O at 60 °C, degradation was monitored by ^{1}H NMR spectroscopy. PMHPAC was degraded into the MHPAC repeating unit and further broken down into bis-MPA as time progressed (Figure 3.11 and 3.12). The degradation products were also confirmed by ESI-MS (Figure 3.13).

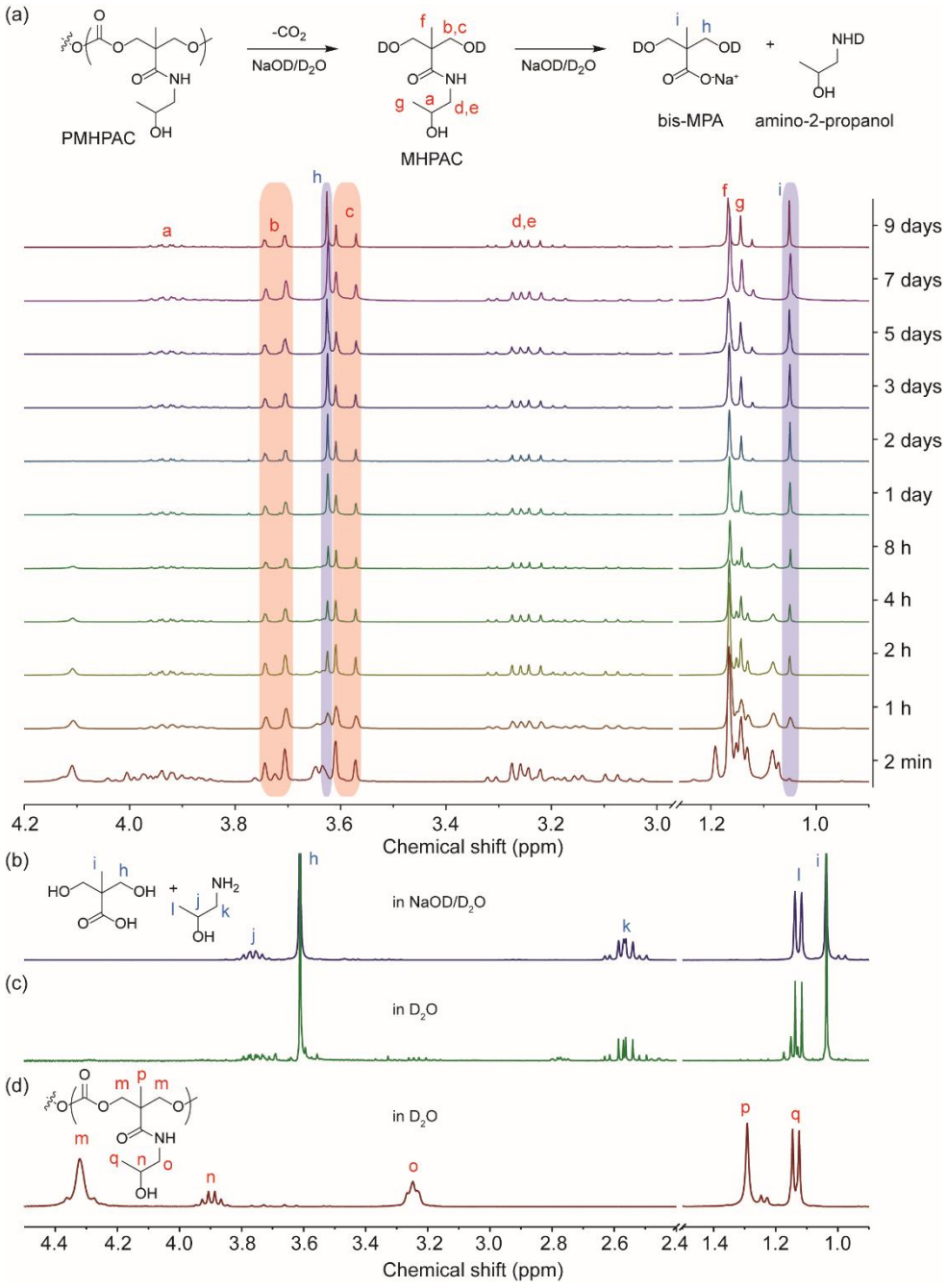

Figure 3.11. ^{1}H NMR spectra of (a) $PMHPAC_{27}$ in 0.1 M $NaOD/D_2O$ at 60 °C at various time points, (b) a mixture of bis-MPA and amino-2-propanol co-dissolved in 0.1 M $NaOD/D_2O$, (c) the lyophilized products of $PMHPAC_{27}$ after incubation in 1.0 M $NaOH_{(aq)}$ overnight at 100 °C and dissolved in D_2O, and (d) $PMHPAC_{27}$ in D_2O.

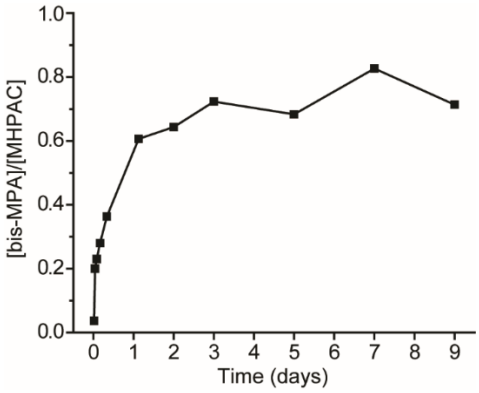

Figure 3.12. Relative molar ratios of bis-MPA *vs* MHPAC by the time interval in the solution of PMHPAC in 0.1 M NaOD/D_2O at 60 °C, calculated by [(the integration of i)/3]/[(the integration of b and c)/4] in Figure 3.11a.

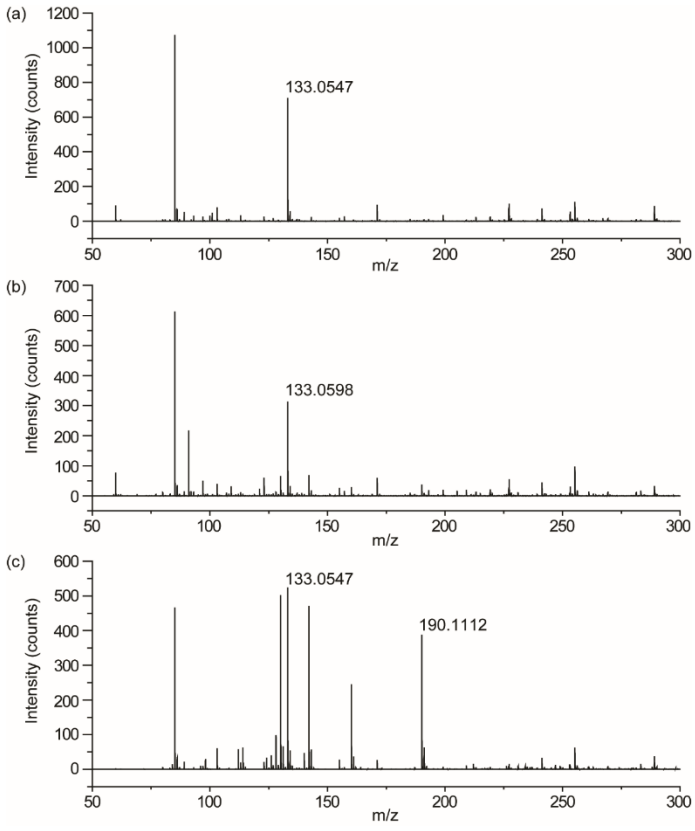

Figure 3.13. ESI MS spectra of (a) a mixture of bis-MPA and amino-2-propanol in 0.1 M NaOD/D_2O, (b) the lyophilized products of $PMHPAC_{27}$ after incubation in 1.0 M $NaOH_{(aq)}$ overnight at 100 °C and dissolved in D_2O, and (c) $PMHPAC_{27}$ in 0.1 M NaOD/D_2O at 60 °C for 9 days in negative mode; *m/z* range of 50–300.

3.2.6. Self assembly of PMHPAC-based amphiphilic block copolymer 10

A potentially fully degradable polymeric nanostructure was prepared from the amphiphilic diblock copolymer containing PMHPAC as a hydrophilic segment. $PMPC_{20}$-*b*-$PMHPAC_{70}$ (10) was self-assembled into spherical micelles by direct dissolution in water (1 mg/mL). The formation and morphology of polymeric nanostructures were confirmed by dynamic light scattering (DLS), transmission electron microscopy (TEM), and atomic force microscopy (AFM) (Figure 3). The number-averaged hydrodynamic diameter of the micelles in water was 16 ± 4 nm. The diameter in the substrate-adsorbed dried state increased to 24 ± 6 nm and 32 ± 6 nm as measured by TEM and AFM, respectively, which might be due to the flattening effect of the viscous polymeric core having a T_g of −13.2 °C and the hygroscopic property of the PMHPAC shell. Unlike the previous report,[104] this PMHPAC-based amphiphilic block copolymer formed smaller micelles, which are suitable for biomedical applications. The ζ−potential, based on surface charge density of the resulting micelles, was −14.4 ± 4.7 mV in nanopure water. It is common that polymeric nanoparticles having neutral polymer-based corona or shells have slightly negative surface charge density values.[112,113]

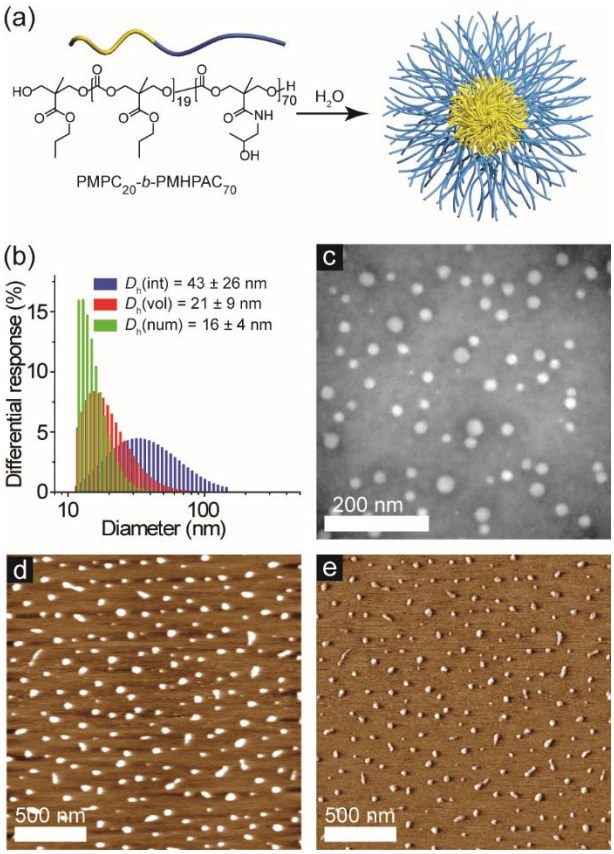

Figure 3.14. Self-assembly of block copolymer, $PMPC_{20}$-*b*-$PMHPAC_{70}$ (10), into spherical micelles. (a) Schematic diagram of micellization. (b) DLS histograms of intensity-averaged (D_h(int)), volume-averaged (D_h(vol)), number-averaged (D_h(num)) hydrodynamic diameters. (c) Bright field TEM image, scale bar = 200 nm, collected for the block copolymer micelle sample drop deposited from water onto a carbon-coated copper grid, diameter = 24 ± 6 nm. (d, e) AFM height (d) and phase (e) images, scale bar = 500 nm, collected for the block copolymer micelle sample spin coated from water onto freshly cleaved mica, diameter = 32 ± 6 nm, height = *ca*. 1.3 nm.

3.3. Experimental Section

3.3.1. Materials

Benzyl alcohol and 1,8-diazabicyclo[5.4.0]undec-7-ene (DBU) were dried over CaH_2, distilled, and stored under inert atmosphere. Methyl methacrylate (MMA) was passed through alumina plug to remove inhibitor before use. A radical initiator, 2,2'-

azobis(2-methylpropionitrile) (AIBN) was recrystallized in methanol and stored in the freezer until use. *a*-Methoxy-*ω*-hydroxy poly(ethylene glycol)s (mPEG, 6 and 10 kDa) were purchased from Rapp Polymere GmbH and dried over P_2O_5 prior to use. Tetrahydrofuran (THF), *N,N*-dimethylformamide (DMF), and dichloromethane (DCM) were purified by passage through solvent purification system (JC Meyer Solvent Systems) and used as dried solvents. The monomers, 5-methyl-5-benzyloxycarbonyl-1,3-dioxan-2-one (MBC)[99] and 5-methyl-5-allyloxycarbonyl-1,3-dioxan-2-one (MAC)[114] were synthesized as reported, recrystallized, and dried over P_2O_5 before use. *N*-(2-Hydroxypropyl)methacrylamide (HPMA) was synthesized as reported.[115] All other solvents and chemicals were purchased from Sigma-Aldrich, TCI America, or Fisher Scientific and were used as received.

3.3.2. Instruments

^{1}H and ^{13}C NMR spectra were recorded on Varian Inova 300 spectrometers. Chemical shifts were referenced to the solvent resonance signals. IR spectra were recorded on an IR Prestige 21 system (Shimadzu Corp., Japan), equipped with an ATR accessory, and analyzed using IRsolution v.1.40 software. Gel permeation chromatography (GPC) eluted with THF or DMF was conducted on a system equipped with an isocratic pump model 1515, a differential refractometer model 2414, and a three-column set of Polymer Laboratories, Inc. (Amherst, MA) Styragel columns (PLgel 5 μm S3Mixed C, 500 Å, and 104 Å, 300 × 7.5 mm columns) and a guard column (PLgel 5 μm, 50 × 7.5 mm)) using THF as the eluent (1.00 mL/min) at 40 °C or a four-column set of 5 μm Guard (50 × 7.5 mm), Styragel HR 4, 5 μm DMF (300 × 7.5 mm), Styragel HR 4E, 5

μm DMF (300 × 7.5 mm), and Styragel HR 2, 5 μm DMF (300 × 7.5 mm) using DMF (0.05 M LiBr) as the eluent (1.00 mL/min) at 70 °C. The differential refractometers were calibrated with Polymer Laboratories, Inc., polystyrene standards (300−467000 Da) for the THF system and poly(ethylene oxide) standards (106−174000 Da) for the DMF system. Polymer solutions were prepared at a concentration of *ca*. 5 mg/mL with toluene (0.05% v/v) as a flow rate marker and an injection volume of 200 μL was used. Data were analyzed using Empower Pro software from Waters Chromatography, Inc. Glass transition temperatures (T_g) were measured by differential scanning calorimetry (DSC) on a Mettler-Toledo DSC822 (Mettler-Toledo, Inc., Columbus, OH) under N_2. Measurements of T_g were taken with a heating rate of 10 °C/min. The measurements were analyzed using Mettler-Toledo STAR^e v.10.00 software. The T_g was taken as the midpoint of the inflection tangent and T_m was taken as the onset point, upon the third scan. Thermogravimetric analysis (TGA) was performed under Ar atmosphere using a Mettler-Toledo model TGA/DSC 1, with a heating rate of 10 °C/min. Dynamic light scattering (DLS) measurements were conducted using DelsaNano C (Beckman Coulter, Inc., Fullerton, CA) equipped with a laser diode operating at 658 nm. Size measurements were made in nanopure water (n = 1.3329, η = 0.890 cP at 25 ± 1 °C). Scattered light was detected at 165° angle and analyzed using a log correlator over 70 accumulations for a 3.0 mL sample in a glass sizing cell (4.0 mL capacity). The samples in a glass sizing cell were equilibrated for 30 min before measurements were made. The photomultiplier aperture and the attenuator were automatically adjusted to obtain a photon counting rate of *ca*. 10

kcps. The calculations of the particle size distributions and distribution averages were performed using CONTIN particle size distribution analysis routines. The ζ−potential of the particles in suspension was obtained by measuring the electrophoretic movement of charged particles under an applied electric field. Scattered light was detected at a 30° angle at 25 °C. The ζ−potential was measured at five regions in the flow cell and a weighted mean was calculated. These five measurements were used to correct for electroosmotic flow that was induced in the cell due to the surface charge of the cell wall. Transmission electron microscopy (TEM) images were collected on a JEOL 1200EX operating at 100 kV and micrographs were recorded at calibrated magnifications using a SIA-15C CCD camera. The samples as aqueous solutions (4 μL) were deposited onto Formvar/carbon-coated copper grids. Excess sample was wicked off using filter paper and the grids were allowed to air-dry for 2 min. Following that, the grids were stained with 4 μL of a 1% phosphotungstic acid aqueous solution. Excess stain was wicked off using filter paper after 1 min. The sample grids were air-dried overnight before analyses. The atomic force microscopy (AFM) imaging was performed on MFP-3D system (Asylum Research) in tapping mode using standard silicon tips (VISTAprobes, CSR-25, resonance constant = 30 kHz, tip radius < 10 nm, spring constant = 0.1 N/m). For AFM sample preparation, nanoparticles were dissolved in nanopure water at 0.025 mg/mL, and 10 μL of the sample was spin-coated onto a mica surface.

3.3.3. Organocatalytic ROP of 5-methyl-5-benzyloxycarbonyl-1,3-dioxan-2-one (MBC)

In a glovebox, MBC and benzyl alcohol initiator were dissolved in dry DCM ([MBC] = 0.5 M). DBU (1 equiv to initiator) was added to the monomer/initiator solution. After the desired time, the polymerization was quenched by addition of benzoic acid in DCM and precipitated into methanol. For example, MBC (2.0 g, 8.0 mmol), benzyl alcohol (21 μL, 0.20 mmol), DBU (30 μL, 0.20 mmol), DCM (16 mL), and benzoic acid solution (37 mg, 0.30 mmol in 300 μL DCM) were used to yield $PMBC_{27}$.

BnO-PMBC$_{27}$-OH (**1**). Yield = 1.26 g, 90% based upon monomer conversion (69%). $M_{n,NMR}$ = 6900 g/mol; $M_{n,GPC}^{THF}$ = 7100 g/mol; $M_{n,GPC}^{DMF}$ = 4000 g/mol; PDI^{THF} = 1.09 and PDI^{DMF} = 1.10. ^{1}H NMR (300 MHz, $CDCl_3$): δ 7.38−7.24 (br, −$OCH_2C_6\boldsymbol{H}_5$), 5.13 (s, −$OC\boldsymbol{H}_2C_6H_5$), 4.39−4.18 (br, −OC(O)$OC\boldsymbol{H}_2$-), 3.70 (m, −$C\boldsymbol{H}_2OH$), 2.45 (br, −$CH_2O\boldsymbol{H}$), 1.22 (s, −$C(C\boldsymbol{H}_3)(CH_2O-)_2$), 1.20 (s, −$C(C\boldsymbol{H}_3)CH_2OH$). ^{13}C NMR (75 MHz, $CDCl_3$): δ 172.0, 154.4, 135.5, 128.7, 128.4, 128.1, 68.7, 67.2, 46.6, 17.5. IR (neat, cm^{-1}): 3125−2825, 1743, 1458, 1381, 1234, 1142, 964, 910, 787, 733, 694. T_g = 17.2 °C. TGA in Ar: 240−390 °C, 96% mass loss; 4% mass remaining above 500 °C.

3.3.5. Preparation of diblock copolymer, PMAC-b-PMBC

The monomer for the first block (MAC) and benzyl alcohol initiator were dissolved in dry DCM ([MAC] = 0.5 M). DBU (1 equiv to initiator) was added to the monomer/initiator solution. After the desired time (~80% conversion), the monomer for the second block (MBC) in DCM was quickly added to the macroinitiator solution. After the desired time, the polymerization was quenched by addition of benzoic acid in DCM

and precipitated into cold methanol. For example, MAC (100 mg, 0.50 mmol) and benzyl alcohol (2.0 μL, 0.020 mmol) in DCM (1 mL, [MAC] = 0.5 M), DBU (3.0 μL, 0.020 mmol), MBC solution in DCM (500 mg, 2.0 mmol in 3 mL) were used to yield $PMAC_{20}$-*b*-$PMBC_{70}$.

$PMAC_{20}$-b-$PMBC_{70}$ (**8**). Yield = 408 mg, 94%. $M_{n,NMR}$ = 21600 g/mol; $M_{n,GPC}^{DMF}$ = 12200 g/mol; PDI = 1.09. ^{1}H NMR (300 MHz, $CDCl_3$): δ 7.39−7.23 (br, −$OCH_2C_6\boldsymbol{H}_5$), 5.96−5.77 (m, −$CH_2C\boldsymbol{H}CH_2$), 5.36−5.20 (m, −$CH_2CHC\boldsymbol{H}_2$), 5.13 (s, −$OC\boldsymbol{H}_2C_6H_5$), 4.65−4.57 (m, −$OC\boldsymbol{H}_2CHCH_2$), 4.39−4.18 (br, −$OC(O)OC\boldsymbol{H}_2$-), 3.70 (m, −$C\boldsymbol{H}_2OH$), 1.27 (s, −$C(C\boldsymbol{H}_3)(CH_2O-)_2$ from PMAC block), 1.22 (s, −$C(C\boldsymbol{H}_3)(CH_2O-)_2$ from PMBC block). ^{13}C NMR (75 MHz, $CDCl_3$): δ 172.0, 154.5, 135.5, 131.7, 128.8, 128.5, 128.1, 118.6, 68.7, 67.2, 66.0, 46.7, 17.6, 17.5. IR (neat, cm^{-1}): 3100−2800, 1744, 1458, 1381, 1227, 1142, 964, 910, 787, 733, 694. T_g = 11.5 °C; T_m = 129.5 °C. TGA in Ar: 215−310 °C, 71% mass loss; 310−410 °C, 27% mass loss; 2% mass remaining above 500 °C.

3.3.6. Representative procedure for catalytic hydrogenolysis

To the flask containing Pd/C (10 wt%), solution of polymers containing PMBC block in ethyl acetate was added. After the flask was flushed and filled with H_2 using balloons of H_2, the reaction mixture was stirred overnight. Pd/C was centrifuged and filtered out and solvent was removed *in vacuo* to yield crude product, which was used in the next reaction without further purification. For example, PMBC (770 mg), ethyl acetate (30 mL), and Pd/C (~10 wt%, 80 mg) were used to yield PMC_{27}.

PMC$_{27}$ (**2**). Yield = 522 mg, ~99%. $M_{n,\,NMR}$ = 4300 g/mol. ^{1}H NMR (300 MHz, DMSO-d_6): δ 13.04 (br, −C(O)O***H***), 4.14 (br, −OC(O)OC***H***$_2$−), 3.51 (d, J = 10.6 Hz, -C***H***H'OH), 3.41 (d, J = 10.6 Hz, −CH***H'***OH), 1.13 (s, −C(C***H***$_3$)(CH$_2$O−)$_2$), 1.05 (s, −C(C***H***$_3$)CH$_2$OH). ^{13}C NMR (75 MHz, DMSO-d_6): δ 173.6, 154.0, 68.9, 45.7, 17.0. IR (neat, cm^{-1}): 3675−2400, 1713, 1466, 1396, 1234, 1150, 964, 880, 779, 633. T_g = 72.5 °C. TGA in Ar: 180−265 °C, 31% mass loss; 265−401 °C, 65% mass loss; 4% mass remaining above 500 °C.

PMPC$_{20}$-b-PMC$_{70}$ (**9**). Yield = 270 mg, ~99%. $M_{n,\,NMR}$ = 15200 g/mol. ^{1}H NMR (300 MHz, DMSO-d_6): δ 13.06 (br, −C(O)O***H***), 4.28−4.13 (br, −OC(O)OC***H***$_2$−), 4.01 (t, J = 7.1 Hz, −OC***H***$_2$CH$_2$CH$_3$), 3.53-3.39 (m, −C***H***$_2$OH), 1.55 (m, −OCH$_2$C***H***$_2$CH$_3$), 1.16 (s, −C(C***H***$_3$)(CH$_2$O−)$_2$ from PMPC block), 1.13 (s, −C(C***H***$_3$)(CH$_2$O−)$_2$ from PMC block), 1.08 (s, −C(C***H***$_3$)CH$_2$OH, PMPC end), 1.05 (s, −C(C***H***$_3$)CH$_2$OH, PMC end), 0.85 (t, J = 7.4 Hz, −OCH$_2$CH$_2$C***H***$_3$). ^{13}C NMR (75 MHz, DMSO-d_6): δ 173.5, 154.0, 153.8, 68.9, 66.3, 46.1, 45.7, 21.4, 16.9, 16.8, 10.0. IR (neat, cm^{-1}): 3750−2400, 1713, 1466, 1389, 1227, 1165, 964, 719, 640. T_g = −7.0 and 69.0 °C. TGA in Ar: 200−275 °C, 30% mass loss; 275−400 °C, 67% mass loss; 3% mass remaining above 500 °C.

3.3.7. Representative procedure for amidation between polymers containing PMC and amine compounds

To a stirred solution of PMC (or PMC containing block copolymers) in DMSO, 1-hydroxybenzotriazole (HOBt, 1.1 equiv to carboxylic acids) and *O*-(benzotriazol-1-yl)-

N,N,N',N'-tetramethyluronium hexafluorophosphate (HBTU, 1.1 equiv to carboxylic acids) in DMSO were added and stirred for 30 min at room temperature. Then, amine (1.5 equiv to carboxylic acids) and *N,N*-diisopropylethylamine (DIPEA, 1.5 equiv to carboxylic acids) in DMSO were added and stirred overnight at room temperature. The resulting solution was dialyzed against nanopure water for 3 days and lyophilized. For example, PMC (100 mg, 0.63 mmol for repeat units) in DMSO (2 mL), HOBt (105 mg, 0.78 mmol) and HBTU (296 mg, 0.78 mmol) in DMSO (1 mL), and amino 2-propanol (72 μL, 0.94 mmol) and DIPEA (162 μL, 0.94 mmol) in DMSO (1 mL) were used to yield $PMHPAC_{27}$.

$PMHPAC_{27}$ [Poly(5-methyl-5-(2-hydroxypropyl)aminocarbonyl-1,3-dioxan-2-one)] (**4**). Yield = 105 mg, 77%. $M_{n,NMR}$ = 5800 g/mol; $M_{n,GPC}^{DMF}$ = 740 g/mol; PDI = 1.20. ^{1}H NMR (300 MHz, DMSO-d_6): δ 7.85−7.70 (br, −C(O)N***H***-), 7.61−7.52 (br, −C(O)N***H***−, end group), 4.66 − 4.56 (m, − $NHCH_2CH(O\boldsymbol{H})CH_3$), 4.28 − 4.06 (br, − $OC(O)OC\boldsymbol{H}_2$−), 3.69−3.55 (m, $-NHCH_2C\boldsymbol{H}(OH)CH_3$), 3.49−3.44 (br, $-C\boldsymbol{H}_2OH$), 3.10−2.90 (m, $-NHC\boldsymbol{H}_2CH(OH)CH_3$), 1.13 (s, $-C(C\boldsymbol{H}_3)(CH_2O-)_2$), 1.04 (s, $-C(C\boldsymbol{H}_3)CH_2OH$), 0.95 (d, J = 6.2 Hz, $-NHCH_2CH(OH)C\boldsymbol{H}_3$). ^{1}H NMR (300 MHz, D_2O): δ 7.92−7.80 (br, −C(O)N***H***−), 4.42−4.20 (br, $-OC(O)OC\boldsymbol{H}_2-$), 3.97−3.84 (m, $-NHCH_2C\boldsymbol{H}(OH)CH_3$), 3.76 (d, J = 11.7 Hz, −C***H***H'OH), 3.66 (d, J = 11.3 Hz, -CH***H'***OH), 3.34 − 3.18 (m, − $NHC\boldsymbol{H}_2CH(OH)CH_3$), 1.30 (s, $-C(C\boldsymbol{H}_3)(CH_2O-)_2$), 1.24 (s, $-C(C\boldsymbol{H}_3)CH_2OH$), 1.15 (d, J = 6.5 Hz, $-NHCH_2CH(OH)C\boldsymbol{H}_3$). ^{13}C NMR (75 MHz, DMSO-d_6): δ 171.2, 154.1, 69.3, 65.0, 46.6, 45.6, 20.8, 17.1. IR (neat, cm^{-1}): 3750−3150, 3050–2800, 1744, 1643, 1535,

1458, 1389, 1234, 1103, 957, 787. T_g = 59.5 °C. TGA in Ar: 182−325 °C, 89% mass loss; 11% mass remaining above 500 °C. Solubility in water: >300 mg/mL.

N-Allyl Amide Functional PC (**5**). Yield = 62 mg, ~99%. $M_{n,NMR}$ = 5000 g/mol; $M_{n,GPC}^{DMF}$ = 3800 g/mol; PDI = 1.13. ^{1}H NMR (300 MHz, DMSO-d_6): δ 8.12−8.00 (br, −C(O)N***H***−), 7.82−7.74 (br, −C(O)N***H***−, end group), 5.81−64 (m, −NHCH$_2$C***H***CH$_2$), 5.14-4.96 (m, − NHCH$_2$CHC***H***$_2$), 4.32 − 4.10 (br, − OC(O)OC***H***$_2$-), 3.76 − 3.62 (br, − NHC***H***$_2$CHCH$_2$), 1.15 (s, −C(C***H***$_3$)(CH$_2$O-)$_2$), 1.07 (s, −C(C***H***$_3$)CH$_2$OH). ^{13}C NMR (75 MHz, DMSO-d_6): δ 171.0, 154.1, 135.1, 114.5, 69.3, 45.6, 40.9, 17.1. IR (neat, cm^{-1}): 3500−3200, 3100−2800, 1748, 1640, 1535, 1475, 1386, 1233, 961, 844, 787.

N-Ethyl Amide Functional PC (**6**). Yield = 58 mg, ~99%. $M_{n,NMR}$ = 4700 g/mol; $M_{n,GPC}^{DMF}$ = 4200 g/mol; PDI = 1.12. ^{1}H NMR (300 MHz, DMSO-d_6): δ 7.88−7.78 (br, −C(O)N***H***−), 7.60−7.53 (br, −C(O)N***H***−, end group), 4.95 (t, J = 5.2 Hz, −O***H***), 4.28−4.08 (br, −OC(O)OC***H***$_2$−), 3.12−3.00 (m, −NHC***H***$_2$CH$_3$), 1.11 (s, −C(C***H***$_3$)(CH$_2$O−)$_2$), 1.03 (s, −C(C***H***$_3$)CH$_2$OH), 0.96 (d, −NHCH$_2$C***H***$_3$). ^{13}C NMR (75 MHz, DMSO-d_6): δ 170.7, 154.1, 69.3, 45.5, 33.7, 17.1, 14.5. IR (neat, cm^{-1}): 3500−3200, 3100−2800, 1746, 1640, 1535, 1460, 1380, 1231, 962, 845, 786.

PMPC$_{20}$-b-PMHPAC$_{70}$ (**10**). Yield = 218 mg, 75%. $M_{n,NMR}$ = 19200 g/mol; $M_{n,GPC}^{DMF}$ = 1230 g/mol; PDI = 1.23. ^{1}H NMR (300 MHz, DMSO-d_6): δ 7.85−7.55 (br, −C(O)N***H***−), 4.70−4.50 (br, −NHCH$_2$CH(O***H***)CH$_3$), 4.28−4.05 (br, −OC(O)OC***H***$_2$−), 4.01 (t, J = 6.3 Hz, −OC***H***$_2$CH$_2$CH$_3$), 3.69−3.55 (m, −NHCH$_2$C***H***(OH)CH$_3$), 3.10−2.90 (m, −

NHC***H***$_2$CH(OH)CH$_3$), 1.55 (m, −OCH$_2$C***H***$_2$CH$_3$), 1.16 (s, −C(C***H***$_3$)(CH$_2$O−)$_2$ from PMPC block), 1.13 (s, −C(C***H***$_3$)(CH$_2$O−)$_2$ from PMHPAC block), 1.04 (s, −C(C***H***$_3$)CH$_2$OH), 0.95 (d, J = 6.2 Hz, -NHCH$_2$CH(OH)C***H***$_3$), 0.85 (t, J = 7.3 Hz, −OCH$_2$CH$_2$C***H***$_3$). ^{13}C NMR (75 MHz, DMSO-d_6): δ 171.7, 171.2, 154.1, 153.8, 69.3, 68.8, 66.3, 64.9, 46.5, 46.1, 45.5, 21.4, 20.8, 17.0, 16.8, 10.0. IR (neat, cm^{-1}): 3650−3150, 3030−2800, 1744, 1643, 1543, 1466, 1389, 1234, 1134, 964, 787. T_g = −13.2 and 65.6 °C. TGA in Ar: 180−260 °C, 64% mass loss; 260−320 °C, 27% mass loss; 8% mass remaining above 500 °C.

3.3.8. Functionalization of PMHPAC

To a stirred solution of PMHPAC$_{27}$ (50 mg, 0.23 mmol for repeat units), 4-pentenoic acid (26 μL, 0.25 mmol), and 4-dimethylaminopyridine (DMAP, 2.8 mg, 0.023 mmol) in DMF (2 mL), *N,N*'-dicyclohexylcarbodiimide (DCC, 52 mg, 0.25 mmol) in DMF (minimum amount to dissolve) was added dropwise at 0°C. After stirring 20 h at room temperature, the resulting solution was dialyzed against DMF for a day and nanopure water for 2 days and lyophilized to yield white solid (**7**). Yield = 64 mg, 96% based on 81% conversion. $M_{n,NMR}$ = 7700 g/mol; $M_{n,GPC}^{DMF}$ = 4200 g/mol; PDI = 1.25. ^{1}H NMR (300 MHz, DMSO-d_6): δ 8.00−7.90 (br, −C(O)N***H***−), 7.80−7.72 (br, −C(O)N***H***−, end group), 5.87−5.70 (m, −C(O)CH$_2$CH$_2$C***H***CH$_2$), 5.07−4.92 (m, −C(O)CH$_2$CH$_2$CHC***H***$_2$), 4.89−4.76 (m, −C(O)NHCH$_2$C***H***(CH$_3$)O−), 4.62−4.56 (m, −NHCH$_2$CH(O***H***)CH$_3$), 4.34−4.02 (br, −OC(O)OC***H***$_2$−), 3.68−3.54 (m, −NHCH$_2$C***H***(OH)CH$_3$), 3.29−3.06 (m, −C(O)NHC***H***$_2$CH(CH$_3$)O−), 3.05−2.90 (m, −NHC***H***$_2$CH(OH)CH$_3$), 2.40−2.29 (m, −

C(O)CH$_2$C***H***$_2$CHCH$_2$), 2.29 − 2.19 (m, −C(O)C***H***$_2$CH$_2$CHCH$_2$), 1.22 and 1.11 (s, −C(C***H***$_3$)(CH$_2$O−)$_2$), 1.06 (d, J = 6.0 Hz, −C(O)NHCH$_2$CH(C***H***$_3$)O−), 0.95 (d, J = 6.0 Hz, −NHCH$_2$CH(OH)C***H***$_3$). ^{13}C NMR (75 MHz, DMSO-d_6): δ 171.7, 171.4, 171.1, 154.1, 137.0, 115.4, 69.2, 68.7, 64.9, 46.5, 45.5, 42.8, 32.9, 28.4, 20.8, 17.2, 17.0. IR (neat, cm^{-1}): 3500–3225, 3050–2800, 1732, 1643, 1537, 1454, 1383, 1234, 1177, 1096, 962, 918, 787, 644. T_g = 34.0 °C. TGA in Ar: 180–380 °C, 94% mass loss; 4% mass remaining above 500 °C.

3.3.9. Thiol-ene "click" reaction of pendant allyl functionality of PMAC-b-PMBC with ethyl mercaptoacetate

PMAC-*b*-PMBC (**8**) (260 mg, 0.24 mmol for alkene functionalities), 2,2-dimethoxy-2-phenylacetophenone (DMPA, 12 mg, 0.050 mmol), and ethyl 2-mercaptoacetate (260 μL, 2.4 mmol) were dissolved in 15 mL of DMF. The solution were bubbled with N_2 for 10 min and irradiated by UV (365 nm, 6 W) for 2 h. The reaction mixture was precipitate into methanol and dried *in vacuo* to yield colorless sticky liquid (**11**). Yield = 245 mg, 85%. $M_{n,NMR}$ = 24000 g/mol. ^{1}H NMR (300 MHz, $CDCl_3$): δ 7.36 −7.23 (br, −OCH$_2$C$_6$***H***$_5$), 5.13 (s, −OC***H***$_2$C$_6$H$_5$), 4.26−4.10 (m, −OC(O)OC***H***$_2$− and −C(O)OC***H***$_2$CH$_2$CH$_2$−), 3.70 (m, −C***H***$_2$OH), 3.24–3.16 (m, −SC***H***$_2$C(O)O−), 2.74–2.63 (m, −C(O)OCH$_2$CH$_2$C***H***$_2$S−), 2.02 − 1.86 (m, −C(O)OCH$_2$C***H***$_2$CH$_2$S−), 1.32 − 1.18 (m, −C(C***H***$_3$)(CH$_2$O−)$_2$ and −C(O)OCH$_2$C***H***$_3$). ^{13}C NMR (75 MHz, $CDCl_3$): δ 172.0, 154.5, 35.5, 128.7, 128.5, 128.1, 68.7, 67.2, 63.9, 61.5, 46.7, 33.6, 29.0, 28.0, 17.5, 14.3. IR (neat, cm^{-1}): 3150–2800, 1744, 1458, 1381, 1234, 1142, 972, 787, 740, 702.

3.3.10. Self-assembly of diblock copolymer, $PMPC_{20}$-b-$PMHPAC_{70}$

$PMPC_{20}$-*b*-$PMHPAC_{70}$ (2 mg) was dissolved in nanopure water (2 mL) and the solution was allowed to stir overnight. Hydrodynamic diameter by DLS: D_h (intensity) = 43 ± 26 nm, D_h (volume) = 21 ± 9 nm, D_h (number) = 16 ± 4 nm. D^{TEM} = 24 ± 6 nm (measured for more than 300 nanoparticles). D^{AFM} = 32 ± 6 nm (measured for more than 100 nanoparticles from phase images). $Height^{AFM}$ = *ca*. 1.3 nm (measured from height image). ζ−potential in nanopure water: − 14.4 ± 4.7 mV (averaged from three measurements: −9.54 mV, −14.81 mV, −18.90 mV).

3.3.11. Cytotoxicity assays

RAW 264.7 mouse macrophages (2×10^4 cells/well) and OVCAR-3 cells (5×10^3 cells/well) were plated in 96-well plate in DMEM and RPMI-1640 medium (10% and 20% fetal bovine serum, for the RAW 264.7 and OVCAR-3, respectively and 1% penicillin/streptomycin). Cells were incubated at 37 °C in a humidified atmosphere containing 5% CO_2 for 24 h to adhere. Then, the medium was replaced with a fresh medium 1 h prior to the addition of 20 μL of polymer stock solutions to 100 μL of the medium (final concentrations ranged from 1 to 3000 μg/mL). The cells were incubated with the various formulations for 72 h and then the medium was replaced with 100 μL of fresh medium prior to the addition of 20 μL MTS combined reagent to each well (Cell Titer 96 Aqueous Non-Radioactive Cell Proliferation Assay, Promega Co., Madison, WI). The cells were incubated with the reagent for 2 h at 37 °C in a humidified atmosphere containing 5% CO_2 protected from light. Absorbance was measured at 490 nm using

SpectraMax M5 (Molecular Devices Co., Sunnyvale, CA). The cell viability was calculated based on the relative absorbance to the control-untreated cells.

3.3.12. Multiplex assay

RAW 264.7 mouse macrophages (2×10^4 cells/well) were plated in 96-well plate in DMEM (10% fetal bovine serum, and 1% penicillin/streptomycin). The RAW 264.7 cells were treated with medium (control) and polymers (500 μg/mL) for 24 h. The supernatants were then collected and centrifuged for 10 min at 13000 rpm. Serial dilutions of standards of cytokines were also prepared in the same diluent utilized for the samples (*i.e*. cell-culture medium). Control, standards and polymer-treated samples (50 μL) were incubated with antibody-conjugated magnetic beads for 30 min in the dark. After washing, the detection antibody was added to the wells and incubated in the dark for 30 min under continuous shaking (300 rpm). After washing, streptavidin-phycoerythrin was added to every well and incubated while protected from light for 10 min under the same shaking conditions. Finally, after several washings and resuspension in the assay buffer and shaking, the expression of the mouse cytokines, interleukin (IL)-1α, IL-1β, IL-2, IL-3, IL-4, IL-5, IL-6, IL-9, IL-10, IL-12 (P40), IL-12 (P70), IL-13, IL-17, eotaxin, granulocyte-colony-stimulating factor (G-CSF), granulocyte macrophage-colony-stimulating factor (GM-CSF), interferon-γ (IFN-γ), keratinocyte-derived chemokine (KC), monocyte chemotactic protein (MCP)-1, macrophage inflammatory protein (MIP)-1α, MIP-1β, regulated upon activation normal T-cell expressed and presumably secreted (RANTES) and tumor necrosis factor-α (TNF-α) was measured immediately using the

Bioplex 200 system with HTF and Pro II Wash station (Bio-Rad Laboratories, Inc., Hercules, CA), and the data were analyzed using the Bioplex Data Pro software.

3.3.13. Methylation of carboxylic acid functionalities[109] in PMC (synthesis of PMMC, 3)

To a stirred solution of PMC_{27} (50 mg, 0.012 mmol) in 1 mL of toluene:MeOH (3:2), an etheric solution (2 M in diethyl ether) of (trimethylsilyl)diazomethane ($TMSCHN_2$) was added dropwise until the yellow color persisted (~250 μL). The mixture was stirred for 30 min at RT and concentrated *in vacuo* to give poly(5-methyl-5-methyloxycarbonyl-1,3-dioxan-2-one), $PMMC_{27}$ (**3**). $M_{n,NMR}$ = 4700 g/mol; $M_{n,GPC}^{THF}$ = 6700 g/mol; PDI = 1.09. ^{1}H NMR (300 MHz, $CDCl_3$): δ 4.35−4.23 (m, −OC(O)OC***H***$_2$−), 3.73 (s, −OC***H***$_3$), 1.25 (s, −C(C***H***$_3$)(CH_2O−)$_2$), 1.20 (s, −C(C***H***$_3$)CH_2OH). ^{13}C NMR (75 MHz, $CDCl_3$): δ 172.7, 154.5, 69.0, 52.7, 48.4, 46.6, 17.6. IR (neat, cm^{-1}): 3100−2800, 1736, 1458, 1389, 1227, 1142, 972, 872, 787, 733.

4.3.14. PEG 6kDa (12)

T_g = −12.5 °C (−17 °C, as reported[116]), T_m = 57.8 °C. TGA in Ar: 320−430 °C, 92% mass loss; 8% mass remaining above 500 °C.

3.3.15. Synthesis of PEG-b-PMAC (14)

mPEG (10 kDa, 100 mg, 0.010 mmol) and MAC (160 mg, 0.80 mmol) were dissolved in dry DCM (1.6 mL, [MAC] = 0.5 M). DBU (1.5 μL, 0.010 mmol) was added to the monomer/initiator solution. After the desired time, the polymerizations were quenched by addition of a DCM solution of benzoic acid (1.8 mg, 0.015 mmol in 200 μL DCM) and precipitated directly into cold diethyl ether to yield PEG-*b*-PMAC (**14**) as a

white powder. Yield = 130 mg, 95% based upon 25% conversion. $M_{n,NMR}$ = 13800 g/mol; $M_{n,GPC}^{DMF}$ = 12000 g/mol; PDI = 1.05. ^{1}H NMR (300 MHz, $CDCl_3$): δ 5.86 (m, −$CH_2C\boldsymbol{H}CH_2$), 5.33−5.18 (m, −$CH_2CHC\boldsymbol{H}_2$), 4.61 (d, J = 5.6 Hz, −$OC\boldsymbol{H}_2CHCH_2$), 4.33−4.24 (m, −OC(O)$OC\boldsymbol{H}_2$−), 3.80−3.46 (br, −$OC\mathbf{H}_2C\boldsymbol{H}_2$−), 3.36 (s, $C\boldsymbol{H}_3O$−), 2.50 (t, J = 6.8 Hz, −$CH_2O\boldsymbol{H}$), 1.25 (s, −$C(C\boldsymbol{H}_3)(CH_2O-)_2$), 1.21 (s, −$C(C\boldsymbol{H}_3)CH_2OH$). ^{13}C NMR (75 MHz, $CDCl_3$): δ 171.8, 154.5, 131.7, 118.6, 70.7, 68.7, 66.0, 46.6, 17.6. IR (neat, cm^{-1}): 3100−2700, 1751, 1466, 1342, 1234, 1096, 957, 841, 787. T_g = −18.5 °C; T_m = 48.5 °C. TGA in Ar: 200−300 °C, 24% mass loss; 300−420 °C, 65% mass loss; 7% mass remaining above 500 °C.

3.3.16. Synthesis of $PHPMA_{40}$ (13)

To a flame-dried Schlenk flask (10 mL) equipped with a magnetic stir bar under N_2 atmosphere was added 4-cyano-4-[(dodecylsulfanylthiocarbonyl)sulfanyl]pentanoic acid (CTA, 8.5 mg, 0.020 mmol), HPMA (300 mg, 2.1 mmol), AIBN (1.0 mg, 6.3 μmol) and 2.5 mL of dimethylacetamide (DMAc). The mixture was stirred for 10 min at RT, deoxygenated through three cycles of freeze-pump-thaw and back-filled with N_2. After the last cycle, the reaction mixture was stirred for 15 min at RT and immersed into a pre-heated oil bath at 70 °C to start the polymerization. After 5 h, the polymerization was quenched by cooling the reaction flask with liquid N_2. The polymer was purified by precipitation into cold diethyl ether twice. The yellow precipitate was collected through centrifugation and kept under vacuum overnight to remove residual solvents. Yield 110 mg of product, 92% yield based upon ~40% conversion. $M_{n,NMR}$ = 6100 g/mol; $M_{n,GPC}^{DMF}$

= 2100 g/mol; PDI = 1.30. ^{1}H NMR (300 MHz, DMSO-d_6): δ 7.40−7.04 (br, −C(O)N***H***−), 4.80−4.64 (br, −$CH_2CH(CH_3)(O\boldsymbol{H})$), 3.74−3.60 (br, −$CH_2C\boldsymbol{H}(CH_3)(OH)$), 3.28−3.20 (br, −$SC\boldsymbol{H}_2$−), 3.04−3.28 (br, −$C\boldsymbol{H}_2CH(CH_3)(OH)$), 2.35−2.26 (m, −$CH_2C\boldsymbol{H}_2C(O)OH$), 2.02−1.37 (m, −$C\boldsymbol{H}_2C(CH_3)(C(O)-)-$), 1.37−1.20 (m, −$SCH_2CH_2(C\boldsymbol{H}_2)_9CH_3$), 1.20−0.60 (m, −$CH_2C(C\boldsymbol{H}_3)(C(O)-)-$, −$CH_2CH(C\boldsymbol{H}_3)(OH)$ and $S(CH_2)_{11}C\boldsymbol{H}_3$). ^{13}C NMR (75 MHz, DMSO-d_6): δ 177.1, 65.0, 64.9, 64.8, 54.6, 47.6, 45.1, 44.6, 31.3, 29.0, 21.6, 21.4, 17.8, 16.5, 15.2, 14.02. IR (neat, cm^{-1}): 3650−3100, 3050−2700, 1751, 1636, 1528, 1466, 1342, 1242, 1103, 957, 841, 787. T_g = 157.0 °C. TGA in Ar: 220−475 °C, 92% mass loss; 6% mass remaining above 500 °C.

3.3.17. Synthesis of $PMMA_{28}$

To a flame-dried Schlenk flask (10 mL) equipped with a magnetic stir bar under N_2 atmosphere was added CTA (202 mg, 0.50 mmol), MMA (3.00 g, 30 mmol), AIBN (8.2 mg, 0.050 mmol) and 1.5 mL of anisole. The mixture was stirred for 10 min at RT, deoxygenated through three cycles of freeze-pump-thaw and back-filled with N_2. After the last cycle, the reaction mixture was stirred for 15 min at RT and immersed into a pre-heated oil bath at 65 °C to start the polymerization. After 4 h, the polymerization was quenched by cooling the reaction flask with liquid N_2. The polymer was purified by precipitation into a methanol:water (4/1) mixture twice. The yellow precipitate was collected through centrifugation and kept under vacuum overnight to remove residual solvents. Yield 1.3 g of product, 87% yield based upon ~47% conversion. $M_{n,NMR}$ = 3200 g/mol; $M_{n,GPC}^{THF}$ = 4500 g/mol; PDI = 1.11. ^{1}H NMR (300 MHz, $CDCl_3$): δ 3.70−3.52

(br, −OC***H***$_3$), 3.21 (t, J = 7.3 Hz, −SC***H***$_2$CH$_2$−), 2.61−2.46 (m, −C***H***$_2$C(O)OH), 2.38−2.06 (m, −CH$_2$C***H***$_2$C(O)OH), 2.06−1.74 (br, −C***H***$_2$C(CH$_3$)(C(O)O−)−), 1.68 (s, −C(CN)(C***H***$_3$)−), 1.62 (m, −SCH$_2$C***H***$_2$−), 1.48−1.10 (m, −SCH$_2$CH$_2$(C***H***$_2$)$_9$CH$_3$), 1.09−0.70 (m, −CH$_2$C(C***H***$_3$)(C(O)O−)− and −S(CH$_2$)$_{11}$C***H***$_3$). ^{13}C NMR (75 MHz, CDCl$_3$): δ 178.2, 177.9, 177.1, 105.1, 60.1, 59.8, 54.5, 53.0, 51.9, 45.6, 45.1, 45.0, 44.6, 37.0, 34.2, 32.0, 29.7, 29.6, 29.5, 29.4, 29.2, 29.0, 27.1, 22.8, 18.8, 16.5, 14.2. IR (neat, cm^{-1}): 3100−2800, 1728, 1443, 1389, 1242, 1150, 988, 841, 810, 748. T_g = 96.0 °C. TGA in Ar: 160−210 °C, 34% mass loss; 210−300 °C, 9% mass loss; 300−370 °C, 19% mass loss; 370−430 °C, 29% mass loss; 8% mass remaining above 500 °C.

3.3.18. Synthesis of PMMA$_{28}$-b-PHPMA$_{90}$ (15)

To a flame-dried Schlenk flask (10 mL) equipped with a magnetic stir bar under N$_2$ atmosphere was added PMMA$_{28}$ (45 mg, 14 μmol), HPMA (300 mg, 2.1 mmol), AIBN (1.0 mg, 6.3 μmol) and 2.5 mL of DMAc. The mixture was stirred for 10 min at RT, deoxygenated through three cycles of freeze-pump-thaw and back-filled with N$_2$. After the last cycle, the reaction mixture was stirred for 15 min at RT and immersed into a pre-heated oil bath at 70 °C to start the polymerization. After 7 h, the polymerization was quenched by cooling the reaction flask with liquid N$_2$. The copolymer was purified by precipitation into cold diethyl ether twice. The yellow precipitate was collected through centrifugation and kept under vacuum overnight to remove residual solvents. Yield 210 mg of product, 93% yield based upon ~60% conversion. $M_{n,NMR}$ = 16100 g/mol; $M_{n,GPC}^{DMF}$ = 3400 g/mol; PDI = 1.56. ^{1}H NMR (300 MHz, DMSO-d_6): δ 7.40−7.04 (br,

−C(O)N***H***−), 4.80−4.64 (br, −$CH_2CH(CH_3)(O\boldsymbol{H})$), 3.74−3.61 (br, −$CH_2C\boldsymbol{H}(CH_3)(OH)$), 3.61−3.48 (br, −$C(O)OC\boldsymbol{H}_3$), 3.04−3.28 (br, −$C\boldsymbol{H}_2CH(CH_3)(OH)$), 2.37−2.26 (m, −$CH_2C\boldsymbol{H}_2C(O)OH$), 2.02 − 1.37 (m, − $C\boldsymbol{H}_2C(CH_3)(C(O) -) -)$, 1.37 − 1.20 (m, −$SCH_2CH_2(C\boldsymbol{H}_2)_9CH_3$), 1.20−0.60 (m, −$CH_2C(C\boldsymbol{H}_3)(C(O)-)-$, −$CH_2CH(C\boldsymbol{H}_3)(OH)$ and $S(CH_2)_{11}C\boldsymbol{H}_3$). ^{13}C NMR (75 MHz, DMSO-d_6): δ 177.4, 177.1, 177.0, 104.5, 64.9, 64.8, 64.7, 54.4, 53.7, 51.8, 47.6, 47.4, 45.0, 44.5, 44.3, 43.9, 21.5, 21.4, 18.5, 17.9, 16.5, 15.2. IR (neat, cm^{-1}): 3650−3050, 3050−2700, 2361, 1728, 1636, 1520, 1458, 1250, 1196, 1134, 949, 841. T_g = 105.5 and 162.0 °C. TGA in Ar: 250−390 °C, 37% mass loss; 390−480 °C, 49% mass loss; 12% mass remaining above 500 °C.

3.4. Conclusions

A polycarbonate-based degradable analogue of hydrophilic PHPMA was prepared *via* amidation of carboxylic acid-functional PCs with 1-amino-2-propanol, and found to exhibit similarly high water solubility and low cyto-/immunotoxicity, while having differences of lower glass transition temperature and, importantly, possessing hydrolytic degradability. Metal-free organocatalytic ROP of a bis-MPA-derived benzyl ester-functional cyclic carbonate monomer and subsequent hydrogenolysis afforded the well-defined polycarbonate precursor for postpolymerization amidation to yield the degradable PHPMA analogue. This method could be utilized as a general procedure to prepare diverse functional PCs. High water solubility and low cyto-/immuno-toxicities as well as facile functionalization *via* pendant hydroxyl groups are promising characteristics of

PMHPAC as a degradable alternative to PEG and PHPMA. In addition, a potentially fully degradable polymeric nanostructure was formed by self-assembly of a PMHPAC-based amphiphilic block copolymer, which has spherical morphology and suitable size for biomedical applications. We believe that degradable PMHPAC may increase the diversity of macromolecular architectures and nanostructures, especially for advances in nanomedicines.

CHAPTER IV

ALDEHYDE-FUNCTIONAL POLYCARBONATES AS REACTIVE PLATFORMS*

4.1. Introduction

Aldehydes are among the most reactive functional groups under mild reaction conditions, which can allow for entry to the construction of a diverse range of functional dynamic and/or static polymer materials. Aldehydes undergo a wide variety of chemical reactions with nucleophiles, resulting in both reversible and irreversible bonds.[117,118] Among them, condensation reactions with nitrogen-containing nucleophiles such as hydrazines or alkoxyamines are classified as "click" reactions, due to the facile formation of stable hydrazones or oximes.[119,120] Also, the condensation of aldehyde with primary amines yields imine derivatives (Schiff bases) and imine reduction provides stable amino bonds. Efforts to develop polymers bearing pendant aldehyde functionalities have been made since the 1950s. Conventional radical polymerization of aldehyde-bearing monomers yielded polymers with uncontrolled molecular weight and dispersity.[121,122] Anionic polymerization was employed to produce well-defined aldehyde-functional polymers.[123,124] However, the rigorous polymerization conditions required for controlled anionic polymerization limited their applications. Since the development of controlled radical polymerizations (CRPs), a few research groups have studied the synthesis and

---

* Reprinted with permission from "Aldehyde-functional polycarbonates as reactive platforms" by Gyu Seong Heo, Sangho Cho, and Karen L. Wooley, *Polym. Chem.* **2014**, *5*, 3555-3558.

application of aldehyde-functional polymers. Maynard and coworkers prepared poly(3,3'-diethoxypropyl methacrylate) (pDEPMA) by atom transfer radical polymerization (ATRP) and reversible addition–fragmentation chain transfer (RAFT) polymerization.[125-127] Aldehydes were produced by hydrolysis of the acetals and were then conjugated with aminooxy- or hydrazine-functionalized compounds including peptides and dyes *via* oxime or hydrazone linkages, respectively. Aldehyde-functional polymers were also synthesized from unprotected monomers by RAFT polymerization[128,129] and ring-opening metathesis polymerization (ROMP).[130]

Although several examples of polymers having aldehyde side chain groups have been reported, most are comprised of nondegradable backbones. While this work was in progress, Hedrick, Yang and coworkers reported the synthesis of poly(ethylene oxide)-*b*-polycarbonates (PEO-*b*-PCs) with pendant aldehyde groups *via* organocatalytic ring-opening polymerization (ROP) of aldehyde-functional cyclic carbonate monomers using PEO as a macroinitiator.[131] Aliphatic PCs are remarkable candidates for biomedical applications on account of their biodegradability, biocompatibility, and low toxicity *in vivo*.[100,101] In particular, various pendant functionalities can be introduced on the PC backbones by ROP of functionalized cyclic carbonate monomers.[100,132] These well-established synthetic methods for functional PCs expand potential applications of these types of materials.

We built a different strategy to prepare aldehyde-functional PCs. Our strategy involved the introduction of aldehyde functionalities via post-polymerization modification of functional PCs. Among many synthetic pathways to aldehydes, ozonolysis of alkenes

is one of the most intriguing methods to attempt, due to: (1) aldehyde groups can be readily introduced by selective cleavage of alkenyl groups using ozone together with a reducing agent; (2) the initial alkenes can instead be utilized for other post-polymerization modifications, such as by thiol–ene reaction, epoxidation, halogenation, hydroboration, etc.; (3) the alkene precursors and resulting aldehydes are orthogonal functional groups for further conjugation reactions. In this study, we prepared allyl-functional PCs by ROP of a functionalized cyclic carbonate monomer using 1,8-diazabicyclo [5.4.0]- undec-7-ene (DBU) in order to develop a readily accessible synthetic method for versatile allyl-functional PCs. Aldehydefunctionalities were introduced by ozonolysis of the pendant alkene groups. The resulting aldehydes were conveniently functionalized with aminooxy-containing compounds *via* aldehyde–aminooxy "click" reactions. Furthermore, PC-based statistical copolymers bearing alkene and aldehyde functionalities were synthesized by partial ozonolysis and functionalized by stepwise aldehyde–aminooxy and thiol–ene "click" reactions in an orthogonal fashion.

4.2. Results and Discussion

Allyl-functional PCs [poly(5-methyl-5-allyloxycarbonyl-1,3-dioxan-2-one), PMAC] were synthesized by organocatalytic ROP of the functionalized cyclic carbonate monomer, 5-methyl-5-allyloxycarbonyl-1,3-dioxan-2-one (MAC). MAC was synthesized by a simple two-step procedure, as reported previously.[114] Dove reported the ROP of MAC using the dual catalyst system of (-)-sparteine in combination with a thiourea.[133] However, the limited availability of (-)-sparteine could hinder the further application of these conditions. Thus, our focus turned to DBU as a catalyst (Scheme 4.1).

In Dove's report, polymerizations using DBU as a catalyst were retarded beyond *ca*. 70% monomer conversion, and led to isolated polymers having broad molecular weight distributions and bimodal GPC traces. In this study, polymerizations were carried out under more dilute conditions ($[MAC]_0$ = 0.5 M in this study *vs*. 2 M as reported), in order to provide enhanced control, which was expected to occur by maintaining uniform solubility throughout the polymerization while also inhibiting transesterification reactions. Investigation of the living characteristics of the polymerization was performed in dichloromethane (DCM) at ambient temperature in a glovebox (29 ˚C) with $[M]_0/[I]_0$ = 50. Application of DBU revealed a linear correlation between the number-average molecular weight (M_n) against monomer conversion until *ca*. 80% monomer conversion, at which point the ROPs became sluggish. However, minimal transesterification was observed until 2 h after polymerization was suspended (Figure 4.1). After the polymerizations were quenched by addition of benzoic acid in DCM, residual monomer and catalyst were removed by column chromatography using silica gel to yield the purified polymers (Figure 4.2). Both the molecular weight and molecular weight distribution could be manipulated by polymer fractionation using column chromatography (Figure 4.3). Furthermore, chain extension experiments after complete monomer conversion or retardation of polymerization showed that the catalyst and chain end remained active for ring opening of monomers for growth of a second block (Table 4.1).

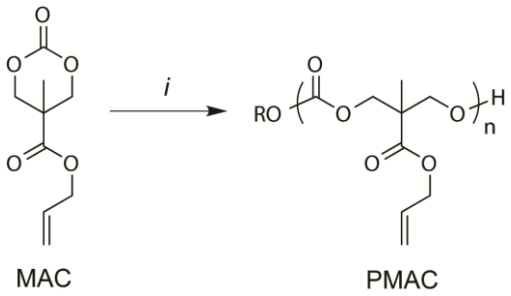

Scheme 4.1. Ring-opening polymerization (ROP) of 5-methyl-5-allyloxycarbonyl-1,3-dioxan- 2-one, MAC. Conditions: (i) ROH, DBU, DCM, 29 °C in the glovebox.

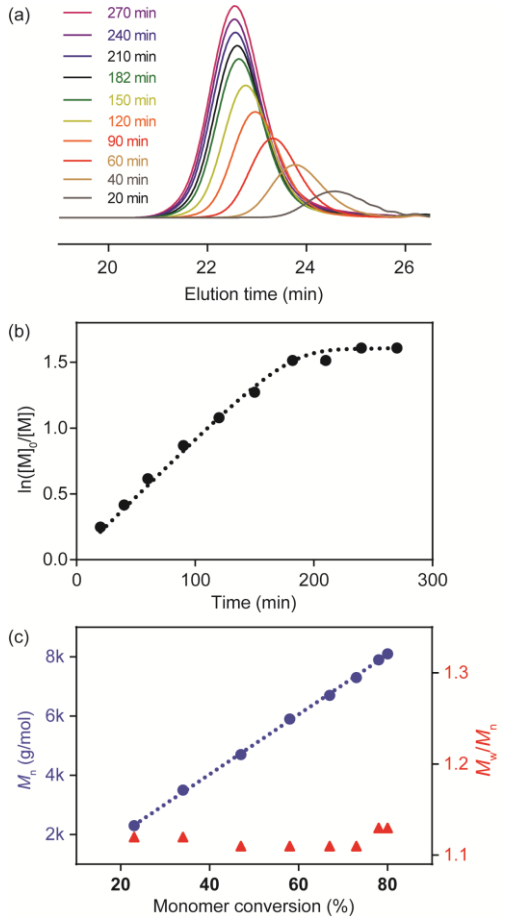

Figure 4.1. (a) GPC profiles (THF as eluent, 1 mL/min) as a function of polymerization time, for the ROP of MAC; (b) Plot of $\ln([M]_0/[M])$ against time, obtained from ^{1}H NMR spectroscopy data; (c) Plot of number-average molecular weight (M_n) and polydispersity (M_w/M_n) against % monomer conversion in the ROP of MAC. Conditions: $[MAC]_0$ = 0.5 M in DCM at 29 °C in the glovebox, [MAC] : [BnOH] : [DBU] = 50 : 1 : 1.

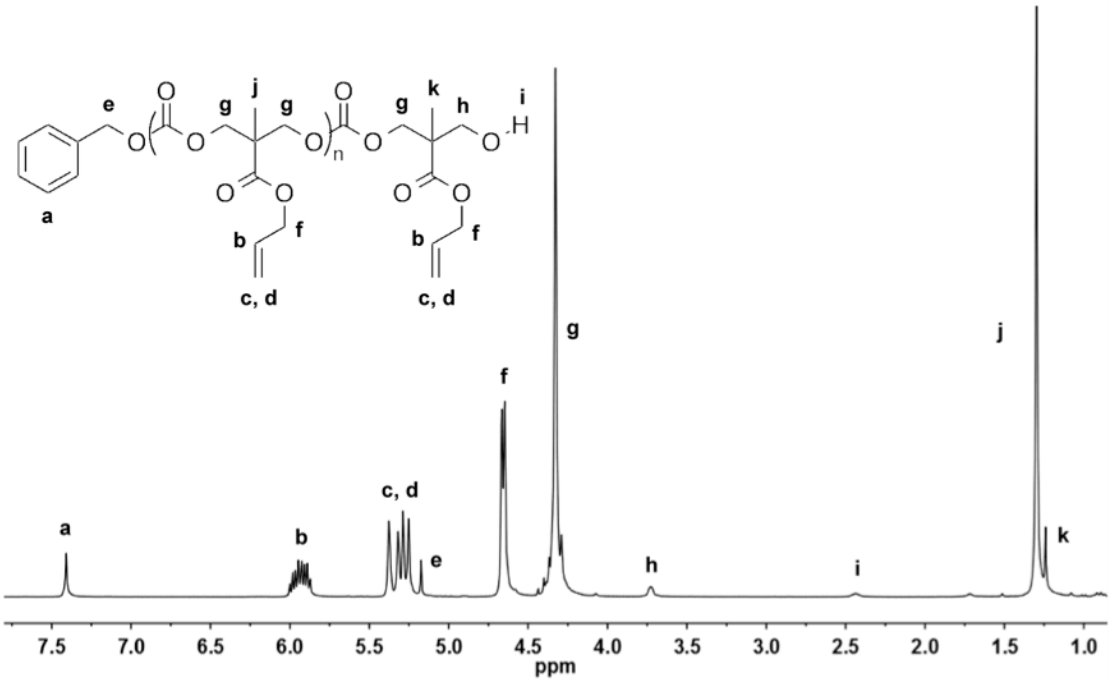

Figure 4.2. ^{1}H NMR spectrum of BnO-PMAC$_{15}$-OH initiated from benzyl alcohol using DBU. Conditions: $[MAC]_0$ = 0.5 M in DCM at 29 °C in the glovebox, [MAC] : [BnOH] : [DBU] = 20 : 1 : 1.

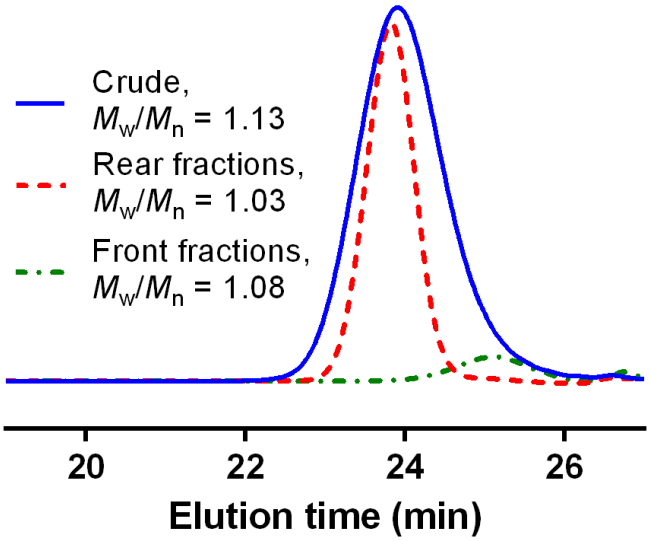

Figure 4.3. GPC profiles (THF as eluent, 1 mL/min) of BnO-PMAC$_{15}$-OH before and after purification using column chromatography. Conditions: $[MAC]_0$ = 0.5 M in DCM at 29 °C in the glovebox, [MAC] : [BnOH] : [DBU] = 20 : 1 : 1.

Table 4.1. Block copolymers of MAC.

Polymer	M_n (NMR) (g/mol)	M_n (GPC) (g/mol)	PDI
N_3-PEG_{68}-*b*-$PMAC_{10}$-OH	5 000	5 100	1.09
BnO-$PMAC_{37}$-*b*-$PLLA_{20}$-OH	10 400	4 300[a)]	1.09
BnO-$PLLA_{20}$-*b*-$PMAC_{15}$-OH	6 000	5 600	1.12

[a)]GPC flow marker was shifted.

Aldehyde-functional PCs [poly(5-methyl-5-oxoethyloxycarbonyl-1,3-dioxan-2-one), PMOC] were prepared by ozonolysis of allyl-functional polymer precursors and their reductive work-up (Scheme 4.2). Ozone serves as "molecular scissors", cutting double bonds in molecules,[134] at specific sites to produce new functional groups. We hypothesized that the PC backbones would remain intact under ozonolysis conditions. Initial ozonolysis studies were conducted in CD_2Cl_2 (20 mg of $PMAC_{15}$ in 2 mL of CD_2Cl_2) at 78 ˚C. Ozone was delivered at a rate of 100 mg h^{-1} as a mixture of column-dried compressed air (2 L min^{-1}) from a Red Sea AquaZone 100 ozone generator. For unknown reasons, the characteristic blue color of the unreacted ozone in both DCM and methanol (MeOH) was difficult to be recognized, even in the solvents themselves. In order to determine the time to halt the exposure to ozone, aliquots of the reaction mixture were collected, dried *in vacuo*, and analyzed by ^{1}H NMR spectroscopy to monitor the disappearance of alkene proton resonances (a and b in Figure 4.4) after the allotted period of time (1, 3, 5, 7, 9 or 11 min). The cleavage of alkene double bonds was complete within

9 min (Figure 4.5) and reductive workup provided aldehyde groups (d in Figure 4.4). The resulting polymer was isolated by precipitation into cold diethyl ether. Unfortunately, after full conversion to PMOC, the isolated polymers had limited solubility in common organic solvents, except trifluoroacetic acid (TFA). Inter- and intra-molecular hydrogen bonding and dipole–dipole interactions of pendant aldehydes might contribute to the observed solubility challenges.[126,130] As a result, further reactions with polymers bearing aldehyde groups were performed by the *in situ* generation of the aldehyde functionalities and reaction directly without an initial purification. Under ideal conditions, ozonolysis and reductive work-up with dimethyl sulfide (Me_2S) give only dimethyl sulfoxide (DMSO) and volatile formaldehyde as the by-products, neither of which would interfere with the subsequent reactions with the aldehydes.

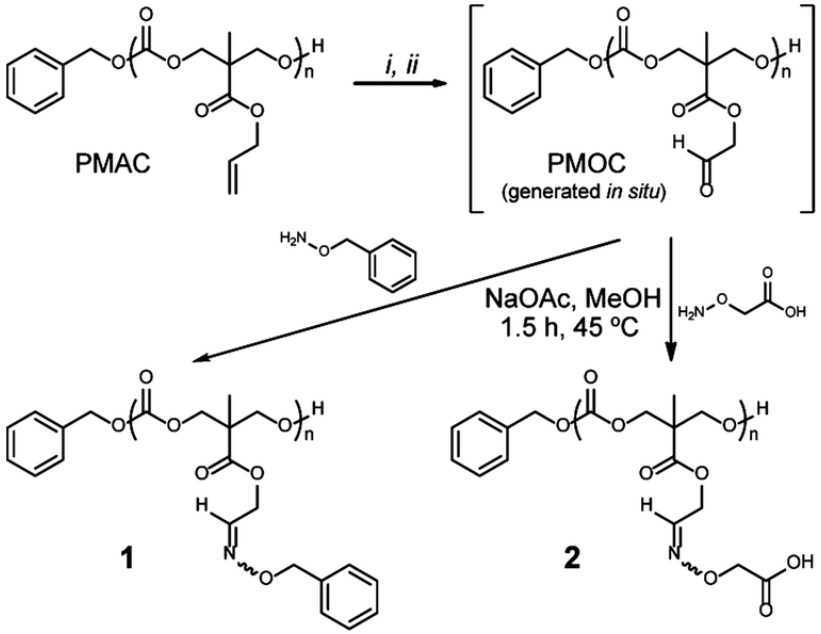

Scheme 4.2. Ozonolysis of PMAC and functionalization by aldehyde–aminooxy "click" reaction. Conditions: (i) O_3, DCM, −78 °C; (ii) Me_2S, −78 °C to RT.

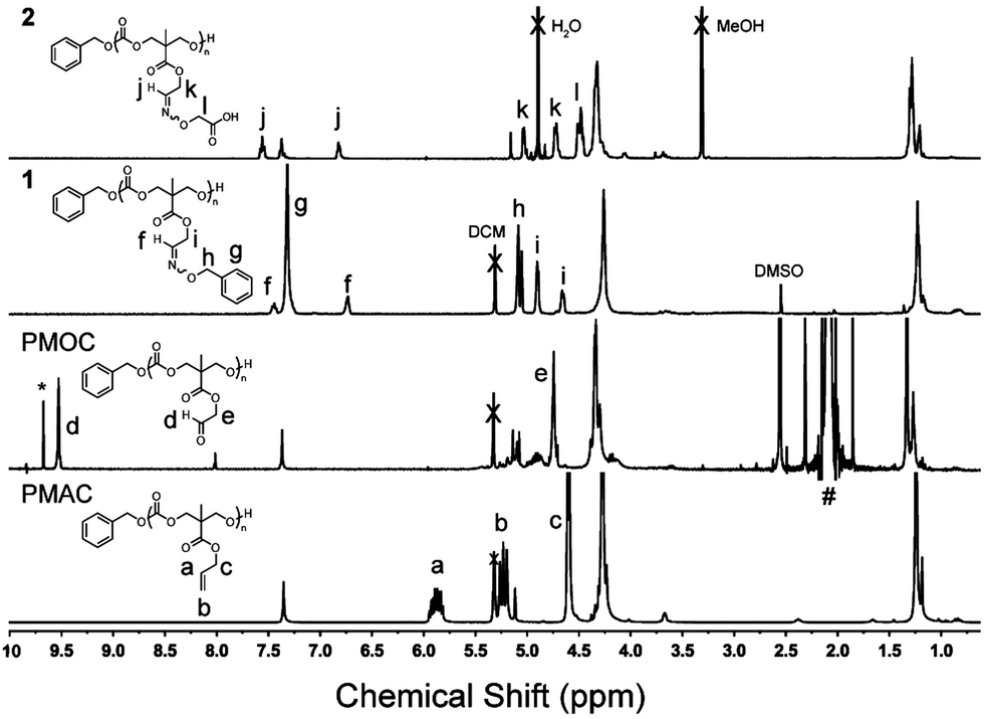

Figure 4.4. ^{1}H NMR spectra (300 MHz) of PMAC (in DCM), PMOC (generated *in situ*, in DCM), and conjugates after functionalization *via* aldehyde–aminooxy "click" reactions with *O*-benzylhydroxylamine (conjugate **1**, in DCM) and *O*-(carboxymethyl)hydroxylamine (conjugate **2**, in MeOD). *: formaldehyde, #: Me_2S.

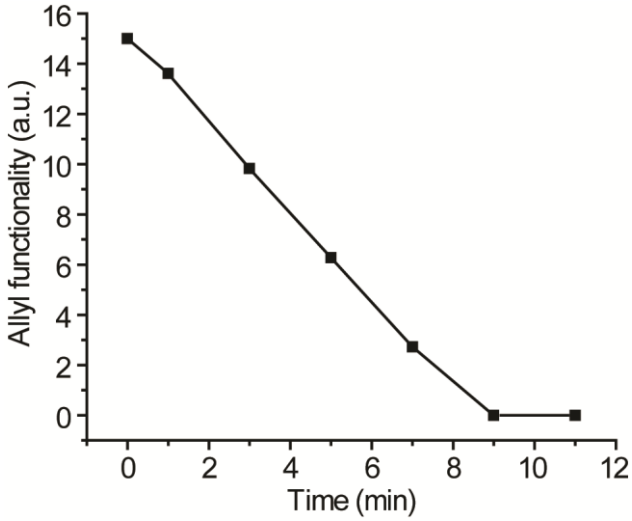

Figure 4.5. Ozonolysis kinetics of $PMAC_{15}$ Conditions: PMAC (20 mg) in DCM (2 mL), (i) O_3, DCM, -78 ºC; (ii) aliquots were dried *in vacuo* before measuring ^{1}H NMR spectra.

The availability of *in situ*-generated aldehyde groups for further functionalization was confirmed by aldehyde–aminooxy "click" reactions. We chose two model compounds to study formation of oxime bonds: *O*-benzylhydroxylamine as a model hydrophobic compound and *O*-(carboxymethyl)hydroxylamine as a model hydrophilic compound (Scheme 4.2). In particular, the latter can be useful for applications, in terms of conjugation with various compounds having alcohol or amine functionalities, such as peptides, drugs, *etc*. The desired aminooxy compound and sodium acetate (NaOAc) in MeOH were added to the *in situ*-generated PMOC in DCM and stirred at 45 ˚C for 1.5 h. The resulting polymers were purified by precipitation into water for hydrophobic conjugate 1 and dialysis against water (or centrifugal filtration) for hydrophilic conjugate 2. Formation of conjugates was verified by monitoring disappearance of aldehyde resonances (d) of PMOC and appearance of the trans and cis protons (f and j) of the oxime bonds using ^{1}H NMR spectroscopy (Figure 4.4). Also, the chemical shifts of the methylene proton resonances of the side chain (c, e, i, and k) were changed. The ^{1}H NMR integrations indicated that conjugation yields were quantitative. GPC profiles verified that transesterification and/or degradation of the PC backbone linkages by ozonolysis and/or over-oxidation were not significant up to the time of completion of the reaction (Figure 4.6). Moreover, we found that insoluble PMOCs became soluble during conjugation reactions. Therefore, isolated PMOCs, despite their limited solubility, are applicable to further reactions, without the requirement of in situ generation and reaction of the aldehyde functionalities.

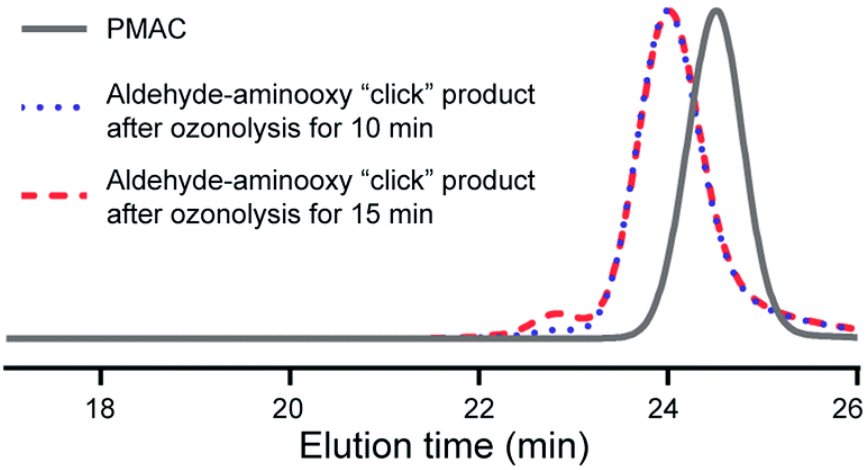

Figure 4.6. GPC profiles (THF as eluent, 1 mL min^{-1}) of BnO-$PMAC_{15}$-OH and isolated products of aldehyde–aminooxy "click" reactions with *O*-benzylhydroxylamine after ozonolysis of PMAC, with application of ozone for 10 or 15 min, each followed by reduction with Me_2S overnight.

The properties of the resulting polymer conjugates were readily modified by varying the aminooxy compounds (Table 4.2). Introduction of aldehydes to the PMAC, which was a viscous liquid with a low T_g of 16.0 ˚C, led to an obvious morphology change, as PMOC was a white solid (T_g = 49.0 ˚C). After aldehyde–aminooxy "click" reactions, conjugate 1 was a viscous liquid (T_g = 0.0 C), while 2 was a white solid (T_g = 76.0 ˚C). Thus, the polymer bulk properties could be readily modified by alteration of the aminooxy compounds. Also, as expected, the solubilities of the conjugates were distinctive. Conjugate 1 was soluble in most organic solvents, while conjugate 2 was soluble in water and MeOH.

Table 4.2. Thermal properties and solubility of synthesized polymers.

	Thermal properties (ºC)			Solubility	
Polymer	T_g [a)]	$T_{d,\,5\%}$ [b)]	$T_{d,\,50\%}$ [b)]	*Organic solvent*	*Aqueous solvent*
$PMAC_{15}$	-16.0	277	333	most	none
$PMOC_{15}$	49.0	245	305	limited[c)]	none
1	0.0	235	262	most	none
2	76.0	183	265	limited[d)]	soluble

[a)]Glass transition temperature, measured by DSC analysis at the third scan.; [b)]Temperatures at 5 and 50% weight degradation by TGA; [c)]soluble in TFA; [d)]soluble in MeOH.

Orthogonal functional groups, alkenes and aldehydes, were easily introduced into the well-defined polymer scaffold. Partial conversions of alkenes to aldehydes were controlled simply by adjusting the times of exposure to ozone. After 3 and 5 min of bubbling ozone and reductive work-up, *ca*. 33% and 60% of alkenes were converted to aldehydes, respectively. The kinetics of ozonolysis made conversions predictable (Figure 4.5). Aldehyde–aminooxy "click" reaction of the resulting alkeneand aldehyde-functional PC (PMAC-*co*-PMOC) with *O*-benzylhydroxylamine and consecutive thiol–ene reaction with ethyl 2-mercaptoacetate demonstrated orthogonal functionalization of the resulting statistical copolymer (Scheme 4.3 and Figure 4.7).

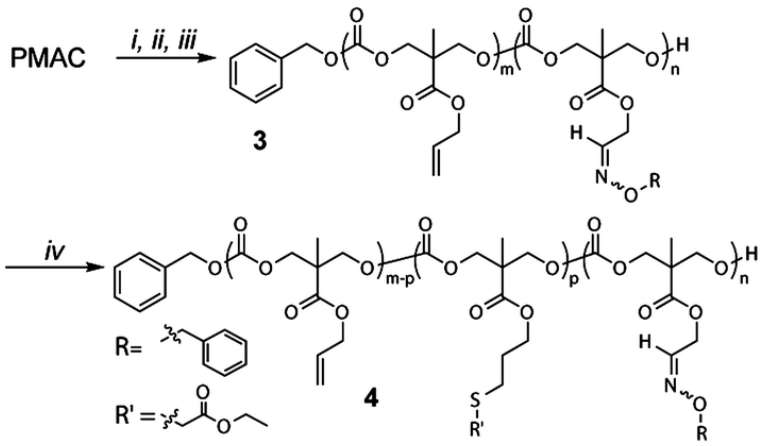

Scheme 4.3. Synthesis of PMAC-*co*-PMOC by partial ozonolysis of PMAC (i and ii), followed by *in situ* functionalization *via* consecutive aldehyde–aminooxy (iii) and thiol–ene "click" (iv) reactions. Conditions: (i) O_3, DCM, −78 °C, 3 min; (ii) Me_2S, −78 °C to RT; (iii) *O*-benzylhydroxylamine, NaOAc, MeOH, 45 °C, 1.5 h; (iv) ethyl 2-mercaptoacetate, DMPA, DMSO, $UV_{365\ nm}$, 2 h.

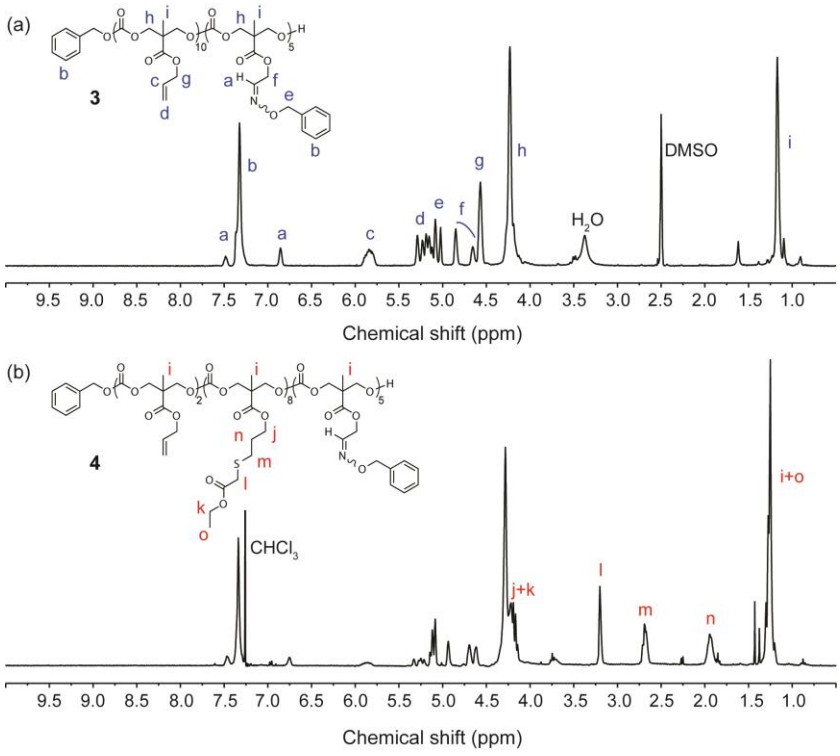

Figure 4.7. ^{1}H NMR spectra of polymer 3 (partial ozonolysis of $PMAC_{15}$ and consecutive functionalization by aldehyde-aminooxy "click" reaction with *O*-benzylhydroxylamine and polymer 4 (thiol-ene reaction of polymer 3 with ethyl 2-mercaptoacetate).

4.3. Experimental Section

4.3.1. Materials

α-Hydroxy-*ω*-azido poly(ethylene glycol) 3,000 Da (HO-PEG_{68}-N_3) was purchased from Rapp Polymere, dried in a desiccator over P_2O_5 and stored under inert atmosphere. Benzyl alcohol and 1,8-diazabicyclo[5.4.0]undec-7-ene (DBU) were dried over CaH_2, distilled, and stored under inert atmosphere. Tetrahydrofuran (THF), *N,N*-dimethylformamide (DMF), and dichloromethane (DCM) were purified by passage through solvent purification system (JC Meyer Solvent Systems) and used as dried solvents. The monomer, 5-methyl-5-allyloxycarbonyl-1,3-dioxan-2-one (MAC) was synthesized as reported,[114] recrystallized several times before use, and dried over P_2O_5. All other solvents and chemicals were obtained from Sigma-Aldrich, TCI America, or Fisher Scientific and used as received.

4.3.2. Instruments

All polymerizations were performed under inert atmosphere in a glovebox. ^1H and ^{13}C NMR spectra were recorded on Varian Mercury 300 spectrometers. Chemical shifts were referenced to the solvent resonance signals.

IR spectra were recorded on an IR Prestige 21 system (Shimadzu Corp., Japan), equipped with an ATR accessory, and analyzed using IRsolution v.1.40 software.

Gel permeation chromatography (GPC) eluted with THF was conducted on a system equipped with Waters chromatography, Inc. (Milford, MA) model 1515 isocratic pump and a model 2414 differential refractometer with a three-column set of Polymer Laboratories, Inc (Amherst, MA). Styragel columns (PLgel 5 μm Mixed C, 500 Å, and

104 Å, 300 × 7.5 mm columns) and a guard column (PLgel 5 μm, 50 × 7.5 mm). The system was equilibrated at 40 °C in THF, which served as the polymer solvent and eluent (flow rate set to 1.00 mL/min). The differential refractometer was calibrated with Polymer Laboratories, Inc., polystyrene standards (300–467,000 Da). Polymer solutions were prepared at a concentration of ca. 3 mg/mL with 0.05% vol toluene as flow rate marker and an injection volume of 200 μL was used. Data were analyzed using Empower Pro software from Waters Chromatography, Inc.

Glass transition temperatures (T_g) were measured by differential scanning calorimetry (DSC) on a Mettler-Toledo DSC822 (Mettler-Toledo, Inc., Columbus, OH) under N_2. Measurements of T_g were taken with a heating rate of 10 °C/min. The measurements were analyzed using Mettler-Toledo Stare v. 10.00 software. The T_g was taken as the midpoint of the inflection tangent, upon the third scan. Thermogravimetric analysis (TGA) was performed under Ar atmosphere using a Mettler-Toledo model TGA/DSC 1, with a heating rate of 10 °C/min.

Column chromatography was performed on CombiFlash Rf4x (Teledyne ISCO) with RediSepRf Column (Teledyne ISCO).

4.3.3. Organocatalytic ROP of 5-methyl-5-allyloxycarbonyl-1,3-dioxan-2-one (MAC)

In a typical experiment, MAC and benzyl alcohol initiator were dissolved in dry DCM ($[MAC]_0$ = 0.5 M). DBU (1 equiv to initiator) was added to the monomer/initiator solution. After the desired time, the polymerizations were quenched by benzoic acid solution in DCM and precipitated directly into hexanes. Impurities were removed by column chromatography on silica gel in hexanes/ethyl acetate (4:1 to 1:1). The polymer

containing fractions were concentrated then dissolved in a minimal amount of DCM and precipitated into hexanes. For example, MAC (1.0 g, 5.0 mmol), benzyl alcohol (26 μL, 27 mg, 0.25 mmol), DBU (37 μL, 38 mg, 0.25 mmol), DCM (10 mL), benzoic acid solution (36 mL, 46 mg, 0.38 mmol in 200 μL DCM) were used to yield BnO-PMAC$_{15}$-OH.

BnO-PMAC$_{15}$-OH. Yield = 670 mg, 87% based upon monomer conversion (75%). Crude: $M_{n,\,GPC}$ = 3,000 g/mol. PDI = 1.13. $M_{n,\,NMR}$ = 3,100 g/mol. After fractionation, fractions 11–12: Mn, GPC = 1,200 g/mol. PDI = 1.08, fractions 14–16: $M_{n,\,GPC}$ = 2,800 g/mol. PDI = 1.03. ^{1}H NMR (300 MHz, $CDCl_3$, 7.26 ppm): δ 7.35 (m, OBn–ArH), 5.86 (m, CH_{vinyl}), 5.33–5.20 (m, $CH_{2\text{-}vinyl}$), 5.13 (s, OBn–CH_2), 4.61 (d, OCH_2CHCH_2), 4.43–4.24 (m, $OC(O)OCH_2$), 3.70 (m, CH_2OH), 2.50 (t, OH), 1.25 (s, CH_3), 1.21 (s, $C(CH_3)CH_2OH$). ^{13}C NMR (75 MHz, $CDCl_3$, 77.16 ppm): δ 171.8, 154.5, 135.1, 131.6, 128.6, 118.5, 68.6, 66.0, 46.6, 17.6. IR (neat, cm^{-1}): 3150–2800 (br), 1736 (s), 1649 (w), 1470 (m), 1402 (m), 1379 (m), 1231 (s), 1138 (s), 968 (s), 785 (m), 739 (w), 698 (w). T_g = -16.0 °C (-17.5 °C, onset). TGA in N_2: 255–280 °C, 7% mass loss; 280–415 °C, 74% mass loss; 415–450 °C, 10% mass loss; 9% mass remaining above 500 °C.

4.3.4. Synthesis of diblock copolymer, α-azido poly(ethylene glycol)$_{68}$-block-poly(5-methyl-5- allyloxycarbonyl-1,3-dioxan-2-one)$_n$, N$_3$-PEG$_{68}$-b-PMAC$_n$

N_3-PEG-*b*-PMAC block copolymer was synthesized using the above-mentioned method with commercially available *α*-hydroxy-*ω*-azido poly(ethylene glycol) 3,000 Da (HO-PEG$_{68}$-N_3) as an initiator ([M]/[I] = 20).

For the synthesis of PMAC-*b*-PLLA block copolymers, MAC (or L-lactide) and benzyl alcohol initiator were dissolved in dry DCM. DBU was added to the monomer/initiator solution. After the desired time (~80% conversion for MAC and >90% conversion for L-lactide), L-lactide (or MAC) was dissolved separately in DCM and added to the reaction mixture. After the desired time, the polymerizations were quenched by benzoic acid solution in DCM and precipitated directly into cold diethyl ether. Otherwise, the mixture was purified by column chromatography on silica gel in hexanes/ethyl acetate (4:1 to 1:1). The polymer containing fractions were concentrated and then dissolved in a minimal amount of DCM and precipitated into hexanes.

N_3-PEG_{68}-b-$PMAC_{10}$-OH. Yield = 234 mg, 90% based upon monomer conversion. $M_{n,\ GPC}$ = 5,100 g/mol. PDI = 1.09. $M_{n,\ NMR}$ = 5,000 g/mol. ^{1}H NMR (300 MHz, $CDCl_3$, 5.32 ppm): δ 5.89 (CH_{vinyl}), 5.34–5.20 ($CH_{2\text{-}vinyl}$), 4.61 (OCH_2CHCH_2), 4.39–4.23 ($OC(O)OCH_2$), 3.59 (OCH_2CH_2), 3.36 ($N_3CH_2CH_2O$), 1.25 (s, CH_3), 1.20 (s, $C(CH_3)CH_2OH$).

BnO-$PMAC_{37}$-b-$PLLA_{20}$-OH. Yield = 162 mg, 74% based upon monomer conversion. $M_{n,\ GPC}$ = 4,300 g/mol (flow marker was shifted). PDI = 1.09. $M_{n,\ NMR}$ = 10,400 g/mol. ^{1}H NMR (300 MHz, $CDCl_3$, 7.26 ppm): δ 7.34 (OBn-ArH), 5.86 (CH_{vinyl}), 5.32–5.10 ($CH_{2\text{-}vinyl}$, PLLA-CH and OBn-CH_2), 4.60 (OCH_2CHCH_2), 4.32–4.24 ($OC(O)OCH_2$ and CHOH), 1.55 (PLLA-CH_3), 1.25 (s, PMAC-CH_3).

BnO-$PLLA_{20}$-b-$PMAC_{15}$-OH. Yield = 197 mg, 71% based upon monomer conversion. $M_{n,\ GPC}$ = 5,600 g/mol. PDI = 1.12. $M_{n,\ NMR}$ = 6,000 g/mol. ^{1}H NMR (300 MHz, $CDCl_3$, 5.32 ppm): δ 7.35 (OBn-ArH), 5.89 (CH_{vinyl}), 5.35–5.13 ($CH_{2\text{-}vinyl}$, PLLA-CH and OBn-CH_2),

4.61 (OCH_2CHCH_2), 4.40–4.25 ($OC(O)OCH_2$ and CHOH), 3.69 (CH_2OH), 1.55 (PLLA-CH_3), 1.26 (s, PMAC-CH_3).

4.3.5. Ozonolysis of PMAC [synthesis of poly(5-methyl-5-oxoethyloxycarbonyl-1,3-dioxan-2- one, PMOC]

$PMAC_{15}$ (20 mg, 0.10 mmol repeat unit, 1 equiv) was dissolved in DCM (2.0 mL), and the solution was cooled to –78 ºC (dry ice/acetone cooling bath). Ozone was bubbled through the cooled solution until a slight blue color was obtained (10 min). When a slight blue color was not recognizable, an aliquot was collected, dried *in vacuo*, and analyzed by ^{1}H NMR to determine conversion. N_2 was then bubbled through for 10 min., and then dimethyl sulfide (37 μL, 31 mg, 0.50 mmol, 5 equiv) was added. The reaction was slowly allowed to warm to room temperature and stir overnight. The resulting solution was used without further purification or was precipitated in diethyl ether to yield PMOC as a white solid (quantitative). For kinetic study of ozonolysis, aliquots were collected, dried *in vacuo*, and analyzed by ^{1}H NMR at the allotted period of time (1, 3, 5, 7, 9, or 11 min). $M_{n,\,NMR}$ = 3,100 g/mol. ^{1}H NMR (300 MHz, CD_2Cl_2, 5.32 ppm): δ 9.52 (br, CHO), 7.36 (br, OBn– ArH), 4.74 (m, OCH_2CHO), 4.34 (m, $OC(O)OCH_2$), 1.33 and 1.27 (br s, CH_3). ^{1}H NMR (300 MHz, TFA-d, 11.5 ppm) δ 9.63 (br, CHO), 7.37 (br, OBn–ArH), 5.07 (br s, OCH_2CHO), 4.56 (br s, $OC(O)OCH_2$), 1.47 (br s, CH_3). ^{13}C NMR (75 MHz, TFA-d, 164.2 ppm): δ 201.7, 176.2, 158.2, 88.1, 72.0, 49.5, 18.4. IR (neat, cm^{-1}): 3675–3075 (br), 3075–2775 (br), 2843 (w), 2725 (w), 1736 (s), 1468 (m), 1402 (m), 1383 (m), 1233 (s), 1142 (s), 961 (s), 858 (m), 783 (m), 738 (w), 700 (w). T_g = 49.0 °C (41.0 °C, onset). TGA

in N_2: 210–355 °C, 76% mass loss; 355–420 °C, 9% mass loss; 15% mass remaining above 500 °C

4.3.6. Functionalization of aldehyde-functional polycarbonates (PMOC)

Isolated or in situgenerated PMOC (50 mg, 0.25 mmol for repeat unit) in DCM (5.0 mL) was mixed with aminooxy compound [*O*-benzylhydroxylamine hydrochloride (80 mg, 0.50 mmol) for 6 conjugate 1, *O*-(carboxymethyl)hydroxylamine (55 mg, 0.50 mmol) for conjugate 2] and NaOAc (136 mg, 1.0 mmol) in MeOH (5.0 mL). The mixture was stirred for 1.5 h at 45 ºC. The conjugate 1 was purified by precipitation into water. The conjugate 2 was concentrated and diluted with nanopure water. The resulting solution was purified by dialysis against nanopure water for 2 days and lyophilized.

Conjugate 1. Yield = 61 mg, 80%. $M_{n,\,GPC}$ = 2,400 g/mol (flow marker was shifted). PDI = 1.10. $M_{n,\,NMR}$ = 4,700 g/mol. ^{1}H NMR (300 MHz, $CDCl_3$, 7.26 ppm): δ 7.43 (br, HC=NO), 7.30 (br, OBn–ArH), 6.72 (br, HC=NO), 5.07 and 5.04 (s, OBn–CH_2), 4.98 (m, OCH_2CHNO), 4.64 (m, OCH_2CHNO), 4.25 (m, $OC(O)OCH_2$), 1.22 (s, CH_3). ^{13}C NMR (75 MHz, $CDCl_3$, 77.16 ppm): δ 171.9, 165.2, 154.5, 147.0, 144.7, 137.4, 137.2, 128.8, 128.6, 128.5, 128.3, 76.7, 76.5, 68.7, 62.0, 60.0, 46.8, 46.7, 17.6. IR (neat, cm^{-1}): 3100–2800 (br), 1746 (s), 1497 (w), 1470 (m), 1454 (m), 1400 (m), 1377 (m), 1236 (s), 1140 (s), 974 (s), 909 (s), 864 (w), 785 (m), 729 (s), 698 (s). T_g = 0.0 °C (-0.2 °C, onset). TGA in N_2: 200–320 °C, 85% mass loss; 320–500 °C, 5% mass loss; 10% mass remaining above 500 °C

Conjugate 2. Yield = 52 mg, 76%. $M_{n,\,NMR}$ = 4,200 g/mol. ^{1}H NMR (300 MHz, CD_3OD, 4.78) δ 7.45 (br, HC=NO), 7.26 (br, OBn–ArH), 6.71 (br, HC=NO), 5.05 (s, OBn–CH_2), 4.92 (m, OCH_2CHNO), 4.62 (m, OCH_2CHNO), 4.37 (m, CH_2COOH), 4.22 (m, $OC(O)OCH_2$), 4.34 (m, CCH_2OH), 1.18 (s, CH_3). ^{13}C NMR (75 MHz, D_2O): δ 174.2, 155.7, 150.0, 148.2, 130.0, 72.8, 69.9, 62.8, 61.0, 47.6, 17.9. IR (neat, cm^{-1}): 3700–3100 (br), 3020–2840 (br), 1738 (s), 1601 (s), 1458 (m), 1406 (m), 1236 (s), 1142 (s), 1059 (m), 1024 (m), 968 (m), 922 (w), 883 (w), 866 (w), 785 (m), 698 (w). T_g = 76.0 °C (-71.0 °C, onset). TGA in N_2: 155–220 °C, 28% mass loss; 220–330 °C, 36% mass loss; 320–500 °C, 9% mass loss; 27% mass remaining above 500 °C.

4.3.7. Synthesis of alkene- and aldehyde-functional polycarbonates (PMAC-co-PMOC) and functionalization by consecutive aldehyde-aminooxy and thiol-ene "click" reactions

$PMAC_{15}$ (20 mg, 0.10 mmol for repeat units, 1 equiv) was dissolved in DCM (2.0 mL), and the solution was cooled to -78 ºC (dry ice/acetone cooling bath). Ozone was bubbled through 7 the cooled solution. After the allotted period of time (3 and 5 min), N_2 was then bubbled through for 10 min., and then dimethyl sulfide (37 μL, 31 mg, 0.50 mmol, 5 equiv) was added. The reaction was slowly allowed to warm to room temperature and stir overnight. The resulting PMAC-*co*-PMOC solution in DCM was mixed with aminooxy compound (*O*-benzylhydroxylamine, 0.20 mmol) and NaOAc (0.40 mmol) in MeOH (5.0 mL). The mixture was stirred for 1.5 h at 45 ºC. The conjugate 3 was purified by precipitation into water.

A solution of conjugate 3 (20 mg, 5.5 μmol, 55 μmol for alkene functionalities), ethyl 2-mercaptoacetate (61 μL, 66 mg, 550 μmol), and DMPA (3.0 mg, 11 μmol) in 0.70 mL of DMSO was irradiated under UV irradiation (365 nm, 6 W) for 2 h. The reaction mixture was purified by dialysis (MWCO 6–8 kDa) in THF overnight. A viscous liquid was collected after the removal of solvent *in vacuo*.

Conjugate 3. Yield = 20 mg, 85%. $M_{n,\,NMR}$ = 3,600g/mol. ^{1}H NMR (300 MHz, DMSO-d6, 7.26 ppm): δ 7.49 (br, HC=NO), 7.32 (br, OBn–ArH), 6.86 (m, HC=NO), 5.84 (m, CH_{vinyl}), 5.29–5.13 (m, $CH_{2\text{-}vinyl}$), 5.08 and 5.02 (s, OBn–CH_2), 4.85 and 4.66 (s, OCH_2CHNO), 4.57 (s, OCH_2CHCH_2), 4.23 (m, $OC(O)OCH_2$), 1.17 (s, CH_3).

Conjugate 4. Yield = 19 mg, 76%. $M_{n,\,NMR}$ = 4,600 g/mol. ^{1}H NMR (300 MHz, $CDCl_3$, 7.26 ppm) δ 7.47 (br, HC=NO), 7.34 (br, OBn–ArH), 6.75 (br, HC=NO), 5.86 (m, CH_{vinyl}), 5.33–5.33 (m, $CH_{2\text{-}vinyl}$), 5.12 and 5.09 (s, OBn–CH_2), 4.94 and 4.69 (s, OCH_2CHNO), 4.62 (s, OCH_2CHCH_2), 4.28 (m, $OC(O)OCH_2$), 4.23–4.14 (m, $OCH_2CH_2CH_2S$ and OCH2CH3), 3.20 (s, $SCH_2C(O)O$), 2.69 (m, $OCH_2CH_2CH_2S$), 1.94 (m, $OCH_2CH_2CH_2S$), 1.25 (m, CH_3 and OCH_2CH_3).

4.4. Conclusions

In summary, we have developed aldehyde-functional PCs *via* ozonolysis and reductive work-up of allyl-functional PCs. Ozone efficiently cleaves the double bonds without damage to the PC backbone. The resulting aldehydes were functionalized with aminooxy compounds under mild conditions. Furthermore, alkene- and aldehyde-bearing PCs were prepared by partial ozonolysis and functionalized by consecutive aldehyde–aminooxy and thiol–ene "click" reactions in an orthogonal fashion. Although we demonstrated a few examples, aldehyde-functional PCs are potentially excellent platforms for divergent research directions, due to their capability to form various conjugates *via* combinations of oxime, hydrazone, and/or Schiff base linkages with aldehydes and also thioether or other linkages to the alkenes.

CHAPTER V

A VINYL ETHER-FUNCTIONAL POLYCARBONATE AS A TEMPLATE FOR MULTIPLE POSTPOLYMERIZATION MODIFICATIONS

5.1. Introduction

There has been constant interest in development of functional polymers due to their lower cost, easier processibility, and diverse properties. In particular, polymers bearing reactive functional groups provide unique opportunity, since modulation of functionalities at the molecular level by postpolymerization modification helps tune material properties and widens potential range of applications. Hence, introductions of new functionalities to polymers have been widely investigated.

Vinyl ether is an interesting functional group, as it has an electron-rich double bond due to an adjacent electron-donating oxygen, which helps the formation of a stable carbocation next to the oxygen.[135] Although the majority of applications of vinyl ethers are as monomers for cationic polymerizations[136] and radical copolymerizations, this highly-reactive functional group can also undergo a variety of reactions, including acetalization, thioacetalization, thiol-ene reaction, hydrolysis, and so on. One of the advantages of the vinyl ether functionality is its capability to form both stable covalent bonds as well as dynamic covalent bonds. While thiol-ene reactions with various thiols yield robust thioether linkages, acetalizations with alcohols can also provide acid-labile acetal bonds. Therefore, this exceptional reactivity enables a variety of applications, ranging from radiation curable coatings *via* formation of poly(vinyl ethers) to conjugation

and stimuli-responsive release of biologically-active molecules *via* acetal or thioacetal linkages.

To date, there are few studies that have investigated vinyl ether-bearing polymers. In 2011, Frey and Wurm *et al*. developed vinyl ether-functionalized poly(ethylene glycol) (PEG) and demonstrated their functionalization *via* two postpolymerization modifications: thiol-ene reaction and acetal formation.[92] Meng, Zhong, and coworkers reported vinyl ether-functionalized PEG-*b*-poly(acrylic acid) to conjugate paclitaxel (PTX) *via* its acid-labile acetal linkage and demonstrated pH-dependent release of PTX from self-assembled polymeric micelles.[137] However, the non-degradable backbone of both polymers could limit further utilization for biomedical applications.

Our group recently developed a vinyl ether-functionalized polyphosphoester (PPE) to tackle this degradability issue.[138] However, difficulty in purification of the cyclic phosphotriester monomer as well as the instability of PPE backbone under acetalization conditions with nucleophiles (alcohols or thiols) and an acid catalyst (*p*-toluenesulfonic acid, PTSA) impede further applications. In this study, we introduced vinyl ether moieties, which have been proven to be a versatile functionality for multiple postpolymerization modifications on the more stable but still degradable polycarbonate (PC) backbones. Well-defined PCs can be prepared *via* metal-free organocatalytic ring-opening polymerization (ROP) of functional cyclic carbonate monomers,[100,133,139] and a variety of functionalities can also be introduced by postpolymerization modifications.[107,140] We hypothesized that the stability of the vinyl ether functionality under basic conditions allows the organobase-catalyzed ROP of functional monomers,

which has been previously tested with vinyl ether-functionalized cyclic phosphotriester monomer.[138] Hence, we designed and synthesized a novel vinyl ether-functionalized cyclic carbonate monomer, 5-methyl-5-((2-vinyloxy)ethyl)oxycarbonyl-1,3-dioxan-2-one (MVEC). The organobase, 1,8-diazabicyclo[5.4.0]undec-7-ene (DBU), successfully initiated ROP of this synthesized monomer and yielded well-defined vinyl ether functional homo-/co-polymers. Multiple conjugation chemistries — acetalization, thio-acetalization, and thiol-ene reactions — were demonstrated as postpolymerization methods. In order to establish its capability for stimuli-responsive drug delivery, the amphiphilic block copolymer, mPEG-*b*-PMVEC, was synthesized and model hydroxyl-containing drug compounds were conjugated *via* acetal linkages. After conducting the characterization of their self-assembled nanostructures in aqueous solutions, cleavage kinetics of acetal bonds were studied using ^{1}H NMR spectroscopy.

5.2. Results and Discussion

5.2.1. Monomer design and synthesis

Six-membered cyclic carbonate monomers, the most commonly used monomers for the preparation of PCs by ROP, can be prepared by cyclization of 1,3-diols in various ways.[100] Among them, 2,2-bis(hydroxymethyl)propionic acid (bis-MPA)-based cyclic carbonate monomers have been well-studied due to the facile introduction of functionalities to the carboxylic acid through ester or amide linkages, taking advantage of different reactivity between acid and alcohol of bis-MPA. A vinyl ether-functionalized cyclic carbonate monomer, 5-methyl-5-((2-vinyloxy)ethyl)oxycarbonyl-1,3-dioxan-2-one (MVEC), **2**, was synthesized by a well-established two-step procedure from bis-

MPA.[99,108] Esterification of bis-MPA with 2-chloroethyl vinyl ether, followed by cyclization using ethyl chloroformate, yielded cyclic carbonate monomer with vinyl ether functionality, MVEC, **2**, in 48% overall yield (Scheme 5.1). At the beginning, the esterification step suffered from low reaction yields (~20%) due to the low reactivity of the alkyl chloride. Sodium iodide was added to compensate for the low reactivity by *in situ* halogen exchange reaction, which improved reaction yields to up to 78%. Although the cyclization step was straightforward in moderate yield (~60%), careful purification was necessary since small amounts of impurities hindered crystallization of MVEC. The crude MVEC was yellowish liquid and was not readily crystallized or solidified. After isolation by flash chromatography, the resulting MVEC was slowly crystallized *in vacuo*. Drying MVEC was easier in solid state. Removal of water is imperative to obtain well-defined PCs *via* ROP of cyclic carbonate monomers since hydroxyl chain-end produced from decarboxylation of water-initiated chain-end can yield telechelic PCs. ^{1}H and ^{13}C NMR spectra (Figure 5.1 and 5.2) and electrospray ionization mass spectrometry (ESI-MS) results were consistent with the structure of monomer.

MVEC, **2**, is an interesting molecule due to the versatile reactivity due to both its vinyl ether as well as its cyclic carbonate functionality. It can participate in not only ROP through cyclic carbonate moiety but also cationic and radical polymerization through vinyl ether moiety. In addition, both functional groups can undergo postpolymerization modifications after corresponding polymerizations: crosslinking reaction[141] of cyclic carbonates, thiol-ene "click" reaction, acetalization, thioacetalization, hydrolysis of vinyl

ethers, *etc*.[138] In this study, we exploit this vinyl ether functionality for postpolymerization modification after ROP of the cyclic carbonate.

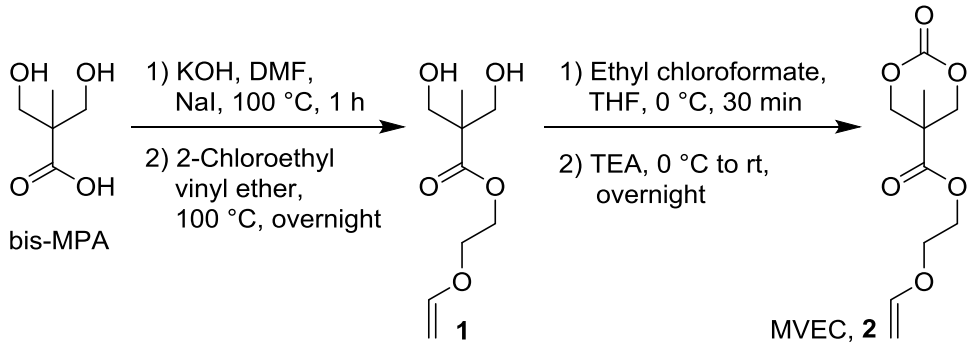

Scheme 5.1. Synthesis of vinyl ether-functionalized cyclic carbonate monomer, MVEC, 2.

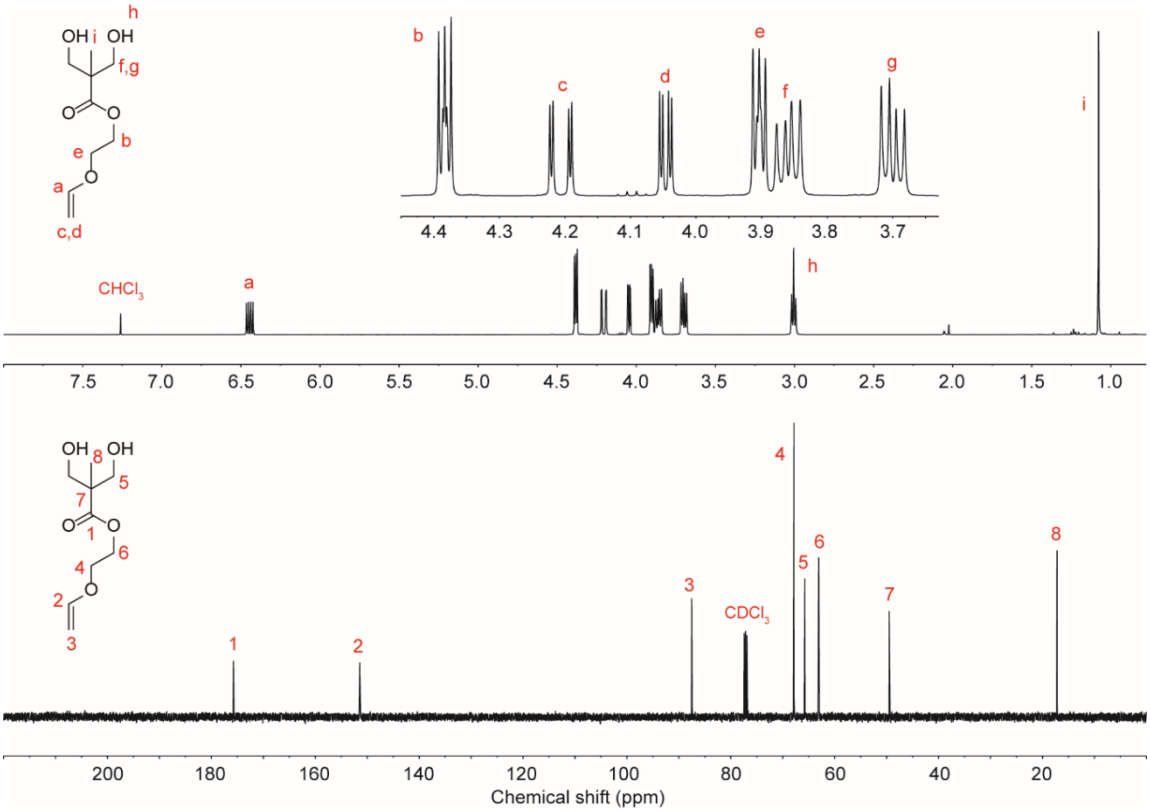

Figure 5.1. ^{1}H and ^{13}C NMR spectra ($CDCl_3$) of (2-vinyloxy)ethyl 2,2-bis(hydroxymethyl)propanoate.

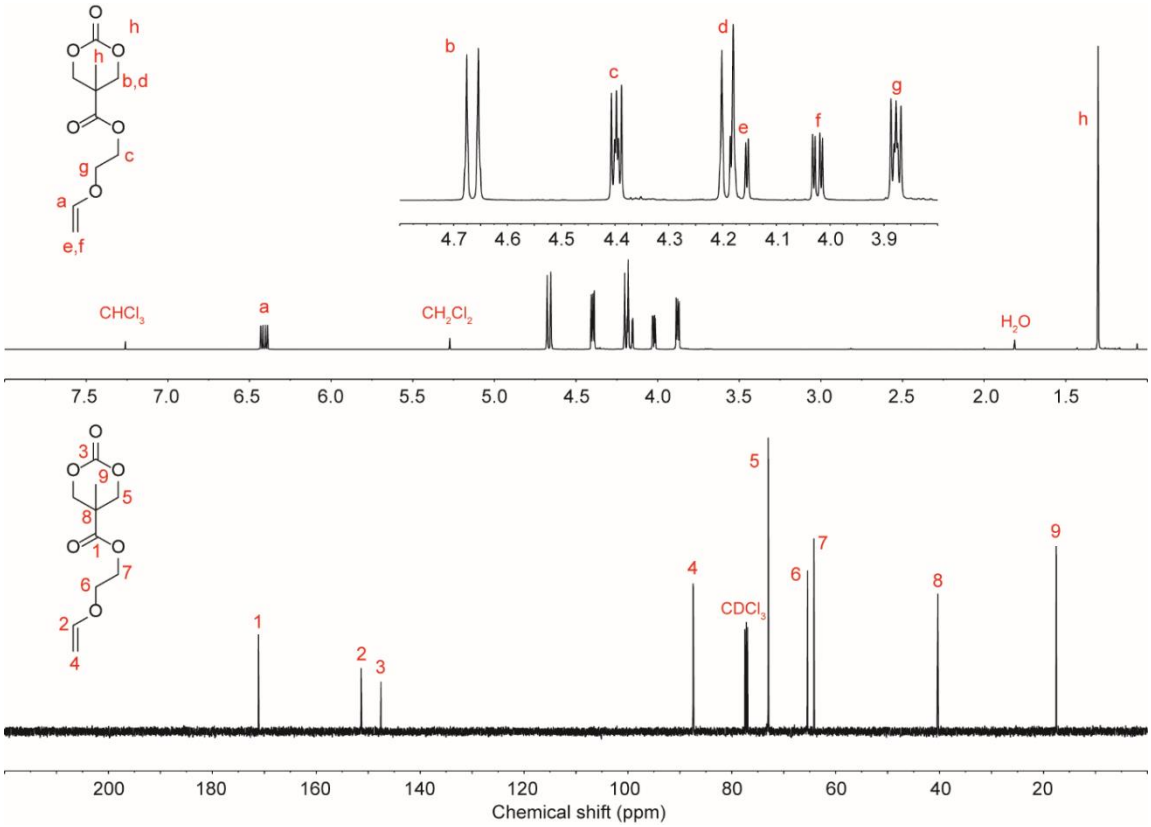

Figure 5.2. ^{1}H and ^{13}C NMR spectra ($CDCl_3$) of MVEC.

5.2.2. Organocatalytic ROP of MVEC, 2

Vinyl ether-functional PCs [poly(5-methyl-5-((2-vinyloxy)ethyl)oxycarbonyl-1,3-dioxan-2-one), PMVEC, **3**] were synthesized by organobase-catalyzed ROP of the functionalized six-membered cyclic carbonate monomer, **2**. The ROP of MVEC was conducted in a glovebox under similar conditions as we previously reported.[107,140] The living characteristics of organobase-catalyzed ROP were demonstrated by a kinetic study

in dichloromethane (DCM) solution of MVEC using benzyl-protected bis-MPA (Bn-MPA) as an initiator and DBU as a catalyst ($[MVEC]_0$ = 0.7 M in DCM, $[MVEC]_0$: [Bn-MPA] : [DBU] = 75:1:2). The semi-logarithmic plot of $[M]_0/[M]$ *vs*. time displayed pseudo-first-order kinetic behavior of ROP (Figure 5.3b). Also, a linear relationship between number average molecular weight (M_n) and monomer conversion indicated that degree of polymerizations (DPs) are pre-determinable (Figure 5.3c). The consistent low dispersities ($Đ_M \leq 1.10$) up to 83% monomer conversion evidenced minimal degree of transesterification of PC backbone during ROP. After the polymerizations were quenched by addition of a DCM solution of benzoic acid, residual monomer, DBU, and benzoic acid were removed by repetitive precipitations into methanol. By ^{1}H NMR spectroscopy, the ratios of numbers of vinyl protons (b, f, and g) and those of PC backbone (e and j) to those of initiator (a and c) were consistent, which indicates vinyl ethers remained intact during ROP and after quenching with benzoic acid (Figure 5.4).

The chemical availability of vinyl ether functionalities for postpolymerization modifications was verified using three types of reactions: thiol-ene "click" reaction, acetalization, and thio-acetalization.

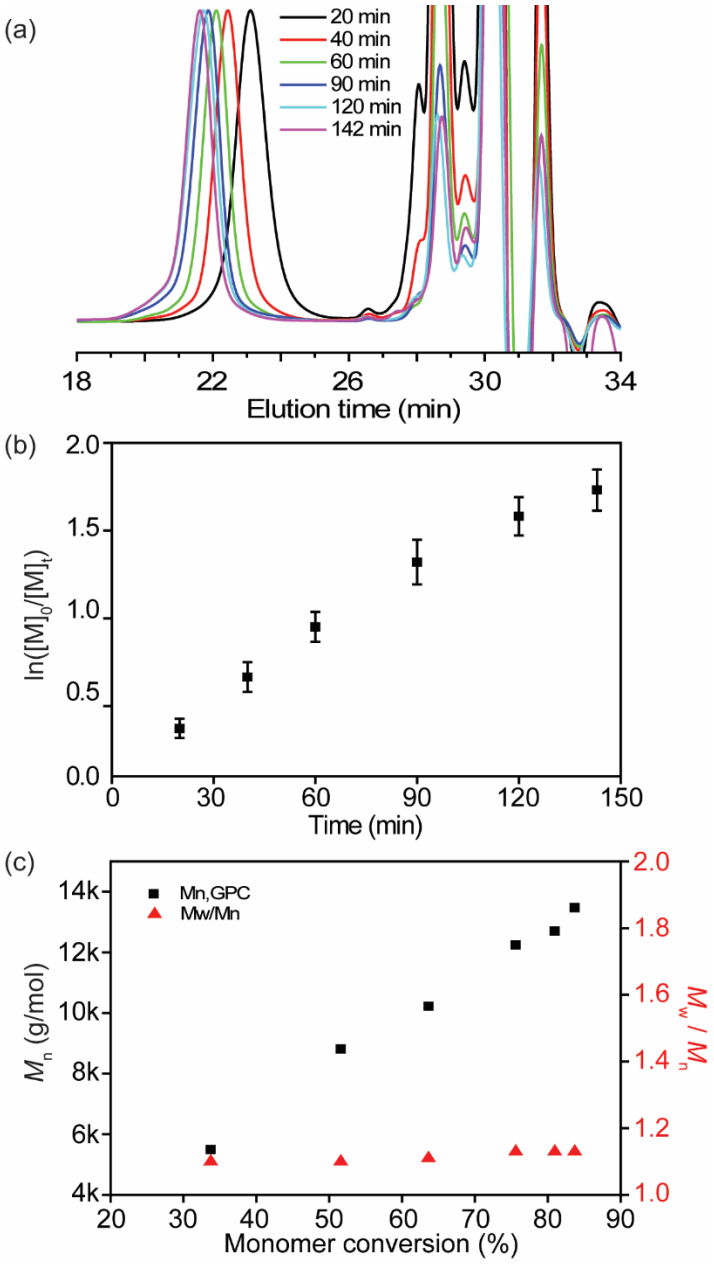

Figure 5.3. (a) GPC profiles (THF as eluent, 1 mL/min) as a function of polymerization time, for the ROP of MVEC; (b) Plot of $\ln([M]_0/[M])$ against time, obtained from ^{1}H NMR spectroscopy data; (c) Plot of number-average molecular weight (M_n) and dispersity ($Đ_M$, M_w/M_n) against % monomer conversion in the ROP of MVEC. *Conditions*: $[MVEC]_0$ = 0.7 M in DCM at 29 °C in the glovebox, $[MVEC]_0$: [Bn-MPA] : [DBU] = 75 : 1 : 2.

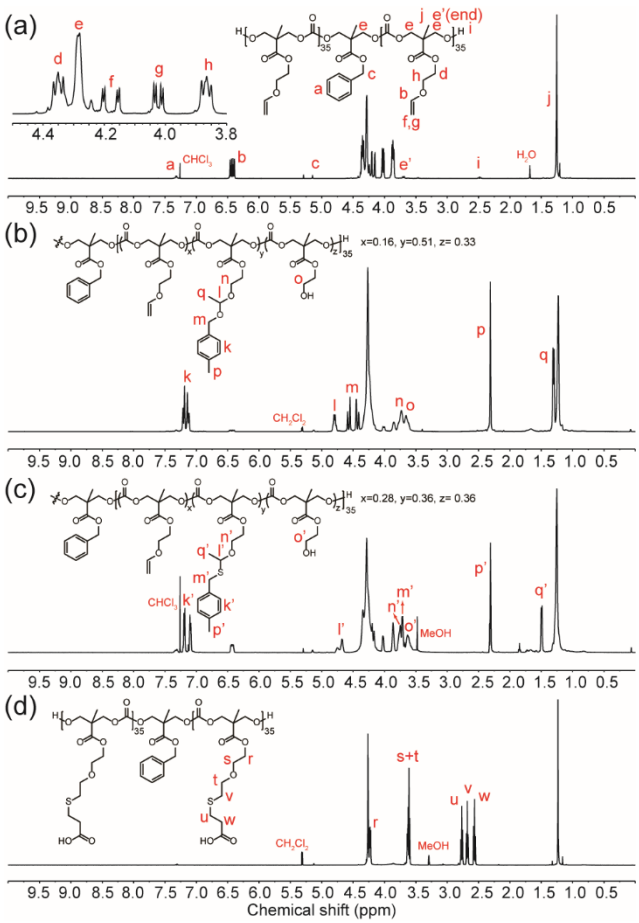

Figure 5.4. ^{1}H NMR spectra of (a) PMVEC, **3** (in $CDCl_3$), (b) after acetalization with 4-methylbenzyl alcohol, **4** (in CD_2Cl_2), (c) after thio-acetalization with 4-methylbenzyl mercaptan, **5** (in $CDCl_3$), (d) after thiol-ene reaction with 3-mercaptopropionic acid, **6** (in CD_2Cl_2/MeOD).

5.2.3. Acetalization and thio-acetalization of the vinyl ether side chain moieties of PMVEC with 4-methylbenzyl alcohol and 4-methylbenzyl mercaptan

Conjugation between the electron-rich vinyl ether moiety of PMVEC and hydroxyl- or thiol-bearing model compounds *via* formation of acetal or thioacetal linkages were demonstrated as postpolymerization modification methods. First, initial acetalization studies were conducted in THF-d_8 to monitor reaction progress by ^{1}H NMR

spectroscopy. ^{1}H NMR spectra were collected at a desired time while a mixture of 4-methylbenzyl alcohol, PMVEC, and PTSA in THF-d_8 was spinning in the NMR spectrometer at 19 °C (Figure 5.5). Formation of acetal linkages was monitored by disappearance of vinyl resonances (a and b) at 6.49 and 4.02 ppm, respectively, of PMVEC and appearance of methine proton (d) at 4.83 ppm and methyl protons (g) at 1.33 ppm of acetal group as well as benzyl protons (e) at 4.62 and 4.49 ppm of conjugated 4-methylbenzyl alcohol using ^{1}H NMR spectroscopy (Figure 5.5). Also, the chemical shift of the methylene proton next to the oxygen of vinyl ether group were changed from 3.85 to 3.75 ppm (from c to f in Figure 5.5). In addition, consumption of vinyl ether groups, calculated by the integral of the vinyl resonances at 6.52 ppm (a in Figure 5.5) at corresponding times divided by that of the initial polymer were plotted against reaction time, showed first order kinetics. With an exponential fit, the half-life of the vinyl ether moieties was estimated to *ca.* 70.6 min at these conditions (Figure 5.6). Because PMVEC, other reagents, and solvent were not dried before the acetalization, water impurities could cause hydrolysis of vinyl ether and resulting acetal functionalities competing with acetalization reaction. Therefore, consumption of vinyl ether groups was not directly correlated to the conversion of acetal linkages. Considering the competition of acetalization and hydrolysis, the reaction time needs to be monitored to control the desired amounts of vinyl, acetalized, and hydrolyzed moieties. In order to prevent further hydrolysis, the reaction was quenched by adding an excess triethylamine (TEA) and unreacted alcohol compounds, acid catalyst, and TEA were removed by dialysis against THF. Figure 1b shows ^{1}H NMR spectrum of PMVEC after acetalization with 4-

methylbenzyl alcohol and purification by dialysis. Precipitations of resulting polymers into organic solvents such as methanol or diethyl ether did not ensure the complete removal of acid catalyst, which led to insoluble materials after concentration *in vacuo*. Residual PTSA likely catalyzed cross-linking reactions *via* trans-acetalization, or acetalization of remaining vinyl ethers with hydrolyzed hydroxyl groups on polymer backbone.[92,138] When vinyl ether moieties of the resulting acetalized polymers were fully consumed, we did not encounter unexpected insoluble materials even after long-term storage in ambient conditions.

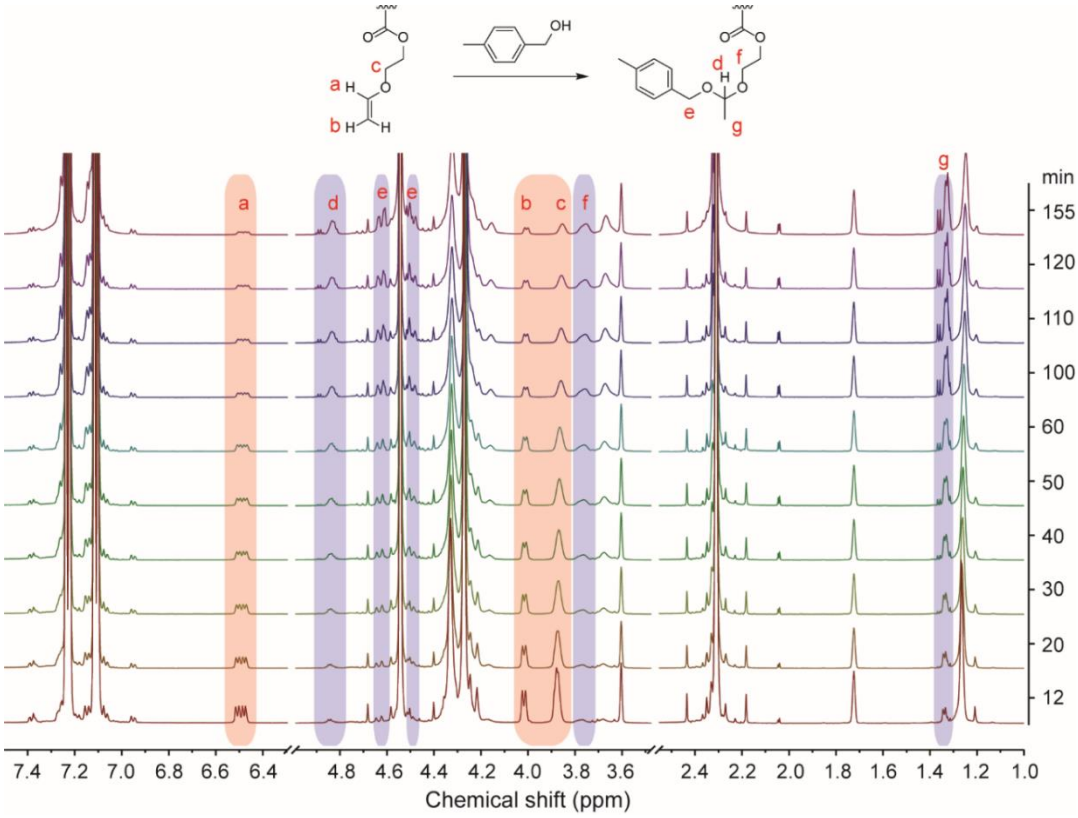

Figure 5.5. Reaction of PMVEC with 4-methylbenzyl alcohol in the presence of PTSA in THF-d_8. For clarity, the relevant part of the spectra are shown.

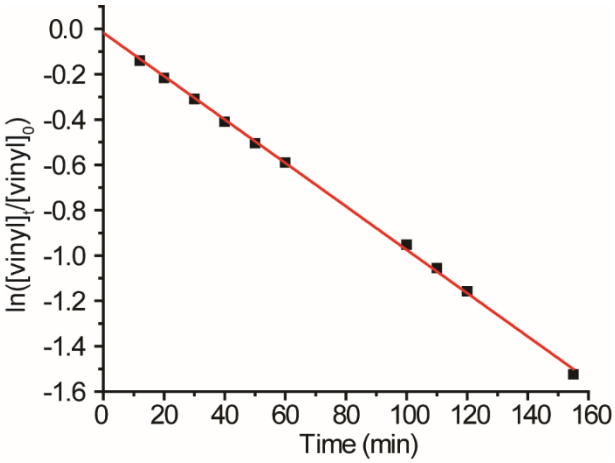

Figure 5.6. Consumption of vinyl ether groups versus time for the reaction of PMVEC with 4-methylbenzyl alcohol. *Conditions*: $[PMVEC_{50}]_0 = 3.8$ mM, $[4\text{-methylbenzyl alcohol}]_0 = 1.88$ M, [PTSA] = 1.18 mM, 19 °C. or *Conditions*: $[PMVEC_{50}]_0 = 3.8$ mM in THF-d_8 at 19 °C. [alkene] : [4-methylbenzyl alcohol]$_0$: [PTSA] = 1 : 10 : 0.01.

The conversions of vinyl ethers to acetals were calculated by chain-end analysis using ^{1}H NMR spectroscopy. The conversion of vinyl ethers to acetal linkages after 2 h reaction was 51%, with 16% of intact vinyl ethers and 33% of hydroxyl groups from the competing hydrolysis reaction of vinyl ethers and resulting acetals (Figure 5.4b). It is noteworthy that all polymers and reagents were not dried for postpolymerization modifications and all conjugations were not conducted in an inert atmosphere to demonstrate suitability for practical applications. The acetal conversion percentages (*ca.* 51%) of PC-based polymers, **4**, were superior to polyphosphoester-based system (*ca.* 18%)[138] since the more stable PC backbone allows for prolonged reaction time.

The thio-acetalization with the model thiol compound, 4-methylbenzyl mercaptan, was also conducted under the similar conditions to acetalization. The conversion of vinyl ethers to thioacetals after 2 h reaction was 36%, with 28% of intact vinyl ethers and 36%

of hydroxyl groups, which were obtained *via* chain-end analysis of ^{1}H NMR spectrum (Figure 5.4c). Comparing the conversion of vinyl ether groups in the two reactions, acetalization (*ca*. 51%) was more efficient than thioacetalization (*ca*. 36%), which might be due to the better nucleophilicity of oxygen than sulfur in the polar aprotic solvent, THF. Although we did not optimize the reaction conditions for thio-acetalization, the conversion was already higher than polyphosphoester-based system (*ca*. 8%).[138]

5.2.4. Thiol−ene "click" reaction of the vinyl ether side chain moieties of PMVEC with 3-mercaptopropionic acid

The thiol-ene "click" reaction was also employed as a postpolymerization modification method to functionalize vinyl ether functionalities of PMVEC to form stable and robust thioether linkages. Previous reports have demonstrated that radical-mediated thiol-ene reaction conditions are compatible with PC backbones.[107,133,139] Conjugation between vinyl ether groups on PMVEC and model thiol, 3-mercaptopropionic acid, was initiated by UV irradiation (365 nm, 6 W) in the presence of a photoinitiator, 2,2-dimethoxy-2-phenylacetophenone (DMPA). Excess amount (10 equiv relative to the vinyl ether functionalities) of thiols was applied to avoid radical-mediated cross-linking of polymers. Formation of conjugate **6** was confirmed by monitoring disappearance of vinyl resonances (b, f, and g) at 6.40, 4.18, and 4.02 ppm, respectively, of PMVEC (Figure 5.4a) and appearance of α proton to the carboxylic acid (w) at 2.57 ppm (Figure 5.4d) and protons of the thio-ether bonds (u and v) at 2.77 and 2.68 ppm, respectively, (Figure 5.4d) using ^{1}H NMR spectroscopy. Also, the signal for the methylene proton resonances of the side chain shifted upfield from (d) at 4.35 ppm and (h) at 3.87 ppm to (r) at 4.23 ppm and

(s) at 3.62 ppm, respectively (Figure 5.4a and d). The ^{1}H NMR integration indicated that conjugation yield was quantitative.

5.2.5. Synthesis of block copolymers and their postpolymerization modifications

The di- and tri-block copolymers containing PMVEC block(s) were synthesized to show versatility of PMVEC as a segment for various block copolymers. First, the amphiphilic diblock copolymer, *α*-methoxy poly(ethylene glycol)-*block*-PMVEC (mPEG-*b*-PMVEC), **7**, was synthesized using mPEG-OH 5 kDa ($mPEG_{5K}$-OH or $mPEG_{113}$-OH) as a macroinitiator and DBU as an organobase catalyst ([$mPEG_{5K}$-OH] : [DBU] : [MVEC] = 1:1:20, $[MVEC]_0$ = 0.5 M in DCM, Scheme 5.2). After the desired time, the polymerization was quenched by adding a DCM solution of benzoic acid and the resulting diblock copolymer was isolated by precipitation into diethyl ether. ^{1}H NMR spectrum of mPEG-*b*-PMVEC showed proton resonances of PMVEC (as in Figure 5.4a) as well as those of mPEG (Figure 5.7). Degrees of polymerization (DP_n) calculated by chain-end analysis by ^{1}H NMR spectroscopy was in agreement with the monomer conversion calculated by ^{1}H NMR spectroscopy. The distinct peak shift on GPC profiles of the macroinitiator and block copolymer verified successful chain extension of PMVEC block from $mPEG_{5K}$-OH (Figure 5.8). The subsequent acetalization of the resulting block copolymer with 4-methylbenzyl alcohol afforded the amphiphilic diblock copolymer with pendant acetal functionalities. After quenching the reaction with TEA, dialysis, and precipitation, ^{1}H NMR spectrum of isolated polymer was consistent with that of model acetalization reaction of PMVEC.

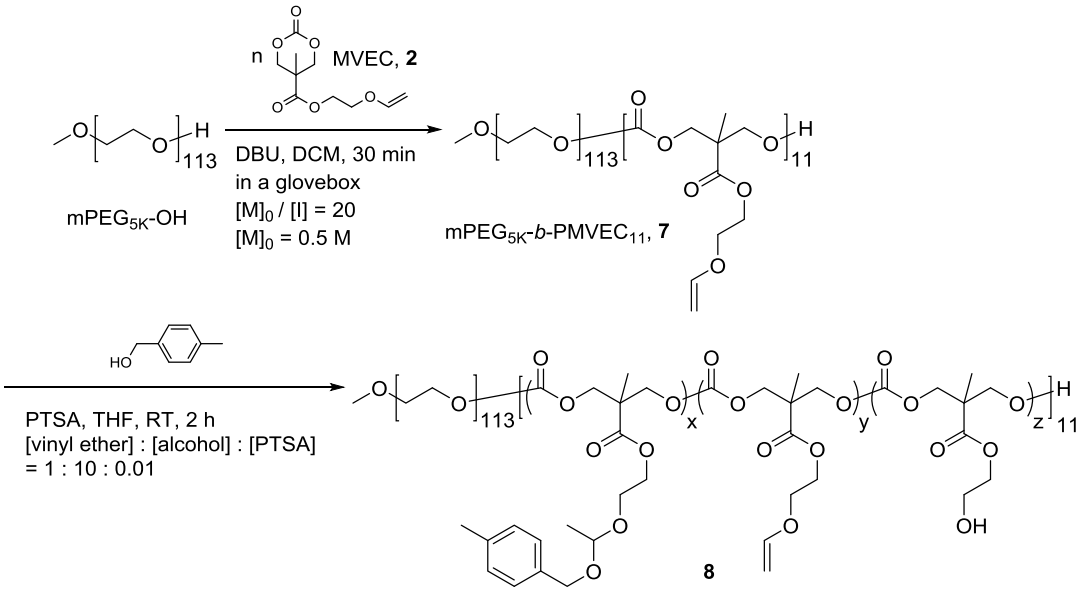

Scheme 5.2. Synthesis of mPEG-*b*-PMVEC and its functionalization *via* acetal formation with a model hydroxyl compound, 4-methylbenzyl alcohol.

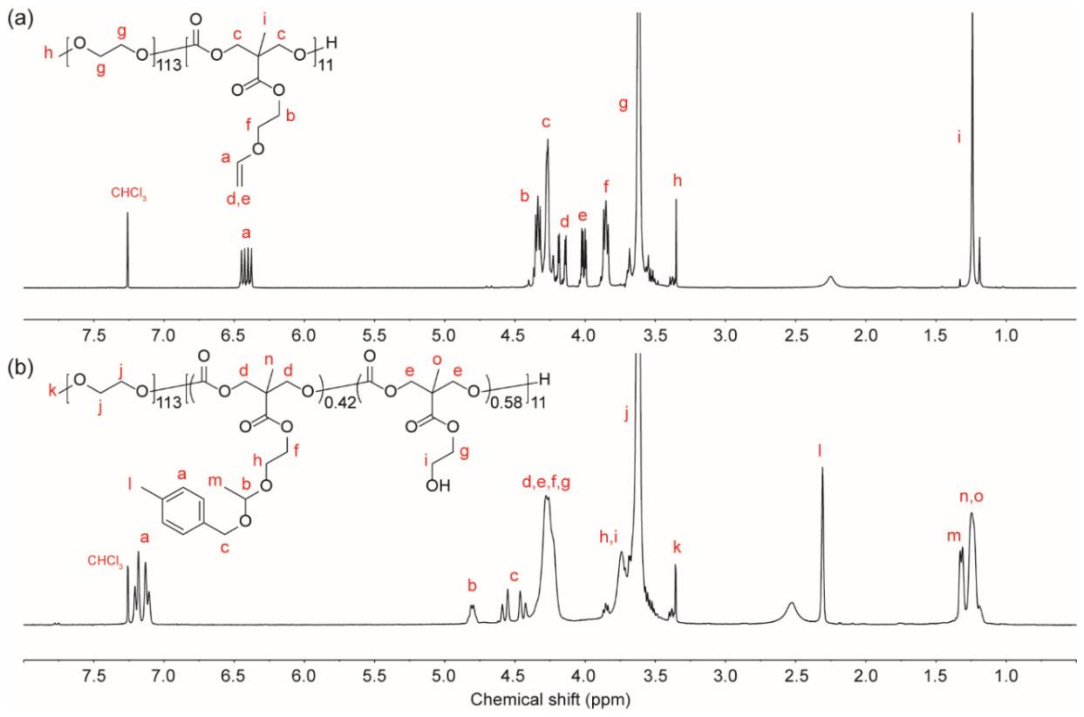

Figure 5.7. ^{1}H NMR spectra of (a) diblock copolymer, mPEG$_{113}$-*b*-PMVEC$_{11}$, **7**, and (b) its acetal-functionalized, **8**.

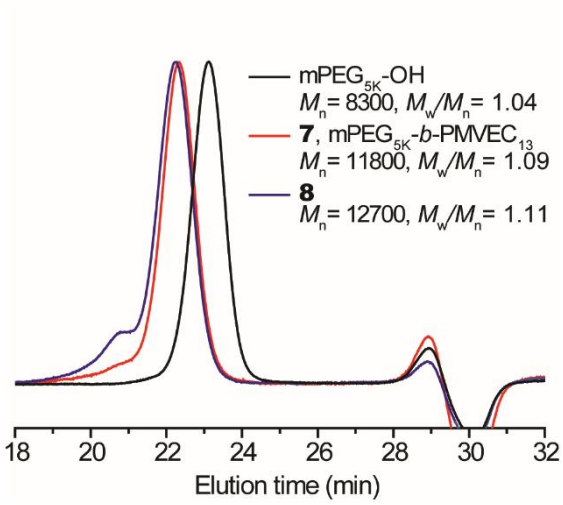

Figure 5.8. GPC traces (DMF as eluent, 1 mL/min) of macroinitiator ($mPEG_{113}$-OH), **7** ($mPEG_{113}$-*b*-$PMVEC_{11}$), and **8** (the acetal-functionalized $mPEG_{113}$-*b*-$PMVEC_{11}$).

In addition, hydroxyl-telechelic triblock copolymers were prepared. One-pot sequential ROP of MBC and then MVEC were conducted with DBU as a catalyst and Bn-MPA as a diol initiator affording triblock copolymer, HO-PMVEC-*b*-PMBC-*b*-PMVEC-OH. Reversed order of addition of two monomers yielded HO-PMBC-*b*-PMVEC-*b*-PMBC-OH (Scheme 5.3). Vinyl ether groups on the triblock copolymers were functionalized with various thiol compounds *via* thiol-ene reaction to introduce new functionalities. We intended to incorporate charged thiols, 3-mercaptopropionic acid, cysteamine hydrochloride, and L-cysteine hydrochloride monohydrate, through robust thioether linkages to achieve differently charged block copolymers (Scheme 5.4 and Figure 5.9).

Synthesis of di- and tri-block copolymers *via* chain extension experiments demonstrated that a variety of PMVEC-based polymers can be synthesized with other

cyclic monomers for ROP such as cyclic carbonates, lactide, and ε-caprolactone, *etc*. Also, postpolymerization modifications of resulting block copolymers will further increase the diversity of PMVEC-based macromolecular structures.

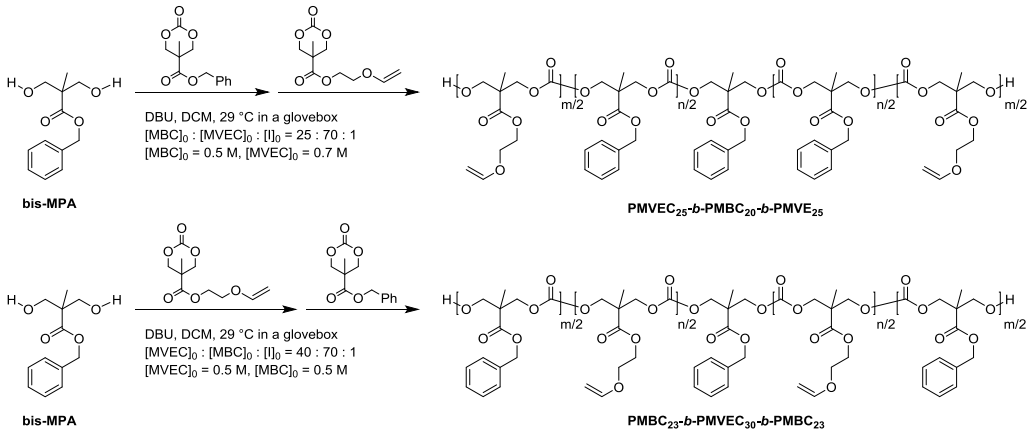

Scheme 5.3. Synthesis of telechelic triblock copolymers.

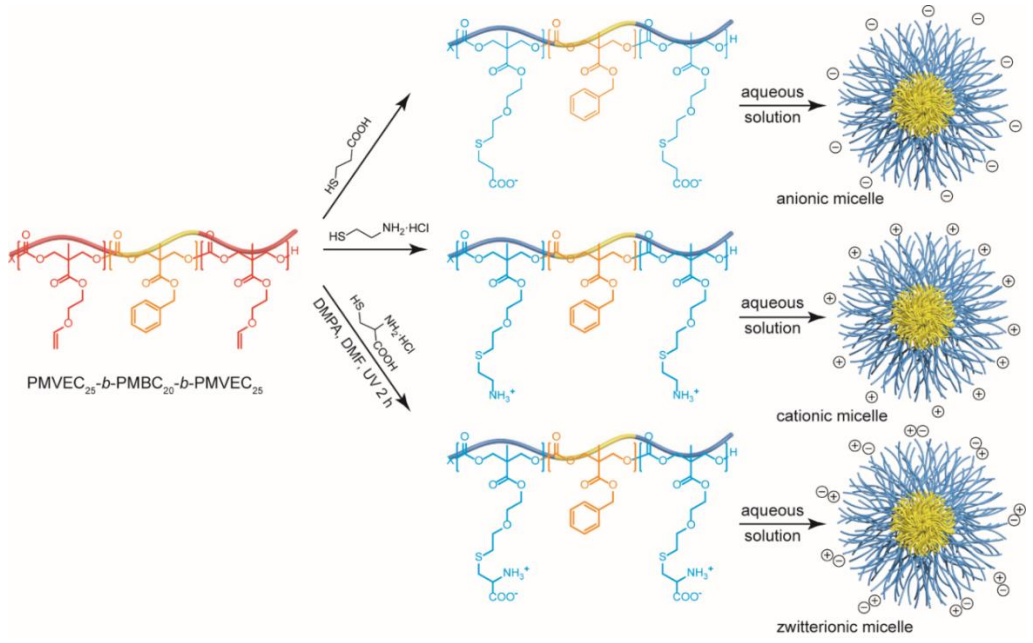

Scheme 5.4. Preparation of functionalized ABA-type block copolymers by thiol-ene reaction of $PMVEC_{25}$-*b*-$PMBC_{20}$-*b*-$PMVEC_{25}$ with charged thiols.

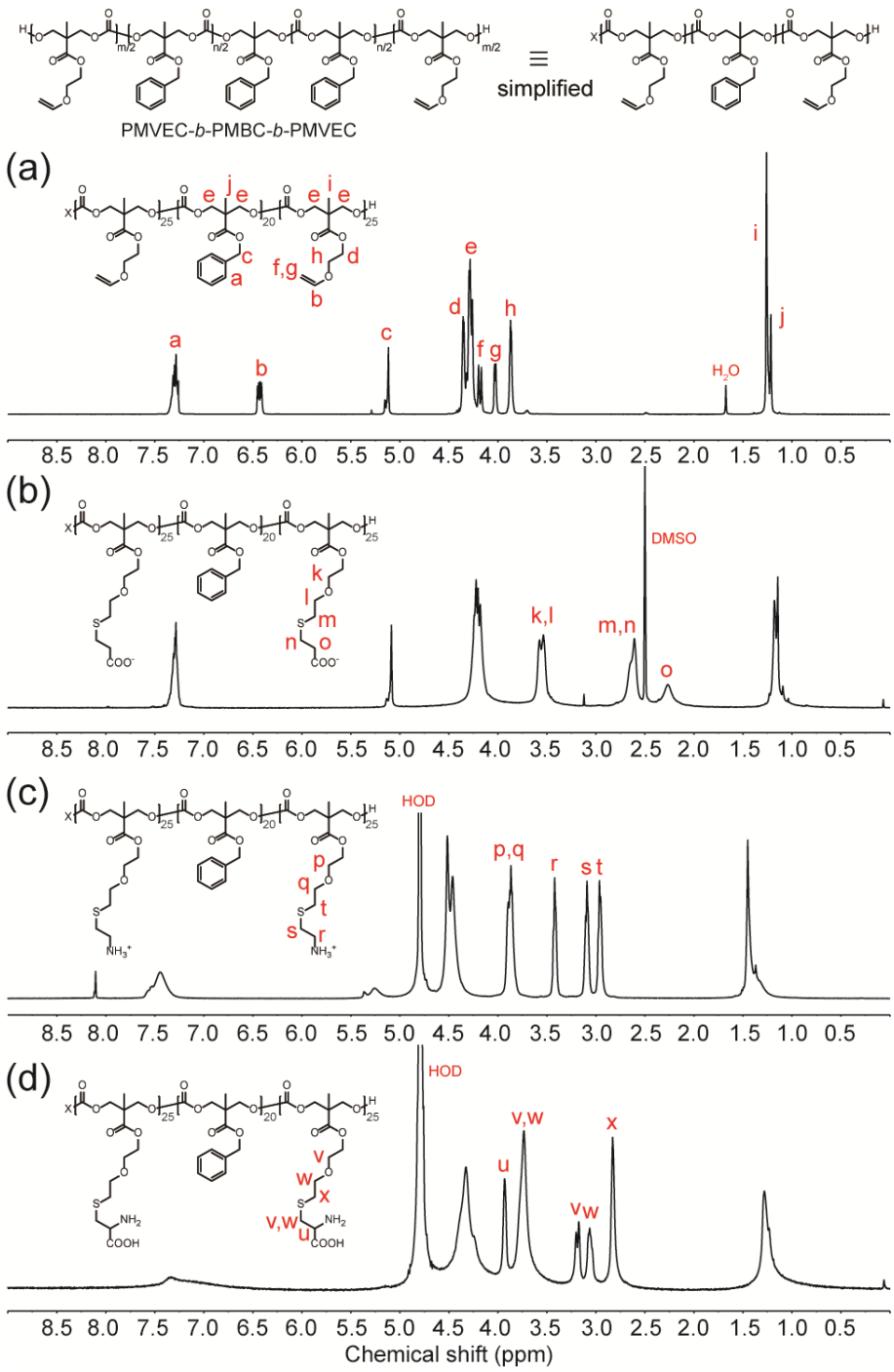

Figure 5.9. ^{1}H NMR spectra of $PMVEC_{25}$-*b*-$PMBC_{20}$-*b*-$PMVEC_{25}$ and its functionalized polymers; (a) in $CDCl_3$, (b) in DMSO-d_6, (c) in DMF-d_7/D_2O (9/1), and (d) in D_2O.

5.2.6. Self-assembly of amphiphilic block copolymers

The self-assembled polymeric nanostructures were readily prepared by direct dissolution of synthesized amphiphilic block copolymers in suitable buffers. First, self-assembly behaviors of mPEG-*b*-PMVEC (**7**), acetal-functionalized mPEG-*b*-PMVEC (**8**), and mPEG-*b*-poly(5-methyl-5-(2-hydroxyethyloxy)carbonyl-1,3-dioxan-2-one (PMHEC) were studied by dynamic light scattering (DLS), ζ-potential measurements, transmission electron microscopy (TEM) (Figure 5.10). PMHEC is the hydrolyzed block of PMVEC or acetalized PMVEC. The number-averaged hydrodynamic diameters of the micellar nanostructures of **7**, **8**, and mPEG-*b*-PMHEC, in buffer solutions measured by DLS were 28 ± 7, 16 ± 5, 9 ± 3 nm, respectively, in acetate buffer (pH 5.0), and 28 ± 8 nm (micelles of **7**) and 16 ± 3 nm (micelles of **8**) in 1X PBS (pH 7.4), with narrow and monomodal size distribution (Figure 5.10a). The spherical shapes of micelles were confirmed by TEM (Figure 5.10b,c). Hydrodynamic diameters of micelles gradually decreased depending on the amount of hydroxyl functionalities, which might be attributed to the increased hydrophilicity of core-forming PC blocks by hydrolysis. Also, critical micelle concentration (CMC) of micelles of mPEG-*b*-PMHEC was higher than those of **7** and **8**, as expected. Although we did not measure CMCs of amphiphilic block copolymers, DLS measurement of micelles of mPEG-*b*-PMHEC was not feasible under the concentration of 5 mg/mL. On the other hand, hydrodynamic diameters of micelles of **7** could be measured at the concentration of 0.25 mg/mL. The PEG corona of resulting micelles makes the ζ-potentials almost neutral, -3.2 ± 0.3, -2.6 ± 0.5, 0.23 ± 1.1 mV,

respectively, in acetate buffer (pH 5.0), and -9.6 ± 2.3 mV (micelles of **7**) and -6.6 ± 2.9 mV (micelles of **8**) in 1X PBS (pH 7.4).

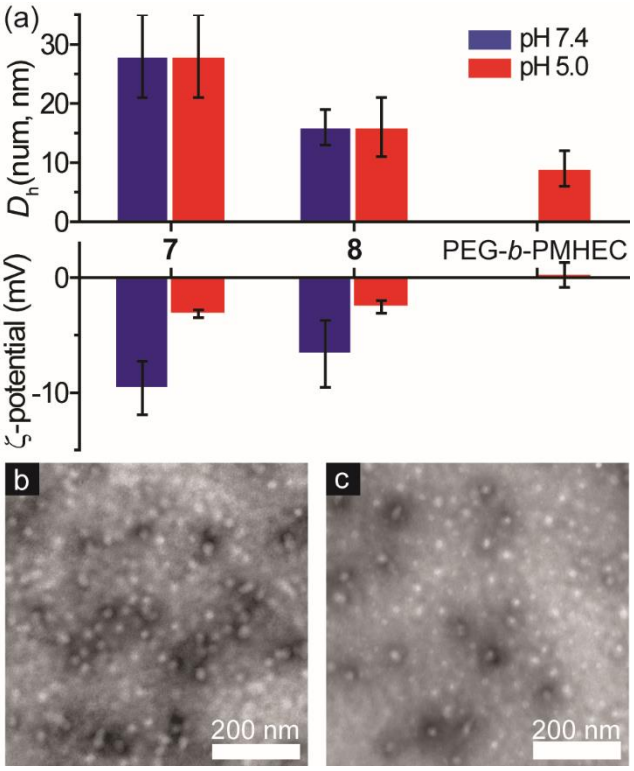

Figure 5.10. Self-assembly of amphiphilic diblock copolymers. (a) Number-averaged (D_h (num)) hydrodynamic diameters and ζ–potential values of **7** ($mPEG_{113}$-*b*-$PMVEC_{11}$), **8** (the acetal-functionalized $mPEG_{113}$-*b*-$PMVEC_{11}$), and $mPEG_{113}$-*b*-$PMHEC_{11}$. (b, c) Bright field TEM images of the block copolymer, **7**, micelles in pH 7.4 (b, 1X PBS) and pH 5 (c, acetate) buffer solutions. Scale bar = 200 nm.

5.2.7. Monitoring cleavage of acetal moieties

The cleavage of acetal functionalities in acidic conditions were monitored using ^{1}H NMR spectroscopy for quantitative analysis of cleavage kinetics. During this process, the residual vinyl ether functionalities can undergo further acetalization with hydrolyzed hydroxyl groups on the PC backbone and/or cleaved 4-methylbenzyl alcohol in acidic

conditions, which could complicate the analysis. Therefore, available vinyl ether groups were completely consumed during acetal formation of $mPEG_{113}$-*b*-$PMVEC_{13}$ with 4-methylbenzyl alcohol, even though it could diminish the final acetal contents *via* competing hydrolysis reaction. Since the acetal-functional mPEG-*b*-PMVEC self-assembles into the micelles in aqueous solution and acetal moieties reside in the core of micelles, *in situ* ^{1}H NMR monitoring of acetal protons is challenging. Instead, an aliquot of micellar solution was collected and purified by dialysis against nanopure water to remove small molecular impurities before ^{1}H NMR analysis in CD_2Cl_2 to observe entire blocks. Two samples were prepared in acetate buffers (pH 4 and 5) and kept in 37 °C shaker. As expected, decrease of acetal content was faster in the more acidic solution. Half-lives of acetal cleavage were *ca*. 10 days at pH 4 and *ca*. 27 days at pH 5, respectively (Figure 5.11). Interestingly, our systems showed slower cleavage rates compared to previously-reported systems. Although we do not have experimental evidence of these phenomena, slower degradation might be attributed to formation of more compactly-aggregated core, which could provide protection against the surrounding acidic environment. The slow cleavage rates will enable more sustained and controlled release of polymeric nanostructure-conjugated therapeutics compared to physically-encapsulated ones, which could reduce patient side effects caused by premature release of payload as well as decrease frequency of dosage for better patient compliance and lower cost of treatment. In addition, after the release of compounds under acidic conditions, remaining hydroxyl groups will further enhance hydrophilicity of resulting polymer, which might help the clearance of polymers from body.

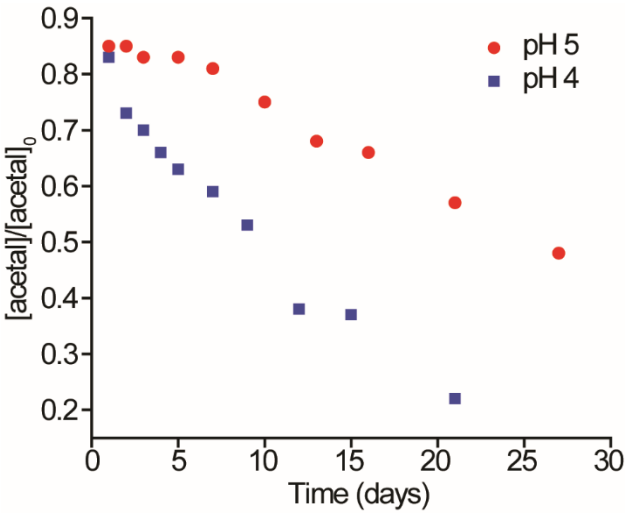

Figure 5.11. Cleavage of acetal moieties within the micelles of acetal functionalized $mPEG_{113}$-*b*-$PMVEC_{11}$, **8**, with 4-methylbenzyl alcohol in pH 4 and pH 5 acetate buffer solutions.

5.3. Experimental Section

5.3.1. Materials

Benzyl alcohol and 1,8-diazabicyclo[5.4.0]undec-7-ene (DBU) were dried over CaH_2, distilled, and stored under inert atmosphere. Tetrahydrofuran (THF), *N,N*-dimethylformamide (DMF), and dichloromethane (DCM) were purified by passage through solvent purification system (JC Meyer Solvent Systems) and used as dried solvents. Benzyl 2,2-bis(hydroxymethyl)propanoate (Bn-MPA) and 5-methyl-5-benzyloxycarbonyl-1,3-dioxan-2-one (MBC) were synthesized as reported, recrystallized, and dried over P_2O_5 before use.[99] All other solvents and chemicals were purchased from Sigma-Aldrich, TCI America, or Fisher Scientific and were used as received.

5.3.2. Characterization

^{1}H and ^{13}C NMR spectra were recorded on Varian NMRS 500 spectrometers. Chemical shifts were referenced to the solvent resonance signals. IR spectra were recorded on an IR Prestige 21 system (Shimadzu Corp., Japan), equipped with an ATR accessory, and analyzed using IRsolution v.1.40 software. Gel permeation chromatography (GPC) eluted with THF was conducted on a system equipped with Waters Chromatography, Inc. (Milford, MA) model 1515 isocratic pump and a model 2414 differential refractometer with a three-column set of Polymer Laboratories, Inc. (Amherst, MA) Styragel columns (PLgel 5 μm Mixed C, 500 Å, and 104Å, 300 × 7.5 mm columns), and a guard column (PLgel 5 μm, 50 × 7.5 mm). The system was equilibrated at 40 °C in THF, which served as the polymer solvent and eluent (flow rate set to 1.00 mL/min). The differential refractometer was calibrated with Polymer Laboratories, Inc., polystyrene standards (300–467,000 Da). Polymer solutions were prepared at a concentration of *ca.* 3 mg/mL with 0.05% vol toluene as flow rate marker and an injection volume of 200 μL was used. Data were analyzed using Empower Pro software from Waters Chromatography, Inc. Glass transition temperatures (T_g) were measured by differential scanning calorimetry (DSC) on a Mettler-Toledo DSC822 (Mettler-Toledo, Inc., Columbus, OH) under N_2. Measurements of T_g were taken with a heating rate of 10 °C/min. The measurements were analyzed using Mettler-Toledo STAR^e v.10.00 software. The T_g was taken as the midpoint of the inflection tangent and T_m was taken as the onset point, upon the third scan. Thermogravimetric analysis (TGA) was performed under Ar atmosphere using a Mettler-Toledo model TGA/DSC 1, with a heating rate of

10 °C/min. Dynamic light scattering (DLS) measurements were conducted using DelsaNano C (Beckman Coulter, Inc., Fullerton, CA) equipped with a laser diode operating at 658 nm. Size measurements were made in nanopure water (n = 1.3329, η = 0.890 cP at 25 ± 1 °C). Scattered light was detected at 165° angle and analyzed using a log correlator over 70 accumulations for a 3.0 mL sample in a glass sizing cell (4.0 mL capacity). The samples in a glass sizing cell were equilibrated for 30 min before measurements were made. The photomultiplier aperture and the attenuator were automatically adjusted to obtain a photon counting rate of *ca*. 10 kcps. The calculations of the particle size distributions and distribution averages were performed using CONTIN particle size distribution analysis routines. The ζ-potential of the particles in suspension was obtained by measuring the electrophoretic movement of charged particles under an applied electric field. Scattered light was detected at a 30° angle at 25 °C. The ζ-potential was measured at five regions in the flow cell and a weighted mean was calculated. These five measurements were used to correct for electroosmotic flow that was induced in the cell due to the surface charge of the cell wall. Transmission electron microscopy (TEM) images were collected on a JEOL 1200EX operating at 100 kV and micrographs were recorded at calibrated magnifications using a SIA-15C CCD camera. The samples as aqueous solutions (4 μL) were deposited onto formvar/carbon-coated copper grids. Excess sample was wicked off using filter paper and the grids were allowed to air-dry for 2 min. Following that, the grids were stained with 4 μL of a 1% phosphotungstic acid aqueous solution. Excess stain was wicked off using filter paper after 1 min. The sample grids were air-dried overnight before analyses.

5.3.3. Synthesis of (2-vinyloxy)ethyl 2,2-bis(hydroxymethyl)propanoate (1)

A mixture of 2,2-bis(hydroxymethyl)propionic acid (5.0 g, 37 mmol), potassium hydroxide (90% assay; 2.6 g, 46 mmol), sodium iodide (1.1g, 7.3 mmol), and DMF (40 mL) was heated to 100 °C for 1 h at which point a homogenous solution was formed. 2-Chloroethyl vinyl ether (3.8 mL, 37 mmol) was added to the warm solution, and stirring was continued at 100°C for 20 h. The reaction was cooled and the solvent was removed under vacuum. The residue was extracted with DCM and water twice and the organic layer was dried over $MgSO_4$ and evaporated. The concentrate was further purified by column chromatography with ethyl acetate and hexane (1:4) as an eluent to yield yellow liquid (5.90 g, 78%). ^{1}H NMR (500 MHz, $CDCl_3$): δ 6.47–6.42 (dd, J = 6.8 and 14.4 Hz, –OC***H***CH_2), 4.40–4.37 (m, –C(O)OC***H***$_2CH_2O$–), 4.23–4.18 (dd, J = 2.3 and 14.2 Hz, -OCHC***H***H'), 4.06–4.03 (dd, J = 2.3 and 6.8 Hz, –OCHCH***H'***), 3.92–3.89 (m, –C(O)OCH_2C***H***$_2$O–), 3.88–3.84 (m, –C***H***$_2$OH), 3.72–3.68 (m, –C***H***$_2$OH), 3.01 (t, J = 6.6 Hz, –CH_2O***H***), 1.08 (s, –C(C***H***$_3$)($CH_2OH)_2$). ^{13}C NMR (125 MHz, $CDCl_3$): δ 175.8, 151.5, 87.6, 67.9, 65.8, 63.2, 49.6, 17.3. ESI MS (m/z): 211.1169 (experimental), 211.1158 (calculated for $C_9H_{16}O_5Li^+$).

5.3.4. Synthesis of 5-methyl-5-((2-vinyloxy)ethyl)oxycarbonyl-1,3-dioxan-2-one (MVEC) (2)

(2-vinyloxy)ethyl 2,2-bis(hydroxylmethyl)propionate (4.2 g, 21 mmol) and ethyl chloroformate (6.0 mL, 63 mmol) were dissolved in THF (80 mL), and the solution was stirred at 0 °C for 30 min under N_2. Subsequently, triethylamine (TEA, 8.5 mL, 61 mmol) was added dropwise over 1 h, after which the reaction mixture was removed from the ice

bath and stirred at room temperature overnight. TEA·HCl precipitate was filtered and the filtrate was concentrated and purified by column chromatography with ethyl acetate and hexane (1:4) as an eluent to yield white solid (2.90 g, 62%). ^{1}H NMR (500 MHz, $CDCl_3$): δ 6.44−6.38 (dd, J = 6.7 and 14.4 Hz, −OC***H***CH_2), 4.67 (d, J = 10.8 Hz, −OC***H***$_2C(CH_3)(CH_2-)-$), 4.41−4.38 (m, −C(O)OC***H***$_2CH_2O-$), 4.21−4.15 (m, −OC***H***$_2C(CH_3)(CH_2-)-$ and −OCHC***H***H'), 4.04−4.01 (dd, J = 2.3 and 6.7 Hz, −OCHCH***H'***), 3.89−3.86 (m, −C(O)OCH$_2$C***H***$_2O-$), 1.30 (s, −C(C***H***$_3)(CH_2-)(CH_2-)$). ^{13}C NMR (125 MHz, $CDCl_3$): δ 171.2, 151.4, 147.6, 87.5, 73.0, 65.4, 64.2, 40.3, 17.5. ESI MS (m/z): 237.0949 (experimental), 237.0950 (calculated for $C_{10}H_{14}O_6Li$+).

5.3.5. Organocatalytic ROP of MVEC (3)

In a glovebox, MVEC and Bn-MPA initiator were dissolved in dry DCM ($[MVEC]_0$ = 0.7 M). DBU (1 equiv to initiator) was added to the monomer/initiator solution. After the desired time, the polymerization was quenched by addition of a DCM solution of benzoic acid and precipitated into methanol. For example, MVEC (365 mg, 1.6 mmol), Bn-MPA (5.9 mg, 26 μmol), DBU (7.9 μL, 53 μmol), DCM (2.5 mL), benzoic acid solution (9.7 mg, 80 μmol in 300 μL DCM) were used to yield $PMVEC_{50}$. *$PMVEC_{50}$*. Yield = 185 mg, 65% based upon monomer conversion (80%). $M_{n,NMR}$ = 11700 g/mol; $M_{n,GPC}^{THF}$ = 11600 g/mol; PDI = 1.06. ^{1}H NMR (500 MHz, $CDCl_3$): δ 7.40−7.29 (m, −OCH$_2$C$_6$***H***$_5$), 6.48−6.38 (m, −OC***H***CH_2), 5.13 (br, −C(O)OC***H***$_2C_6H_5$), 4.39−4.32 (m, −C(O)OC***H***$_2CH_2O-$), 4.32−4.21 (br, −OC(O)OC***H***$_2-$), 4.22−4.14 (m, −OCHC***H***H'), 4.05−4.00 (m, −OCHCH***H'***), 3.91−3.83 (m, −C(O)OCH$_2$C***H***$_2O-$), 3.74−3.66 (m, −C***H***$_2$OH), 2.48 (m, −CH$_2$O***H***), 1.28−1.23 (s, −C(C***H***$_3)(CH_2-)_2$), 1.21 (s,

−C(C***H***$_3$)(CH$_2$−)(CH$_2$OH)). ^{13}C NMR (125 MHz, $CDCl_3$): δ 174.0, 172.2, 155.0, 154.5, 151.6, 135.6, 128.8, 128.6, 128.2, 87.4, 68.7, 65.7, 63.7, 63.3, 48.6, 46.7, 17.6. IR (neat, cm^{-1}): 2965, 1740, 1620, 1460, 1385, 1234, 1200, 1145, 964, 825, 783, 733. T_g = -9.0 °C. TGA in Ar: 270−450 °C, 92% mass loss; 8% mass remaining above 500 °C.

5.3.6. Acetalization of the vinyl ether side chain moieties of PMVEC with 4-methylbenzyl alcohol (4)

To the solution of PMVEC$_{70}$ (54 mg, 0.23 mmol for alkene functionalities) and 4-methylbenzyl alcohol (290 mg, 2.4 mmol) in 0.5 mL THF, *p*-toluenesulfonic acid (PTSA, 0.40 mg, 2.3 μmol) in 0.5 mL THF was added at 0 °C. After stirring for 2 h at room temperature, excess amount of TEA was added to quench the reaction. The reaction mixture was purified by dialysis against THF for 24 h and dried *in vacuo* to yield colorless sticky liquid. Yield = 54 mg, 76%. $M_{n,NMR}$ = 19700 g/mol. ^{1}H NMR (500 MHz, CD_2Cl_2): δ 7.34−7.30 (br, −OCH$_2$C$_6$***H***$_5$), 7.24−7.10 (m, −OCH$_2$C$_6$***H***$_4$CH$_2$), 6.48−6.38 (m, −OC***H***CH$_2$), 5.13 (br, −C(O)OC***H***$_2$C$_6$H$_5$), 4.80 (m, −OC***H***(CH$_3$)O−), 4.57 (d, J = 11.5 Hz, −OC***H***H'C$_6$H$_4$CH$_3$), 4.43 (d, J = 11.5 Hz, −OCH***H'***C$_6$H$_4$CH$_3$), 4.39−4.12 (br, −OC(O)OC***H***$_2$−, −C(O)OC***H***$_2$CH$_2$O−, and −OCHC***H***H'), 4.01 (m, −OCHCH***H'***), 3.89−3.82 (br, −C(O)OCH$_2$C***H***$_2$OCHCH$_2$), 3.80−3.69 (br, −C(O)OCH$_2$C***H***$_2$OCH(CH$_3$)O−), 3.69−3.59 (br, −C(O)OCH$_2$C***H***$_2$OH), 3.40 (s, −CH$_2$O***H***), 2.31 (s, −OCH$_2$C$_6$H$_4$C***H***$_3$, *para*), 1.30 (*d*, J = 5.1 Hz, −C(O)OCH$_2$CH$_2$OCH(C***H***$_3$)O−), 1.28−1.20 (s, −C(C***H***$_3$)(CH$_2$−)$_2$), 1.17 (s, −C(C***H***$_3$)(CH$_2$−)(CH$_2$OH)). ^{13}C NMR (125 MHz, CD_2Cl_2): δ 172.4, 154.8, 151.9, 137.7, 135.7, 129.3, 128.1, 99.6, 87.3, 69.1, 67.5, 66.1, 65.0, 62.7, 60.9, 47.0, 46.9, 21.2, 19.8,

17.6. IR (neat, cm^{-1}): 3700–3300, 3100–2800, 1744, 1458, 1381, 1234, 1134, 1096, 964, 795. T_g = -20.5 °C. TGA in Ar: 90−240 °C, 21% mass loss; 240−390 °C, 68% mass loss; 11% mass remaining above 500 °C.

5.3.7. Kinetic study of acetalization of the vinyl ether side chain moieties of PMVEC

$PMVEC_{50}$ (52 mg, 0.23 mmol of vinyl ether moieties) and 4-methylbenzyl alcohol (280 mg, 2.3 mmol) were dissolved in 1 mL THF-d_8. After addition of PTSA solution (380 μg, 2.3 μmol) in THF-d_8 (200 μL), the solution was transferred to a NMR tube and the reaction was monitored *via* ^{1}H NMR while spinning in the spectrometer (19 °C). Half-life time for this condition was 70.6 min.

5.3.8. Thio-acetalization of the vinyl ether side chain moieties of PMVEC with 4-methylbenzyl mercaptan (5)

To the solution of $PMVEC_{70}$ (78 mg, 0.34 mmol for alkene functionalities) and 4-methylbenzyl mercaptan (0.46 mL, 3.4 mmol) in 1.0 mL THF, PTSA (0.58 mg, 3.4 μmol) in 0.50 mL THF was added at 0 °C. After stirring for 2 h at room temperature, an excess amount of TEA was added to quench the reaction. The reaction mixture was precipitated into methanol and collected by centrifugation followed by drying *in vacuo* to yield colorless sticky liquid. Yield = 61 mg, 67%. $M_{n,NMR}$ = 18900 g/mol. ^{1}H NMR (500 MHz, $CDCl_3$): δ 7.37−7.28 (br, −$OCH_2C_6\boldsymbol{H}_5$), 7.22−7.07 (m, −$OCH_2C_6\boldsymbol{H}_4CH_2$), 6.46−6.39 (m, −$OC\boldsymbol{H}CH_2$), 5.15 (br, −$C(O)OC\boldsymbol{H}_2C_6H_5$), 4.79−4.64 (m, −$OC\boldsymbol{H}(CH_3)S$−), 4.42−4.12 (m, −$OC(O)OC\boldsymbol{H}_2$−, −$C(O)OC\boldsymbol{H}_2CH_2O$−, and −$OCHC\boldsymbol{H}$H'), 4.02 (br, −$OCHCH\boldsymbol{H}'$), 3.89−3.83 (br, −$C(O)OCH_2C\boldsymbol{H}_2OCHCH_2$), 3.80−3.73 (br, −$C(O)OCH_2C\boldsymbol{H}_2OCH(CH_3)S$−), 3.73−3.69 (m, −$SC\boldsymbol{H}_2C_6H_4CH_3$), 3.69−3.56 (br,

−C(O)OCH$_2$C***H***$_2$OH), 2.31 (s, −SCH$_2$C$_6$H$_4$C***H***$_3$, *para*), 1.49 (br, −C(O)OCH$_2$CH$_2$OCH(C***H***$_3$)S−), 1.30−1.20 (s, −C(C***H***$_3$)(CH$_2$−)$_2$). ^{13}C NMR (125 MHz, CDCl$_3$): δ 172.1, 154.5, 151.6, 136.7, 135.5, 129.5, 129.3, 128.9, 128.0, 99.7, 87.3, 80.8, 68.7, 65.7, 64.3, 63.7, 63.6, 62.6, 46.7, 32.4, 29.8, 21.9, 21.2, 19.5, 17.6. IR (neat, cm^{-1}): 3700–3300, 3100–2800, 2361, 1744, 1458, 1381, 1234, 1142, 1103, 972, 918, 864, 787, 733, 648. T_g = 7.3 °C. TGA in Ar: 205−410 °C, 95% mass loss; 4% mass remaining above 500 °C.

5.3.9. Thiol-ene "click" reaction of the vinyl ether side chain moieties of PMVEC with 3-mercaptopropionic acid (6)

PMVEC$_{70}$ (50 mg, 217 μmol for alkene functionalities), 2,2-dimethoxy-2-phenylacetophenone (DMPA, 11 mg, 43 μmol), and 3-mercaptopropionic acid (190 μL, 2.2 mmol) were dissolved in 5 mL DMF. The solution were bubbled with N_2 for 10 min and irradiated by UV (365 nm, 6 W) for 2 h. The reaction mixture was precipitated into ether/pentane (1/4) and dried *in vacuo* to yield colorless sticky liquid. Yield = 46 mg, 63% based on 100% conversion. $M_{n,NMR}$ = 23800 g/mol. ^{1}H NMR (500 MHz, CD$_2$Cl$_2$/MeOD): δ 7.36-7.27 (m, −OCH$_2$C$_6$***H***$_5$), 5.13 (br, −C(O)OC***H***$_2$C$_6$H$_5$), 4.32−4.25 (br, −OC(O)OC***H***$_2$−), 4.25−4.21 (m, −C(O)OC***H***$_2$CH$_2$O−), 3.65−3.59 (m, −C(O)OCH$_2$C***H***$_2$O− and −OC***H***$_2$CH$_2$S−), 2.77 (t, J = 7.3 Hz, −SC***H***$_2$CH$_2$C(O)OH), 2.68 (t, J = 6.6 Hz, −OCH$_2$C***H***$_2$S−), 2.57 (t, J = 7.3 Hz, −SCH$_2$C***H***$_2$C(O)OH), 1.23 (s, −C(C***H***$_3$)(CH$_2$−)$_2$). ^{13}C NMR (125 MHz, CD$_2$Cl$_2$/MeOD): δ 174.8, 172.8, 155.0, 71.4, 69.3, 69.0, 64.9, 47.1, 35.3, 32.0, 27.9, 17.6. IR (neat, cm^{-1}): 3700–2800, 1728, 1458,

1389, 1234, 1119, 964, 787, 710, 633. T_g = -14.8 °C. TGA in Ar: 220−395 °C, 82% mass loss; 18% mass remaining above 500 °C.

5.3.10. Synthesis of mPEG$_{113}$-b-PMVEC$_{13}$ (7)

MVEC (276 mg, 1.2 mmol) and mPEG (5 kDa, 0.30 mg, 60 μmol) were dissolved in DCM (2.4 mL, [MVEC] = 0.5 M). DBU (9.0 μL, 60 μmol) was added to initiate the polymerization. After 30 min, the polymerizations were quenched by addition of a DCM solution of benzoic acid, precipitated into diethyl ether, and collected by centrifugation followed by drying *in vacuo* to yield white powder. Yield = 487 mg, >98%. $M_{n,NMR}$ = 8000 g/mol. $M_{n,GPC}$ = 10500 g/mol. PDI = 1.06. ^{1}H NMR (500 MHz, $CDCl_3$): δ 6.46-6.37 (m, −OC***H***CH_2), 4.36−4.31 (m, −C(O)OC***H***$_2CH_2O$−), 4.31−4.22 (br, −OC(O)OC***H***$_2$−), 4.21−4.13 (m, −OCHC***H***H'), 4.04−3.99 (m, −OCHCH***H'***), 3.89−3.83 (m, −C(O)OCH$_2$C***H***$_2$O−), 3.62 (s, −OC***H***$_2$C***H***$_2$O− for PEG), 3.35 (s, −OC***H***$_3$), 1.24 (s, −C(C***H***$_3$)(CH$_2$−)$_2$), 1.19 (s, −C(C***H***$_3$)(CH$_2$−)(CH$_2$OH)). ^{13}C NMR (125 MHz, $CDCl_3$): δ 172.04, 154.4, 151.5, 87.3, 71.3, 70.6, 70.0, 69.0, 68.6, 68.3, 65.6, 63.5, 46.6, 17.5. . IR (neat, cm^{-1}): 3050–2700, 1751, 1628, 1466, 1342, 1273, 1242, 1103, 957, 841. T_g = -20.4 °C; T_m = 44.5 °C. TGA in Ar: 190−350 °C, 33% mass loss; 350−430 °C, 62% mass loss; 5% mass remaining above 500 °C.

5.3.11. Acetalization of the vinyl ether side chain moieties of mPEG-b-PMVEC with 4-methylbenzyl alcohol (8)

To the solution of mPEG$_{113}$-*b*-PMVEC$_{13}$ (0.30 g, 0.49 mmol for alkene functionalities) and 4-methylbenzyl alcohol (0.60 g, 4.9 mmol) in 1.0 mL THF, PTSA (1.7 mg, 9.8 μmol) in 0.50 mL THF was added at room temperature. After stirring for 4 h at

room temperature, an excess amount of trimethylamine was added to quench the reaction. The reaction mixture was precipitate into diethyl ether twice and dried *in vacuo* to yield white powder. Yield = 296 mg, 93%. $M_{n,NMR}$ = 8400 g/mol. ^{1}H NMR (500 MHz, CD_2Cl_2): δ 7.22−7.09 (m, −OCH$_2$C$_6$***H***$_4$CH$_2$), 6.46-6.37 (m, −OC***H***CH$_2$), 4.85−4.76 (m, −OC***H***(CH$_3$)O−), 4.87 (d, J = 11.5 Hz, −OC***H***H'C$_6$H$_4$CH$_3$), and 4.44 (d, J = 11.5 Hz, −OCH***H'***C$_6$H$_4$CH$_3$), 4.39−4.17 (br, −OC(O)OC***H***$_2$−, −C(O)OC***H***$_2$CH$_2$O−), 3.80−3.50 (m, −C(O)OCH$_2$C***H***$_2$O− and −OC***H***$_2$C***H***$_2$O− for PEG), 2.31 (s, −OCH$_2$C$_6$H$_4$C***H***$_3$, *para*), 1.32 (*d*, J = 5.1 Hz, −C(O)OCH$_2$CH$_2$OCH(C***H***$_3$)O−), 1.25 (s, −C(C***H***$_3$)(CH$_2$−)$_2$), 1.19 (s, −C(C***H***$_3$)(CH$_2$−)(CH$_2$OH)). ^{13}C NMR (125 MHz, CD_2Cl_2): δ 172.4, 154.5, 135.0, 129.1, 127.7, 99.2, 71.3, 70.6, 69.9, 60.6, 46.7, 19.6, 17.5. IR (neat, cm^{-1}): 3700–3200, 2882, 1749, 1466, 1387, 1343, 1277, 1238, 1144, 1103, 1061, 961, 841, 787, 444, 420, 409. T_g = -9.6 °C; T_m = 45.1 °C.

5.3.12. Self-assembly of functionalized diblock copolymers

The functionalized diblock copolymers were suspended into nanopure water (5 mg/mL) and sonicated for 10 min.

5.3.13. Monitoring cleavage of acetal moieties of 8

Cleavage of acetal moieties of **8** was monitored by ^{1}H NMR spectroscopy. **8** (100 mg) was dissolved in 20 mL of acetate buffers (pH 4 and pH 5, final concentrations = 5 mg/mL). After incubation of polymer solutions at 37 °C for desired times, an aliquot (2 mL) of the solution was collected, dialyzed against nanopure water for 1 day, and lyophilized. The resulting polymer powder was dissolved in $CDCl_3$ and ^{1}H NMR spectrum was collected.

5.4. Conclusions

A highly-reactive vinyl ether-functionalized aliphatic polycarbonate and its block copolymers were developed as a template for multiple post-polymerization conjugation chemistries. The vinyl ether-functional six-membered cyclic carbonate monomer was synthesized by a well-established two-step procedure starting from 2,2-bis(hydroxymethyl)propanoate (bis-MPA). An organobase-catalyzed ring-opening polymerization of the synthesized monomer afforded polycarbonates with the pendant vinyl-ether functionalities (PMVEC). The vinyl ether moieties on the resulting polymers were readily conjugated with hydroxyl- or thiol-containing compounds *via* three different post-polymerization modification chemistries — acetalization, thio-acetalization, and thiol-ene reaction. Acetal-functionalized polycarbonates were studied in depth to exploit their acid-labile acetal functionality. The amphiphilic block copolymer of poly(ethylene glycol) and PMVEC was functionalized with the model hydroxyl compound and its self-assembled nanostructure was characterized. Kinetics of acetal cleavage within the block copolymer micelles were examined in acidic buffer solutions (pH 4 and 5) and showed relatively slower rates compared to the previous reports. The results suggested that this polymer system is promising for a stimuli-responsive drug delivery vehicle.

CHAPTER VI

DETECTION OF AN INTERMEDIATE IN RING-OPENING POLYMERIZATION OF L-LACTIDE USING HYPERPOLARIZED NMR

6.1. Introduction

Hyperpolarization of nuclear spins by dissolution dynamic nuclear polarization (D-DNP) has been recognized for its potential to study non-equilibrium chemical processes in solution. Several thousand-folds of signal enhancement provided by D-DNP allows for monitoring diverse reactions in real-time that occur on the NMR time scale, such as protein-ligand interactions,[142-147] enzymatic reaction,[148,149] protein folding,[50] and fast organic reactions,[150-152] without need for signal averaging or isotope-labeling.

This emerging technique can also offer benefits in the field of polymer chemistry, including understanding polymerization mechanisms and studying reaction kinetics, *etc*.[153,154] Recently, olefin polymerization catalyzed by zirconium-based metallocenes has been studied by DNP-NMR to determine tacticity and deactivation mechanisms.[154] In another study, it has been demonstrated that ^{13}C DNP-NMR measurements of "living" anionic polymerization of styrene enables not only observation of the resonances associated with anionic chain-end, but also attainment of information on polymerization kinetics.[153] The previous works supported our hypothesis that "living" characteristics of controlled polymerizations allow D-DNP NMR measurements to detect active chain-ends or intermediate structures due to their constant concentration during polymerization processes. While it is generally challenging to monitor highly reactive and instable species

such as reaction intermediates, D-DNP NMR provides significant insight into reaction mechanism. As a follow-up study, we extended the application of D-DNP NMR into the mechanism study of a less-studied polymerization system organocatalytic ring-opening polymerization (ROP) of L-lactide using 1,5,7-triazabicyclo[4.4.0]dec-5-ene (TBD).

Polylactide (PLA) is an aliphatic polyester, which can be degraded into low molecular weight oligomers or lactic acid by microorganisms or hydrolysis. Due to its biodegradability and biocompatibility, PLAs have been a valuable substitute for petroleum-based products such as polyethylene, polystyrene, *etc*.[155,156] Traditionally, PLAs have been synthesized by ROPs using metal catalysts.[157] However, metal catalysts are not ideal for electronic and medical applications due to the detrimental effects of residual metals. Therefore, organocatalyzed ROPs have been actively investigated. Among various organocatalysts, we are especially interested in 1,5,7-triazabicyclo[4.4.0]dec-5-ene (TBD) due to its high catalytic activity.[158] Its ability to catalyze both acyl transfer and carbonyl activation by hydrogen bonding enables dual activation of monomers, which has been believed to be attributed to its superior catalytic efficiency. Theoretical and experimental studies proposed two possible mechanisms (Scheme 6.1): a nucleophilic catalytic mechanism and an acid-base catalytic mechanism (hydrogen bonding mechanism). Computational studies indicated that the hydrogen bonding mechanism is energetically favorable,[159,160] while experimental studies suggested the presence of the nucleophilic catalytic mechanism based on the model systems.[158] Here, we report the observation of intermediate resonance of ROP by hyperpolarized NMR spectroscopy.

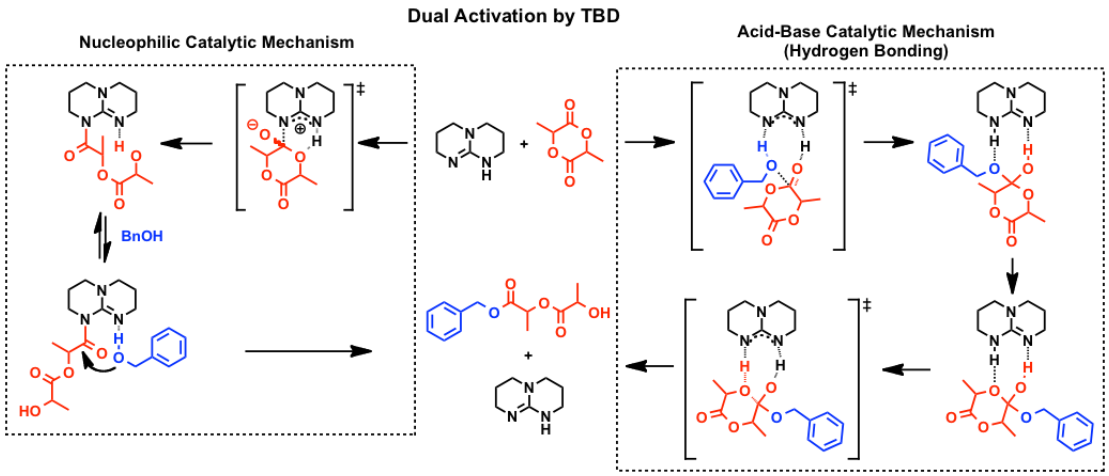

Scheme 6.1. Two proposed mechanisms of ROP of lactide catalyzed by TBD.

6.2. Results and Discussion

Before the hyperpolarized NMR experiments, the test polymerization was performed to check the feasibility of the mechanism study using D-DNP NMR spectroscopy. ROP of L-lactide under similar conditions with DNP experiments yielded poly(L-lactide) (Scheme 6.2), which was confirmed by THF gel permeation chromatography (GPC) (Figure 6.1) and NMR spectroscopy (Figure 6.2). Also, spin-relaxation time of the ester carbon in L-lactide was sufficiently long for monitoring the reaction process before the carbon nuclei lost their hyperpolarization significantly (Figure 6.3).

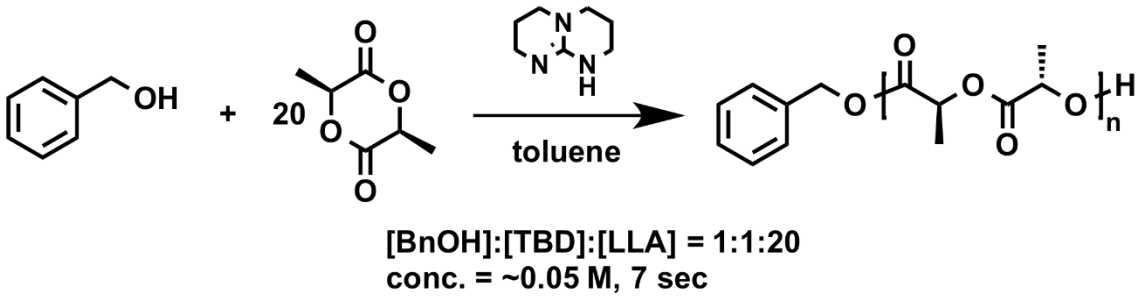

Scheme 6.2. Test polymerization under the similar conditions with DNP experiments.

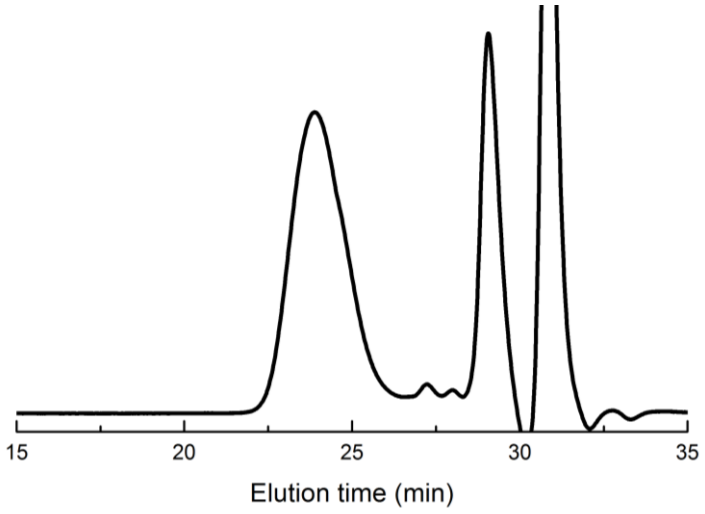

Figure 6.1. GPC trace of PLLA prepared from the test polymerization.

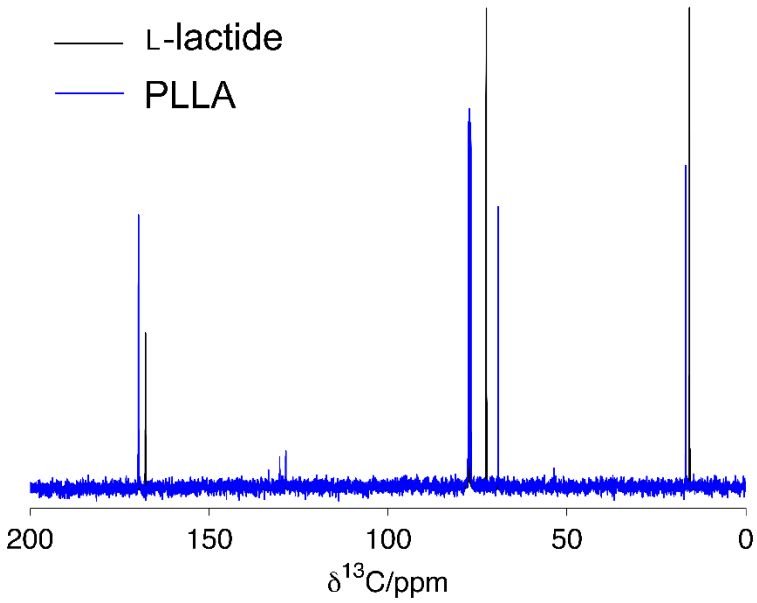

Figure 6.2. ^{13}C NMR spectra of L-lactide (black) and PLLA (blue) synthesized from test polymerization.

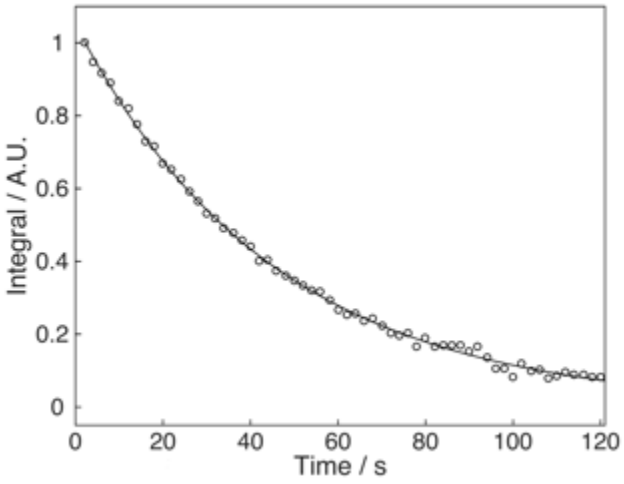

Figure 6.3. Spin-lattice relaxation of the hyperpolarized ester carbon of L-lactide dissolved in toluene. A 5 degree pulse was applied to acquire each data point and the time interval between the subsequent scans was 2 s. The small-flip angle effect was considered to determine the spin-lattice relaxation time (T_1) from the apparent T_1 as discussed in the reference.[151] The single exponential fit results in $T_1 = 50$ s of the lactide ester carbon.

The ROP of L-lactide catalyzed by TBD was monitored by ^{13}C NMR spectroscopy using the D-DNP technique in real-time. The broader range of chemical shifts in ^{13}C NMR spectrum allows for clearer observations of desired signals with minimal overlap of resonances. The hyperpolarized L-lactide in the solid state was rapidly transferred into the NMR spectrometer after dissolution in toluene, which initiates the polymerization in the presence of TBD as an organocatalyst and benzyl alcohol as an initiator in the NMR tube, generating site-specifically hyperpolarized products, *i.e.*, carbon resonances derived from hyperpolarized lactide only have signal enhancement. For DNP experiments, the optimal reaction conditions were found to be the ratio of 10:1:1 ([L-lactide]:[TBD]:[benzyl alcohol]), where the reaction rate was compromised to monitor the polymerization process before the substantial loss of polarization. Figure 6.4 shows the time-resolved DNP-NMR ^{13}C spectra obtained from a single polymerization reaction by a series of small-flip-angle pulse excitation. The consumption of monomer, L-lactide, and the formation of polymer, poly(L-lactide), were observed as a signal decrease at *ca*. 167 ppm (corresponding to the ester carbon of the monomer, C1) and, a signal increase at *ca*. 170 ppm (corresponding to the ester carbon of the polymer, C2), respectively. Both resonances eventually decayed by the spin-lattice relaxation. Interestingly, small signals were additionally observed near 175 ppm (C3), which did not appear in the reference spectra of L-lactide and poly(L-lactide). The earlier appearance of these signals compared to the product signal presents a possibility that the additional peaks might be related to reaction intermediates. In addition, when considering the concomitant spin relaxation and short life-time of the intermediates, relatively constant intensity of resonances around 175 ppm supports the

above hypothesis reflecting "living" characteristics of ROP. Based on the predicted chemical shifts of the proposed intermediates from both mechanisms, we hypothesized that the small peaks near 175 ppm could be a resonance of the polymerization intermediate.

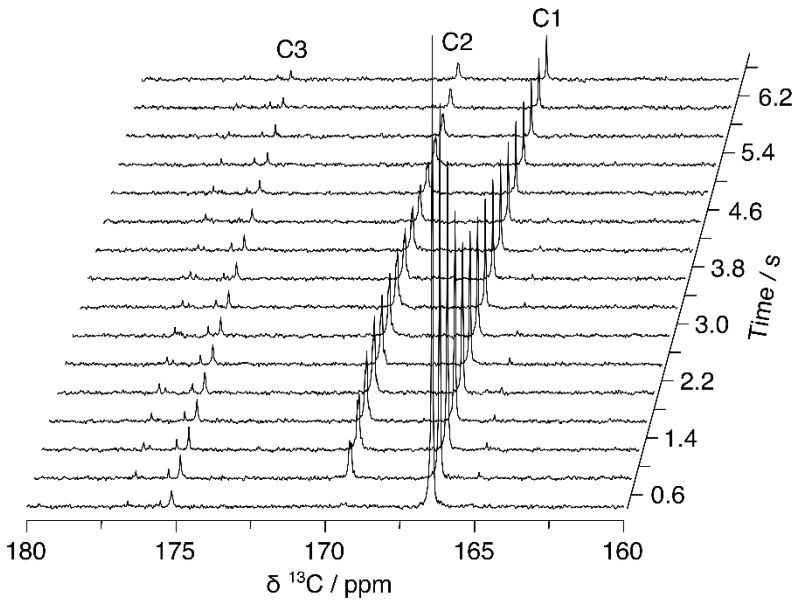

Figure 6.4. Regions of ester carbons from a series of ^{13}C NMR spectra recorded during the course of the ROP of L-lactide catalyzed by TBD. The spectra were acquired by a series of small flip angle pulses with the time resolution of 400 ms. (C1: ester carbon of L-lactide, C2: ester carbon of poly(L-lactide), C3: additionally observed signals)

Intermediates in the nucleophilic catalytic mechanism possess an amide carbon. In order to identify the rough ^{13}C chemical shift of amide carbon derived from TBD, *N*-Acetyl TBD was synthesized as a model intermediate compound, which was confirmed by NMR spectroscopy and ESI-MS. Vinyl acetate can be used for acetylation of TBD since it was used to verify acyl transfer reaction *via* TBD as a bifunctional catalyst in the

previous report.[158] When one amino group of TBD reacts with vinyl acetate, however, the adjacent tertiary amino group will act as a base catalyst, which could make it too unstable to characterize. Therefore, we applied acetyl chloride as an acetylating agent since hydrogen chloride byproduct can deactivate the adjacent basic amino group by protonation after acetylation (Scheme 6.3). The resulting compound was stable enough to be detected by ESI-MS. The ^{13}C chemical shift of amide carbon in *N*-acetyl TBD·HCl salt was *ca*. 170.5 ppm in $CDCl_3$, which supports the possibility that the observed peaks could have originated from an amide carbon formed during ring-opening of lactide by TBD. However, insolubility of *N*-acetyl TBD·HCl salt in toluene prevents attainment of the exact chemical shift of amide carbon in the solvent we used for dissolution, after which we decided not to synthesize more similar model compounds. However, it is worth mentioning that ^{13}C chemical shifts of intermediates in the hydrogen bonding mechanism might appear at similar chemical shifts since the ester carbon resonance of lactide could be shifted downfield by hydrogen bonding with TBD.

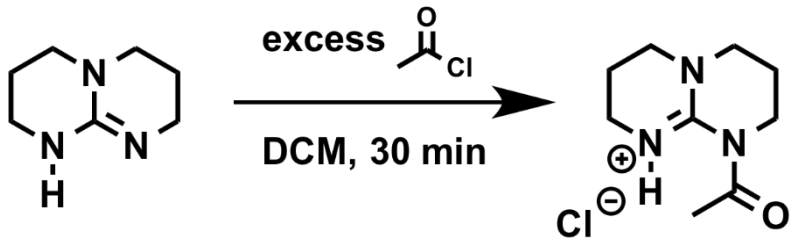

Scheme 6.3. Synthesis of model intermediate compound.

To identify the origins of the hyperpolarized signals observed aside from that of monomer, several ^{13}C temporal correlation experiments were performed. First, a direct temporal correlation between monomer and polymer was established with encoding of the spins by a frequency selective-inversion pulse (IBURP2) applied at the resonance of L-lactide ester carbon, *ca*. 167 ppm. The polymer signal produced from the non-inverted monomer was removed by employing selective-saturation pulses (EBURP2) before acquiring a series of ^{13}C NMR spectra. The obtained spectra clearly showed the transfer of the inverted monomer spins to the signals of the polymer ester carbons at *ca*. 170 ppm, represented by red colored signals (Figure 6.5). Additionally, the signal at *ca*. 175 ppm appears inverted, indicating that it originates from the ester carbon of monomer. The downfield shift of the peak from the resonance of lactide ester carbon along with the ^{13}C chemical shift of amide functionality of the model compound suggested that the inverted peak observed could be derived from either amide or ester functionalities of specific molecular structures comprised of lactide and TBD.

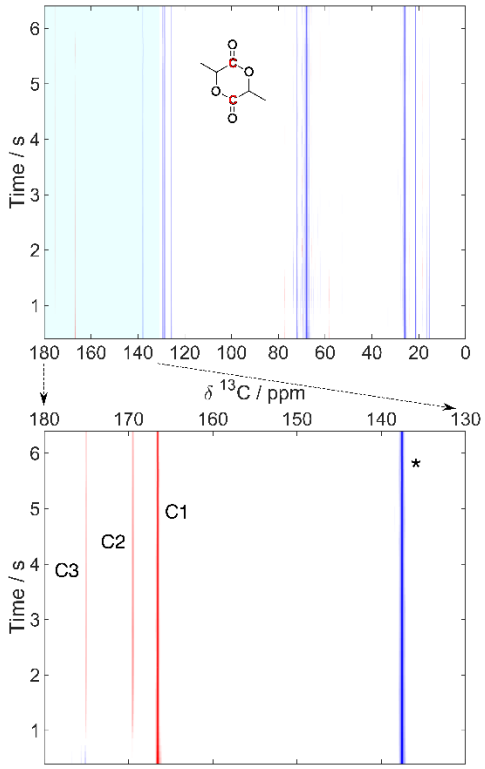

Figure 6.5. Time-resolved DNP-NMR ^{13}C spectra of the ROP of L-lactide catalyzed by TBD. The blue and red colored signals represent a positive and a negative signal, respectively. Top: a full-width spectrum, bottom: a magnified spectrum. (*: solvent: toluene)

From the previous experiment, the correlations between the monomer and polymer, and the monomer and the additional peak at *ca*. 175 ppm, were found. In order to confirm the flow of NMR spins from the additional peak to the polymer, homonuclear selective saturation experiments were designed. In this experiment, a homonuclear decoupling (HD) pulse scheme was used to selectively saturate a spin of interest during the entire measurement. The HD pulse scheme is originally devised for a quick identification of correlated protons of a molecule in a 1D ^{1}H NMR experiment, which has been largely replaced by the 2D COSY experiment. Here, we demonstrate the ^{13}C

temporal correlation experiment using the HD pulse for a frequency-selective saturation during the NMR measurement. By the irradiation of HD pulse on the frequency of potential intermediate species, the polymer signal was expected to be reduced since the hyperpolarization that was transferred from the monomer to the intermediate would be lost upon the selective-saturation. The pulse scheme contains a continuous wave that was applied before the measurement started to eliminate any polymer signal that was produced during the stabilization time after the sample injection, as described in Figure 6.6a. In the experiment, a time-resolved ^{13}C DNP NMR spectra were obtained while the HD pulse was irradiated to the frequency of potential intermediate, *ca.* 175 ppm, which is 8.64 ppm away from the monomer ester carbon signal. For comparison, the off-resonance experiment was conducted where the HD pulse was irradiated to the frequency that was the same offset away from the monomer to the upfield. In this experiment, 10% HD duty cycle was chosen for an effective saturation without a large signal loss due to the reduced detection time. The peaks of ester carbons from both polymer and monomer are integrated and the averaged results from five independent data sets are plotted in Figure 6.6b. In data processing, a signal from THF, a component of glassy matrix used to prepare the sample for DNP experiments, was used for calibrating the signal enhancement by DNP in different measurements, and the maximum integral value of the monomer ester carbon was used to normalize all the other peaks. The signal of polymer ester carbon was noticeably reduced by 42% when the HD pulse was applied on resonance, while that of monomer ester carbon showed similar signal decays in the on and off resonance experiments (Figure 6.6b). This result supports our hypothesis that the peak appears at *ca*. 175 ppm might originate from

the reaction intermediate. In addition, similar results were obtained using EBURP2 pulses instead of the HD pulse as shown in Figure 6.7. Furthermore, we designed a simple pulse sequence that contains EBURP2 pulses to eliminate the resonance near 175 ppm only during the first two scans. Reappearance of the signal at *ca*. 175 ppm from the third scan agrees with regeneration of reaction intermediate. (Figure 6.8).

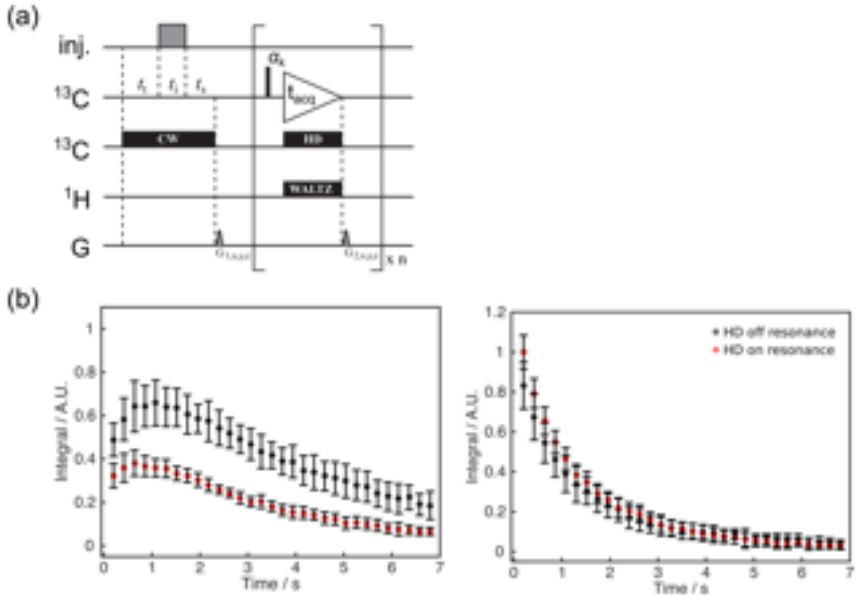

Figure 6.6. (a) Pulse sequence used for the homonuclear selective saturation experiment. The polarized monomer was transferred from the polarizer to the home-built sample injector for a transfer time (t_t). A continuous wave (CW) was irradiated to the frequency at 175 ppm during an injection time (t_i) of 360 ms and a stabilization time (t_s) of 400 ms to saturate the intermediate peak that was generated before the NMR measurement. A series of 15° pulse (α_k) were applied to acquire the time-resolved ^{13}C NMR spectra while the HD pulse was irradiated to the desired frequency. (b) Time evolution of signal integrals of the C2 (left) and C1 (right) from hyperpolarized ^{13}C NMR measurements. The error bars indicate 90 % confidence intervals.

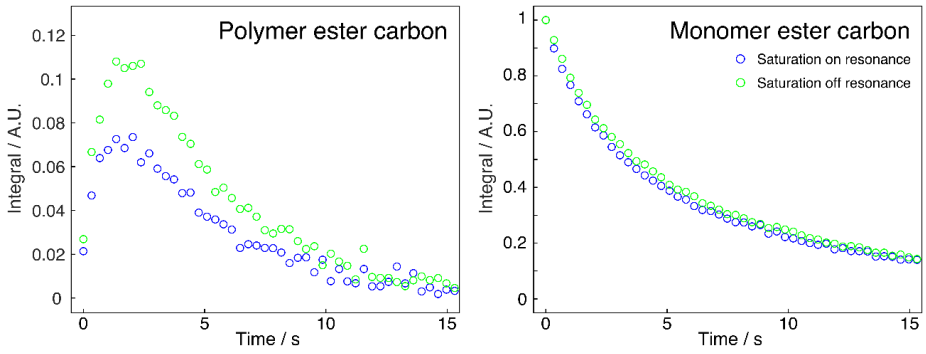

Figure 6.7. The temporal correlation of the intermediate and poly L-lactide was observed using a ^{13}C DNP-NMR selective-saturation experiment. The hyperpolarized monomer was transferred from the polarizer to the home-built sample injector for a transfer time (t_t). The sample was injected into a 5 mm NMR tube, which was preinstalled in a 400 MHz NMR spectrometer, after dissolution with 4 mL of preheated toluene. Benzyl alcohol and TBD were preloaded in the NMR tube in the ratio of 7:1:1 ([L-lactide]:[TBD]:[benzyl alcohol]) for the final sample conditions. The NMR experiment was triggered after an injection time (t_i) of 400 ms and a stabilization time (t_s) of 400 ms. The resonance of ester carbon in the polymer was selectively saturated by EBURP2 shaped π/2 pulse applied for a duration of 20 ms in the beginning and it was repeated three times, followed by a randomized pulsed field gradient $G_{x,y,z}$ to remove polymer signal produced before the intermediate saturation. Then, the EBURP2 shaped π/2 pulses with a duration of 20 ms were used four times to saturate the resonance of intermediate before the small flip angle pulse of 15.9° for the signal detection. In a control experiment, the EBURP2 pulses were turned off. A total of 64 transients were acquired for XX s, and the time between each transient was 0.34 s. Time evolution of signal integrals of the C2 (left) and C1 (right) from hyperpolarized ^{13}C NMR measurements.

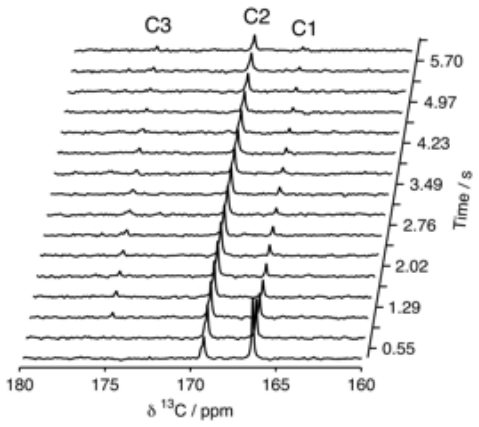

Figure 6.8. Regeneration of ^{13}C signal at *ca*. 175 ppm after removing a selective saturation pulse EBURP2, applied to the intermediate frequency (*ca*. 175 ppm) was observed. The time-resolved spectra were acquired using a pulse sequence, (trigger– [(shaped π/2) – $G_{x,y,z}$ – α_x – acquire FID]$_2$– [α_x – acquire FID – $G_{x,y,z}$]$_{62}$). The duration of EBURP2 shaped π/2 pulse was 20 ms and the flip angle α of the excitation pulse was 15.9° with the pulse strength of γB_1 = 29.4 kHz applied. A randomized $G_{x,y,z}$ pulsed field gradients (35.5 /cm, 1 ms) were used after each scan. 16384 data points were acquired for each scan with the time interval between each transient of 400 ms.

6.3. Experimental Section

6.3.1. Materials

Benzyl alcohol was distilled from calcium hydride and stored over 4 Å molecular sieves. TBD (1,5,7-triazabicyclo[4.4.0]dec-5-ene) was used as received from TCI America. L-lactide (LLA, 98%, Alfa Aesar) was recrystallized twice from ethyl acetate/hexanes, dried by azeotropic distillation in dry toluene twice, dried over 4 Å molecular sieves in dry DCM twice, concentrated *in vacuo*, and stored under inert atmosphere prior to use. Tetrahydrofuran (THF), toluene, and dichloromethane (DCM) were purified by passage through solvent purification system (JC Meyer Solvent Systems) and used as dried solvents. α,γ-bisdiphenylene-β-phenylallyl (BDPA) was obtained from Sigma Aldrich, St. Louis, MO and used as received.

6.3.2. NMR spectroscopy

All hyperpolarized NMR experiments were carried out using a broadband observe (BBO) probe on a 400 MHz NMR spectrometer (Bruker Biospin, Billerica) equipped with three pulsed field gradients at a temperature of 298 K. For the experiment shown in Figure 1, the spectra were acquired using a pulse sequence, (trigger – $[G_z - \alpha_x -$ acquire FID$]_{x64}$). The resulting data set consists of 64 transients and 18432 data points were acquired for each scan with the time resolution of 0.4 s. Prior to every scan, a randomized pulsed field gradient G_z (35.5 G/cm, 1 ms) was applied to remove unwanted coherences present from the previous scan. The flip angle α of the excitation pulse was 21.2°, and the pulse strength γB_1 = 29.4 kHz was applied. During the acquisition, WALTZ-16 ^{1}H decoupling was applied with field strength γB_1 = 2.3 kHz. In the T_1 relaxation measurement of pure L-

lactide, the same pulse scheme was used with a 5-degree pulse and the time interval of 2 s. In the selective-inversion experiment shown in Figure 2, the spectra were acquired using a pulse sequence, (trigger– (shaped π) – $G_{x,y,z}$ – [(shaped π/2) – $G_{x,y,z}$]$_3$ – [α_x – acquire FID – $G_{x,y,z}$]$_{64}$). An IBURP2 shaped π pulse at the resonance frequency of the ester carbon of L-lactide with a duration of 20 ms, three EBURP2 shaped π/2 pulses at the resonance frequency of the ester carbon of poly(L-lactide) with a duration of 20 ms, and $G_{x,y,z}$ pulsed field gradients (35.5 /cm, 1 ms) were used. The flip angle α of the excitation pulse was 15.9° and the pulse strength γB_1 = 29.4 kHz was applied. 16384 data points were acquired for each scan with an acquisition time of 341 ms. In the homonuclear selective saturation experiments, the spectra were acquired using a pulse sequence, (CW – trigger – $G_{x,y,z}$ – [α_x – acquire FID / HD – $G_{x,y,z}$]$_{32}$) (Figure 3a). An HD pulse was applied during the acquisition with 10 % duty cycle and the pulse strength γB_1= 1.5 kHz. The flip angle α of the excitation pulse was 15.9°, and 16384 data points were acquired for each scan with an acquisition time of 218 ms, followed by a $G_{x,y,z}$ pulsed field gradients (35.5 /cm, 1 ms). During the acquisition, WALTZ-16 ^{1}H decoupling was applied with field strength γB_1 = 2.3 kHz.

6.3.3. Sample preparation for DNP experiments

L-lactide (87 mg, 0.60 mmol) and free radical BDPA (2.8 mg, 15 mM) were dissolved in 400 μL of glass-forming solvent (THF:toluene, 85:15, v/v) and the resulting solution was used as a stock solution for DNP experiments. A DCM solution of initiator (benzyl alcohol) and catalyst (TBD) was prepared as a stock solution prior to use.

6.3.4. DNP polarization

L-lactide / BDPA stock solution (40 μL, 1.5 M) was hyperpolarized in a HyperSense DNP polarizer (Oxford Instruments, Tubney Woods, UK), with 60 mW power of 93.965 GHz microwaves, for 3 hours at T = 1.4 K. Prior to the dissolution, a stock solution of TBD and benzyl alcohol in DCM was prepared and 25 μL of the solution was loaded in the NMR tube. The NMR tube was installed in the NMR instrument, and connected to the injection system. Subsequently, the hyperpolarized sample was dissolved with 4 mL of pre-heated toluene, and automatically transferred to a 5 mm NMR tube inside the NMR spectrometer The sample injection was driven by N_2 gas and the gas pressure was optimized for fast and homogeneous mixing of the hyperpolarized sample and the pre-loaded initiator and catalyst in the NMR tube.[161] NMR experiments were triggered after an injection time of 360 ~ 400 ms and a stabilization time of 400 ms. The reaction conditions were the equivalent ratio of 10:1:1 ([L-lactide]:[TBD]:[benzyl alcohol]). Less than 2 s was taken for the transfer of the hyperpolarized sample into the measurement stage and a total sample volume was 450 μL after mixing.

6.3.5. Test ROP of L-lactide

In a 20 mL scintillation vial equipped with a stir bar, benzyl alcohol (3.8 mg, 3.6 μL, 0.035 mmol) and TBD (4.8 mg, 0.035 mmol) were dissolved in DCM (minimum amount to dissolve). L-lactide (100 mg, 0.69 mmol) in toluene (14.5 mL, [L-lactide] = *ca.* 0.05 M, [L-lactide]:[TBD]:[benzyl alcohol] = 20:1:1) was added to initiator/catalyst solution. After 7 sec, the polymerization was quenched by DCM solution of benzoic acid. The conversion was determined by ^{1}H NMR spectroscopy. The polymer was precipitated from toluene into diethyl ether and dried to a constant weight to afford poly(L-lactide).

Molecular weight and PDI were determined by THF GPC. $M_n^{GPC(RI)}$ = 2900 Da, M_w/M_n = 1.21.

6.3.6. Synthesis of model intermediate compound, N-acetyl TBD

In a flame-dried scintillation vial (5 mL) equipped with a stir bar, acetyl chloride (113 mg, 103 μL, 1.44 mmol) was added dropwise to TBD (40.0 mg, 0.287 mmol) in DCM-d_2 (1 mL). After 30 min, the resulting solution was concentrated *in vacuo* to remove excess acetyl chloride. Remaining acetic acid was azeotropically removed with dry benzene (0.3 mL × 2) *in vacuo*. ^{13}C NMR (100 MHz, $CDCl_3$): δ 170.5 ppm. HRMS (ESI-TOF) m/z: $[M + H]^+$ Calcd for $C_9H_{16}N_3O$ 182.1293; Found 182.1295.

6.4. Conclusions

An unprecedented ^{13}C signal, which was not observable by conventional NMR spectroscopy, was detected by hyperpolarized NMR. Signal enhancement, which was achieved by hyperpolarization of nuclear spins using dynamic nuclear polarization (DNP) technique, makes the collection of ^{13}C NMR spectra possible in real time during ROP. ^{13}C temporal correlation experiments and homonuclear selective saturation experiments verified that the observed ^{13}C NMR signal has characteristics of intermediate species. Although further studies will be necessary to gain more advanced understanding for the mechanism of ROP with the chemical structure of the intermediate, this study showed a significant potential of hyperpolarized NMR technique for an investigation of chemical reactions.

CHAPTER VII

CONCLUSIONS

The majority of the most common health problems are infectious diseases or related complications. Although a variety of antimicrobials have been developed, the efficacy of these interventions to manage infectious diseases is compromised by poor bioavailability, side effects, and physical and biological barriers to their efficient delivery to target sites, as well as drug-resistant microorganisms. Moreover, the development of new antimicrobials becomes increasingly difficult and expensive. Therefore, novel treatment strategies are required to improve the efficacy of currently available antimicrobial agents.

Nanotechnology can contribute to more effective treatment of infectious diseases using available antibiotics. Nanomaterials can carry and selectively deliver therapeutics to the site of the disease with enhanced efficacy and reduced side-effects. We have a keen interest in exploiting the polymeric nanostructures due to their capability to incorporate a wide range of therapeutics and targeting ligands as well as their tunability of physicochemical properties by synthesis and modification. This dissertation aims to contribute to fundamental chemistry advances toward the development of degradable polymer-based nanoparticles for the treatment of infectious diseases.

In a first project, bacterial adhesin, $FimH_A$-targeted polymeric nanoparticles were developed *via* amidation between carboxylic acids located in the shell of the poly(acrylic acid)-*block*-polystyrene-based polymeric nanoparticles and primary amine groups of

lysine residues on $FimH_A$. After improving amidation conditions, we prepared $FimH_A$-polymeric nanoparticle conjugates with varying amount of adhesin on the surface of nanostructures in order to optimize cell binding and internalization efficiency. Although the behaviors of these conjugates were not improved compared to those of the previous reports, the improved conjugation conditions in this study can be used for future studies with other $FimH_A$ variants or polymeric nanostructures with different morphologies.

In a second direction involving a series of projects, functional degradable polymers and their self-assembled nanostructures were developed for the biomedical applications. Degradable polycarbonates were synthesized by metal-free organocatalytic ring-opening polymerization of functional cyclic carbonate monomers, and postpolymerization modifications. Hydrophilic polycarbonate analogous to non-degradable PHPMA, and reactive aldehyde- and vinyl ether-functionalized polycarbonates were synthesized and their potential applications were examined. Polycarbonates have higher stability than polyphosphoester analogs that we have previously developed, yet still retaining hydrolytic degradability. These projects contributed an expansion of the type of reactive side chain groups available on polycarbonate backbone.

In a third directon, a mechanistic study of organocatalytic ring-opening polymerization (ROP) of lactide was performed by hyperpolarized NMR spectroscopy. The collection of ^{13}C NMR data in real time during polymerization was possible due to signal enhancement by hyperpolarization of lactide monomer. We observed an unprecedented signal at *ca*. 175 ppm, which showed characteristics of an intermediate for ring-opening polymerization. Even though further studies will be required to reveal the

mechanism of the polymerization, this study demonstrated that hyperpolarized NMR technique can be a valuable method to investigate "living" polymerizations.

In summary, a novel strategy to treat recurrent bacterial infections was explored by mimicking the bacterial mode of cell invasion, which would enable delivery of antimicrobials to reservoir bacteria that evade current/conventional antibiotic treatments by hiding inside the cells. This strategy served as the motivation for several fundamental advances that were made to the compositions of polymers to increase functionality while adjusting degradability and mechanistic studies of their synthesis. This work serves as a guide for future development of functional polycarbonates and their self-assembled nanostructures to be used as degradable nanocarriers for antimicrobial delivery. Further degradation studies of polycarbonates *via* hydrolysis and/or enzymatic hydrolysis will need to be conducted *in vitro* as well as *in vivo*. Furthermore, future studies will need to focus on the influence of nanoparticle size and shape on binding and invasion into the cell.

REFERENCES

(1) Toumey, C. *Nat. Nanotechnol.* **2009**, *4*, 783.

(2) Taniguchi, N. *Proc. Intl. Conf. Prod. Eng. Tokyo, Part II, Japan Society of Precision Engineering* **1974**.

(3) Devadasu, V. R.; Bhardwaj, V.; Kumar, M. N. *Chem. Rev.* **2013**, *113*, 1686.

(4) Brambilla, D.; Luciani, P.; Leroux, J. C. *J. Control. Release* **2014**, *190*, 9.

(5) Elsabahy, M.; Wooley, K. L. *Chem. Soc. Rev.* **2012**, *41*, 2545.

(6) Ensign, L. M.; Cone, R.; Hanes, J. *Adv. Drug Deliv. Rev.* **2012**, *64*, 557.

(7) Minko, T.; Rodriguez-Rodriguez, L.; Pozharov, V. *Adv. Drug Deliv. Rev.* **2013**, *65*, 1880.

(8) Minko, T. *Adv. Drug Deliv. Rev.* **2013**, *65*, 1665.

(9) Prausnitz, M. R.; Langer, R. *Nat. Biotechnol.* **2008**, *26*, 1261.

(10) Lai, S. K.; Wang, Y. Y.; Hanes, J. *Adv. Drug Deliv. Rev.* **2009**, *61*, 158.

(11) Dobrovolskaia, M. A.; McNeil, S. E. *Nat. Nanotechnol.* **2007**, *2*, 469.

(12) Tatem, A. J.; Rogers, D. J.; Hay, S. *Adv. Parasitol.* **2006**, *62*, 293.

(13) Hindi, K. M.; Ditto, A. J.; Panzner, M. J.; Medvetz, D. A.; Han, D. S.; Hovis, C. E.; Hilliard, J. K.; Taylor, J. B.; Yun, Y. H.; Cannon, C. L.; Youngs, W. J. *Biomaterials* **2009**, *30*, 3771.

(14) Marier, J. F.; Brazier, J. L.; Lavigne, J.; Ducharme, M. P. *J. Antimicrob. Chemother.* **2003**, *52*, 247.

(15) Beaulac, C.; Clément-Major, S.; Hawari, J.; Lagacé, J. *Antimicrob. Agents Chemother.* **1996**, *40*, 665.

(16) Flores-Mireles, A. L.; Walker, J. N.; Caparon, M.; Hultgren, S. J. *Nat Rev Micro* **2015**, *13*, 269.

(17) Lai, S.; Wang, Y.; Wirtz, D.; Hanes, J. *Adv. Drug Deliv. Rev.* **2009**, *61*, 86.

(18) Dawson, M.; Wirtz, D.; Hanes, J. *J. Biol. Chem.* **2003**, *278*, 50393.

(19) Henke, M. O.; Ratjen, F. *Paediatr. Respir. Rev.* **2007**, *8*, 24.

(20) Matsumura, Y.; Maeda, H. *Cancer Res.* **1986**, *46*, 6387.

(21) Elsabahy, M.; Wooley, K. L. *Chem. Soc. Rev.* **2013**, *42*, 5552.

(22) Le Garrec, D.; Gori, S.; Luo, L.; Lessard, D.; Smith, D. C.; Yessine, M. A.; Ranger, M.; Leroux, J. C. *J. Control. Release* **2004**, *99*, 83.

(23) Lin, L. Y.; Lee, N. S.; Zhu, J.; Nystrom, A. M.; Pochan, D. J.; Dorshow, R. B.; Wooley, K. L. *J. Control. Release* **2011**, *152*, 37.

(24) Ma, Q.; Remsen, E. E.; Clark, C. G., Jr.; Kowalewski, T.; Wooley, K. L. *Proc. Natl. Acad. Sci. U. S. A.* **2002**, *99*, 5058.

(25) Carr, L. R.; Zhou, Y.; Krause, J. E.; Xue, H.; Jiang, S. *Biomaterials* **2011**, *32*, 6893.

(26) Jiang, S.; Cao, Z. *Adv. Mater.* **2010**, *22*, 920.

(27) Keefe, A. J.; Jiang, S. *Nat. Chem.* **2012**, *4*, 59.

(28) Ishida, T.; Wang, X.; Shimizu, T.; Nawata, K.; Kiwada, H. *J. Control. Release* **2007**, *122*, 349.

(29) Wang, X.; Ishida, T.; Kiwada, H. *J. Control. Release* **2007**, *119*, 236.

(30) Garay, R. P.; El-Gewely, R.; Armstrong, J. K.; Garratty, G.; Richette, P. *Expert Opin. Drug Deliv.* **2012**, *9*, 1319.

(31) Lundberg, P.; Lee, B. F.; van den Berg, S. A.; Pressly, E. D.; Lee, A.; Hawker, C. J.; Lynd, N. A. *ACS Macro Lett.* **2012**, *1*, 1240.

(32) Lux, F.; Mignot, A.; Mowat, P.; Louis, C.; Dufort, S.; Bernhard, C.; Denat, F.; Boschetti, F.; Brunet, C.; Antoine, R.; Dugourd, P.; Laurent, S.; Elst, L. V.; Muller, R.; Sancey, L.; Josserand, V.; Coll, J.; Stupar, V.; Barbier, E.; Rémy, C.; Broisat, A.; Ghezzi, C.; Le Duc, G.; Roux, S.; Perriat, P.; Tillement, O. *Angew. Chem. Int. Ed.* **2011**, *50*, 12299.

(33) Zhao, Y.; Sultan, D.; Detering, L.; Luehmann, H.; Liu, Y. *Nanoscale* **2014**, *6*, 13501.

(34) Kang, N.; Perron, M. E.; Prud'homme, R. E.; Zhang, Y.; Gaucher, G.; Leroux, J. C. *Nano Lett.* **2005**, *5*, 315.

(35) Cui, H.; Chen, Z.; Zhong, S.; Wooley, K. L.; Pochan, D. J. *Science* **2007**, *317*, 647.

(36) Yang, C.; Tan, J. P. K.; Cheng, W.; Attia, A. B. E.; Ting, C. T. Y.; Nelson, A.; Hedrick, J. L.; Yang, Y. Y. *Nano Today* **2010**, *5*, 515.

(37) O'Reilly, R. K.; Hawker, C. J.; Wooley, K. L. *Chem. Soc. Rev.* **2006**, *35*, 1068.

(38) van Nostrum, C. F. *Soft Matter* **2011**, *7*, 3246.

(39) Read, E. S.; Armes, S. P. *Chem. Commun.* **2007**, 3021.

(40) Elsabahy, M.; Wooley, K. L. *J. Polym. Sci. Part A: Polym. Chem.* **2012**, *50*, 1869.

(41) Zhang, F.; Zhang, S.; Pollack, S. F.; Li, R.; Gonzalez, A.; Fan, J.; Zou, J.; Leininger, S. E.; Pavía-Sanders, A.; Johnson, R.; Nelson, L. D.; Raymond, J. E.; Elsabahy, M.; Hughes, D. M. P.; Lenox, M. W.; Gustafson, T. P.; Wooley, K. L. *J. Am. Chem. Soc.* **2015**, *137*, 2056.

(42) Kim, J. O.; Sahay, G.; Kabanov, A. V.; Bronich, T. K. *Biomacromolecules* **2010**, *11*, 919.

(43) Klyachko, N. L.; Manickam, D. S.; Brynskikh, A. M.; Uglanova, S. V.; Li, S.; Higginbotham, S. M.; Bronich, T. K.; Batrakova, E. V.; Kabanov, A. V. *Nanomedicine* **2012**, *8*, 119.

(44) Stamm, W. E.; Norrby, S. R. *Journal of Infectious Diseases* **2001**, *183*, S1.

(45) Schappert, S. M.; Rechtsteiner, E. A. *Vital Health Stat 13* **2011**, 1.

(46) Foxman, B. *Infectious Disease Clinics of North America* **2014**, *28*, 1.

(47) Ducel, G.; Fabry, J.; Nicolle, L. *Prevention of hospital acquired infections: A practical guide*; World Health Organization: Geneva, 2002.

(48) Scott, R. D. **2009**.

(49) Kostakioti, M.; Hultgren, S. J.; Hadjifrangiskou, M. *Virulence* **2012**, *3*, 592.

(50) Chen, H.-Y.; Ragavan, M.; Hilty, C. *Angew. Chem. Int. Ed.* **2013**, *52*, 9192.

(51) Ribet, D.; Cossart, P. *Microbes and Infection* **2015**, *17*, 173.

(52) Wright, K. J.; Hultgren, S. J. *Future Microbiology* **2006**, *1*, 75.

(53) Hadjifrangiskou, M.; Gu, A. P.; Pinkner, J. S.; Kostakioti, M.; Zhang, E. W.; Greene, S. E.; Hultgren, S. J. *J. Bacteriol.* **2012**, *194*, 6195.

(54) Schilling, J. D.; Mulvey, M. A.; Hultgren, S. J. *Journal of Infectious Diseases* **2001**, *183*, S36.

(55) Eto, D. S.; Jones, T. A.; Sundsbak, J. L.; Mulvey, M. A. *PLoS Pathog* **2007**, *3*, e100.

(56) Hannan, T. J.; Totsika, M.; Mansfield, K. J.; Moore, K. H.; Schembri, M. A.; Hultgren, S. J. *FEMS microbiology reviews* **2012**, *36*, 616.

(57) Zhou, G.; Mo, W.-J.; Sebbel, P.; Min, G.; Neubert, T. A.; Glockshuber, R.; Wu, X.-R.; Sun, T.-T.; Kong, X.-P. *J. Cell Sci.* **2001**, *114*, 4095.

(58) Mulvey, M. A.; Lopez-Boado, Y. S.; Wilson, C. L.; Roth, R.; Parks, W. C.; Heuser, J.; Hultgren, S. J. *Science* **1998**, *282*, 1494.

(59) Martinez, J. J.; Mulvey, M. A.; Schilling, J. D.; Pinkner, J. S.; Hultgren, S. J. *The EMBO Journal* **2000**, *19*, 2803.

(60) Hung, C.-S.; Bouckaert, J.; Hung, D.; Pinkner, J.; Widberg, C.; DeFusco, A.; Auguste, C. G.; Strouse, R.; Langermann, S.; Waksman, G.; Hultgren, S. J. *Mol. Microbiol.* **2002**, *44*, 903.

(61) Anderson, G. G.; Palermo, J. J.; Schilling, J. D.; Roth, R.; Heuser, J.; Hultgren, S. J. *Science* **2003**, *301*, 105.

(62) Mulvey, M. A.; Schilling, J. D.; Hultgren, S. J. *Infection and Immunity* **2001**, *69*, 4572.

(63) Mysorekar, I. U.; Hultgren, S. J. *Proc. Natl. Acad. Sci. U.S.A.* **2006**, *103*, 14170.

(64) Lin, L. Y.; Tiemann, K. M.; Li, Y.; Pinkner, J. S.; Walker, J. N.; Hultgren, S. J.; Hunstad, D. A.; Wooley, K. L. *J. Am. Chem. Soc.* **2012**, *134*, 3938.

(65) Thurmond, K. B.; Kowalewski, T.; Wooley, K. L. *J. Am. Chem. Soc.* **1996**, *118*, 7239.

(66) O'Reilly, R. K.; Hawker, C. J.; Wooley, K. L. *Chem. Soc. Rev.* **2006**, *35*, 1068.

(67) Satishkumar, R.; Vertegel, A. *Biotechnol. Bioeng.* **2008**, *100*, 403.

(68) George, A. L.; Borders, C. L. *Biochem. Biophys. Res. Commun.* **1979**, *87*, 59.

(69) Gilles, M. A.; Hudson, A. Q.; Borders Jr, C. L. *Anal. Biochem.* **1990**, *184*, 244.

(70) Hermanson, G. T. *Bioconjugate techniques*; Academic press, 2013.

(71) Gebhardt, J.; Fuerstenau, D. *Colloids and Surfaces* **1983**, *7*, 221.

(72) Xu, J.; Sun, G.; Rossin, R.; Hagooly, A.; Li, Z.; Fukukawa, K.-i.; Messmore, B. W.; Moore, D. A.; Welch, M. J.; Hawker, C. J.; Wooley, K. L. *Macromolecules* **2007**, *40*, 2971.

(73) Gustafson, T. P.; Lim, Y. H.; Flores, J. A.; Heo, G. S.; Zhang, F.; Zhang, S.; Samarajeewa, S.; Raymond, J. E.; Wooley, K. L. *Langmuir* **2014**, *30*, 631.

(74) Shanmugananda Murthy, K.; Ma, Q.; Clark Jr, C. G.; Remsen, E. E.; Wooley, K. L. *Chem. Commun.* **2001**, 773.

(75) Flores, J. A.; Pavía-Sanders, A.; Chen, Y.; Pochan, D. J.; Wooley, K. L. *Chem. Mater.* **2015**, *27*, 3775.

(76) Tang, C.; Qi, K.; Wooley, K. L.; Matyjaszewski, K.; Kowalewski, T. *Angew. Chem. Int. Ed.* **2004**, *43*, 2783.

(77) Hartmann, M.; Lindhorst, T. K. *Eur. J. Org. Chem.* **2011**, *2011*, 3583.

(78) Lundblad, R. L. *Chemical reagents for protein modification*; Fourth ed.; CRC press, 2014.

(79) Chan, V. W. F.; Jorgensen, A. M.; Borders Jr, C. L. *Biochem. Biophys. Res. Commun.* **1988**, *151*, 709.

(80) Svensson, B.; Møller, H.; Clarke, A. *Carlsberg Res. Commun.* **1988**, *53*, 331.

(81) Gee, K. R.; Archer, E. A.; Kang, H. C. *Tetrahedron Lett.* **1999**, *40*, 1471.

(82) Lockett, M. R.; Phillips, M. F.; Jarecki, J. L.; Peelen, D.; Smith, L. M. *Langmuir* **2008**, *24*, 69.

(83) Wu, S. Y.; Lopez-Berestein, G.; Calin, G. A.; Sood, A. K. *Science Translational Medicine* **2014**, *6*, 240ps7.

(84) Lin, L. Y.; Lee, N. S.; Zhu, J.; Nyström, A. M.; Pochan, D. J.; Dorshow, R. B.; Wooley, K. L. *J. Controlled Release* **2011**, *152*, 37.

(85) Kadajji, V. G.; Betageri, G. V. *Polymers* **2011**, *3*, 1972.

(86) Alconcel, S. N. S.; Baas, A. S.; Maynard, H. D. *Polym. Chem.* **2011**, *2*, 1442.

(87) Pelegri-O'Day, E. M.; Lin, E.-W.; Maynard, H. D. *J. Am. Chem. Soc.* **2014**, *136*, 14323.

(88) Knop, K.; Hoogenboom, R.; Fischer, D.; Schubert, U. S. *Angew. Chem. Int. Ed.* **2010**, *49*, 6288.

(89) Barz, M.; Luxenhofer, R.; Zentel, R.; Vicent, M. J. *Polym. Chem.* **2011**, *2*, 1900.

(90) Lundberg, P.; Lee, B. F.; van den Berg, S. A.; Pressly, E. D.; Lee, A.; Hawker, C. J.; Lynd, N. A. *ACS Macro Lett.* **2012**, *1*, 1240.

(91) Lee, B. F.; Kade, M. J.; Chute, J. A.; Gupta, N.; Campos, L. M.; Fredrickson, G. H.; Kramer, E. J.; Lynd, N. A.; Hawker, C. J. *J. Polym. Sci., Part A: Polym. Chem.* **2011**, *49*, 4498.

(92) Mangold, C.; Dingels, C.; Obermeier, B.; Frey, H.; Wurm, F. *Macromolecules* **2011**, *44*, 6326.

(93) Kataoka, K.; Harada, A.; Nagasaki, Y. *Advanced Drug Delivery Reviews* **2001**, *47*, 113.

(94) Kopeček, J.; Kopečková, P. *Advanced Drug Delivery Reviews* **2010**, *62*, 122.

(95) Duncan, R.; Vicent, M. J. *Advanced Drug Delivery Reviews* **2010**, *62*, 272.

(96) Nuhn, L.; Barz, M.; Zentel, R. *Macromolecular Bioscience* **2014**, *14*, 607.

(97) Pissuwan, D.; Boyer, C.; Gunasekaran, K.; Davis, T. P.; Bulmus, V. *Biomacromolecules* **2010**, *11*, 412.

(98) Mohr, N.; Barz, M.; Forst, R.; Zentel, R. *Macromol. Rapid Commun.* **2014**, *35*, 1522.

(99) Pratt, R. C.; Nederberg, F.; Waymouth, R. M.; Hedrick, J. L. *Chem. Commun.* **2008**, 114.

(100) Tempelaar, S.; Mespouille, L.; Coulembier, O.; Dubois, P.; Dove, A. P. *Chem. Soc. Rev.* **2013**, *42*, 1312.

(101) Suriano, F.; Coulembier, O.; Hedrick, J. L.; Dubois, P. *Polym. Chem.* **2011**, *2*, 528.

(102) Feng, J.; Zhuo, R.-X.; Zhang, X.-Z. *Prog. Polym. Sci.* **2012**, *37*, 211.

(103) Coady, D. J.; Horn, H. W.; Jones, G. O.; Sardon, H.; Engler, A. C.; Waymouth, R. M.; Rice, J. E.; Yang, Y. Y.; Hedrick, J. L. *ACS Macro Lett.* **2013**, *2*, 306.

(104) Engler, A. C.; Ke, X.; Gao, S.; Chan, J. M. W.; Coady, D. J.; Ono, R. J.; Lubbers, R.; Nelson, A.; Yang, Y. Y.; Hedrick, J. L. *Macromolecules* **2015**, *48*, 1673.

(105) Engler, A. C.; Chan, J. M. W.; Coady, D. J.; O'Brien, J. M.; Sardon, H.; Nelson, A.; Sanders, D. P.; Yang, Y. Y.; Hedrick, J. L. *Macromolecules* **2013**, *46*, 1283.

(106) Seow, W. Y.; Yang, Y. Y. *J. Controlled Release* **2009**, *139*, 40.

(107) Heo, G. S.; Cho, S.; Wooley, K. L. *Polym. Chem.* **2014**, *5*, 3555.

(108) Al-Azemi, T. F.; Bisht, K. S. *Macromolecules* **1999**, *32*, 6536.

(109) Presser, A.; Hüfner, A. *Monatshefte für Chemie / Chemical Monthly* **2004**, *135*, 1015.

(110) Nahmany, M.; Melman, A. *Organic & Biomolecular Chemistry* **2004**, *2*, 1563.

(111) Cho, S.; Heo, G. S.; Khan, S.; Gonzalez, A. M.; Elsabahy, M.; Wooley, K. L. *Macromolecules* **2015**.

(112) Xiong, M.-H.; Bao, Y.; Yang, X.-Z.; Wang, Y.-C.; Sun, B.; Wang, J. *J. Am. Chem. Soc.* **2012**, *134*, 4355.

(113) Zhang, S.; Zou, J.; Zhang, F.; Elsabahy, M.; Felder, S. E.; Zhu, J.; Pochan, D. J.; Wooley, K. L. *J. Am. Chem. Soc.* **2012**, *134*, 18467.

(114) Hu, X.; Chen, X.; Xie, Z.; Liu, S.; Jing, X. *J. Polym. Sci., Part A: Polym. Chem.* **2007**, *45*, 5518.

(115) Nuhn, L.; Schüll, C.; Frey, H.; Zentel, R. *Macromolecules* **2013**, *46*, 2892.

(116) Faucher, J. A.; Koleske, J. V.; Santee, E. R.; Stratta, J. J.; Wilson, C. W. *J. Appl. Phys.* **1966**, *37*, 3962.

(117) Carey, F. A.; Sundberg, R. J. *Advanced organic chemistry: Part B: Reaction and synthesis*; Springer, 2007.

(118) Smith, M. B.; March, J. *March's advanced organic chemistry: Reactions, mechanisms, and structure*; Wiley, 2007.

(119) Moses, J. E.; Moorhouse, A. D. *Chem. Soc. Rev.* **2007**, *36*, 1249.

(120) Iha, R. K.; Wooley, K. L.; Nystrӧm, A. M. Burke, D. J.; Kade, M. J.; Hawker, C. J. *Chem. Rev.* **2009**, *109*, 5620.

(121) Wiley, R. H.; Hobson, P. H. *J. Polym. Sci.* **1950**, *5*, 483.

(122) Mulvaney, J. E.; Chang, D. M. *Macromolecules* **1980**, *13*, 240.

(123) Hirao, A.; Ishino, Y.; Nakahama, S. *Makromol. Chem.* **1986**, *187*, 141.

(124) Hirao, A.; Nakahama, S. *Macromolecules* **1987**, *20*, 2968.

(125) Hwang, J.; Li, R. C.; Maynard, H. D. *J. Controlled Release* **2007**, *122*, 279.

(126) Li, R. C.; Broyer, R. M.; Maynard, H. D. *J. Polym. Sci., Part A: Polym. Chem.* **2006**, *44*, 5004.

(127) Li, R. C.; Hwang, J.; Maynard, H. D. *Chem. Commun.* **2007**, 3631.

(128) Sun, G.; Cheng, C.; Wooley, K. L. *Macromolecules* **2007**, *40*, 793.

(129) Alconcel, S. N.; Kim, S. H.; Tao, L.; Maynard, H. D. *Macromol. Rapid Commun.* **2013**, *34*, 983.

(130) Yang, S. K.; Weck, M. *Macromolecules* **2007**, *41*, 346.

(131) Ke, X.; Coady, D. J.; Yang, C.; Engler, A. C.; Hedrick, J. L.; Yang, Y. Y. *Polym. Chem.* **2014**, *5*, 2621.

(132) Sanders, D. P.; Fukushima, K.; Coady, D. J.; Nelson, A.; Fujiwara, M.; Yasumoto, M.; Hedrick, J. L. *J. Am. Chem. Soc.* **2010**, *132*, 14724.

(133) Tempelaar, S.; Mespouille, L.; Dubois, P.; Dove, A. P. *Macromolecules* **2011**, *44*, 2084.

(134) Reingold, I. D. *Organic chemistry: An introduction emphasizing biological connections REVISED Edition*; Indo American Books, 2007.

(135) Login, R. B. In *Kirk-Othmer encyclopedia of chemical technology*; John Wiley & Sons, Inc.: 2000.

(136) Kawamura, M.; Kanazawa, A.; Kanaoka, S.; Aoshima, S. *Polym. Chem.* **2015**, *6*, 4102.

(137) Gu, Y.; Zhong, Y.; Meng, F.; Cheng, R.; Deng, C.; Zhong, Z. *Biomacromolecules* **2013**, *14*, 2772.

(138) Lim, Y. H.; Heo, G. S.; Rezenom, Y. H.; Pollack, S.; Raymond, J. E.; Elsabahy, M.; Wooley, K. L. *Macromolecules* **2014**, *47*, 4634.

(139) Tempelaar, S.; Barker, I. A.; Truong, V. X.; Hall, D. J.; Mespouille, L.; Dubois, P.; Dove, A. P. *Polym. Chem.* **2013**, *4*, 174.

(140) Cho, S.; Heo, G. S.; Khan, S.; Gonzalez, A. M.; Elsabahy, M.; Wooley, K. L. *Macromolecules* **2015**, *48*, 8797.

(141) Campagne, B.; David, G.; Améduri, B.; Jones, D. J.; Rozière, J.; Roche, I. *Int. J. Hydrogen Energy* **2015**, *40*, 16797.

(142) Lee, Y.; Zeng, H.; Ruedisser, S.; Gossert, A. D.; Hilty, C. *J. Am. Chem. Soc.* **2012**, *134*, 17448.

(143) Lee, Y.; Zeng, H.; Mazur, A.; Wegstroth, M.; Carlomagno, T.; Reese, M.; Lee, D.; Becker, S.; Griesinger, C.; Hilty, C. *Angew. Chem. Int. Ed.* **2012**, *51*, 5179.

(144) Chappuis, Q.; Milani, J.; Vuichoud, B.; Bornet, A.; Gossert, A. D.; Bodenhausen, G.; Jannin, S. *J. Phys. Chem. Lett.* **2015**, *6*, 1674.

(145) Min, H.; Sekar, G.; Hilty, C. *ChemMedChem* **2015**, *10*, 1559.

(146) Buratto, R.; Bornet, A.; Milani, J.; Mammoli, D.; Vuichoud, B.; Salvi, N.; Singh, M.; Laguerre, A.; Passemard, S.; Gerber-Lemaire, S.; Jannin, S.; Bodenhausen , G. *ChemMedChem* **2014**, *9*, 2509.

(147) Kim, Y.; Hilty, C. *Angew. Chem. Int. Ed.* **2015**, *54*, 4941.

(148) Bowen, S.; Hilty, C. *Angew. Chem. Int. Ed.* **2008**, *47*, 5235.

(149) Jensen, P. R.; Meier, S.; Ardenkjaer-Larsen, J. H.; Duus, J. O.; Karlsson, M.; Lerche, M. H. *Chem. Commun.* **2009**, 5168.

(150) Bowen, S.; Hilty, C. *Anal. Chem.* **2009**, *81*, 4543.

(151) Zeng, H.; Lee, Y.; Hilty, C. *Anal. Chem.* **2010**, *82*, 8897.

(152) Allouche-Arnon, H.; Hovav, Y.; Friesen-Waldner, L.; Sosna, J.; Moshe Gomori, J.; Vega, S.; Katz-Brull, R. *NMR Biomed.* **2014**, *27*, 656.

(153) Lee, Y.; Heo, G. S.; Zeng, H.; Wooley, K. L.; Hilty, C. *J. Am. Chem. Soc.* **2013**, *135*, 4636.

(154) Chen, C.-H.; Shih, W.-C.; Hilty, C. *J. Am. Chem. Soc.* **2015**, *137*, 6965.

(155) Schugens, C.; Maquet, V.; Grandfils, C.; Jerome, R.; Teyssie, P. *Journal of Biomedical Materials Research* **1996**, *30*, 449.

(156) Sinha Ray, S.; Maiti, P.; Okamoto, M.; Yamada, K.; Ueda, K. *Macromolecules* **2002**, *35*, 3104.

(157) Dechy-Cabaret, O.; Martin-Vaca, B.; Bourissou, D. *Chem. Rev.* **2004**, *104*, 6147.

(158) Pratt, R. C.; Lohmeijer, B. G. G.; Long, D. A.; Waymouth, R. M.; Hedrick, J. L. *J. Am. Chem. Soc.* **2006**, *128*, 4556.

(159) Chuma, A.; Horn, H. W.; Swope, W. C.; Pratt, R. C.; Zhang, L.; Lohmeijer, B. G. G.; Wade, C. G.; Waymouth, R. M.; Hedrick, J. L.; Rice, J. E. *J. Am. Chem. Soc.* **2008**, *130*, 6749.

(160) Simón, L.; Goodman, J. M. *The Journal of Organic Chemistry* **2007**, *72*, 9656.

(161) Bowen, S.; Hilty, C. *PCCP* **2010**, *12*, 5766.

APPENDIX A

CFTR-CONJUGATED POLYMERIC NANOPARTICLES FOR THE TARGETED DELIVERY OF ANTIMICROBIAL SILVER COMPOUNDS TO TREAT LUNG INFECTIONS

Lung infections are one of the major health issues worldwide. The leading causes of death for children under the age of five and adults by curable infections are pneumonia and tuberculosis (TB), respectively, according to the World Health Organization.[1,2] What makes situation worse is the emergence of antibiotic resistant bacteria such as *Mycobacterium tuberculosis* (MTB), which makes treatment of pulmonary diseases more challenging.[3] In the case of cystic fibrosis (CF), respiratory failure by lung infections of multiple bacteria leads to patient death and the most common species to cause these infections are *Pseudomonas aeruginosa* (PA).

The goal of this project is the development of multi-functional, biodegradable polymeric nanoparticles, which are capable of loading antimicrobial silver compounds as well as targeting infectious bacteria to localize drugs and/or diagnostic imaging agents (Figure A.1). We envision that directly targeting bacteria at the site of infection may increase the efficacy of conventional antibiotics towards chronic lung infections. In order to treat our target disease, cystic fibrosis (CF), degradable polymeric nanoparticles were conjugated with a peptide sequence corresponding to the first extracellular domain of cystic fibrosis transmembrane conductance regulator (CFTR), given the well described

interaction of this molecule with the disease-causing bacteria, *Pseudomonas aeruginosa* (PA)'s lipopolysaccharide.

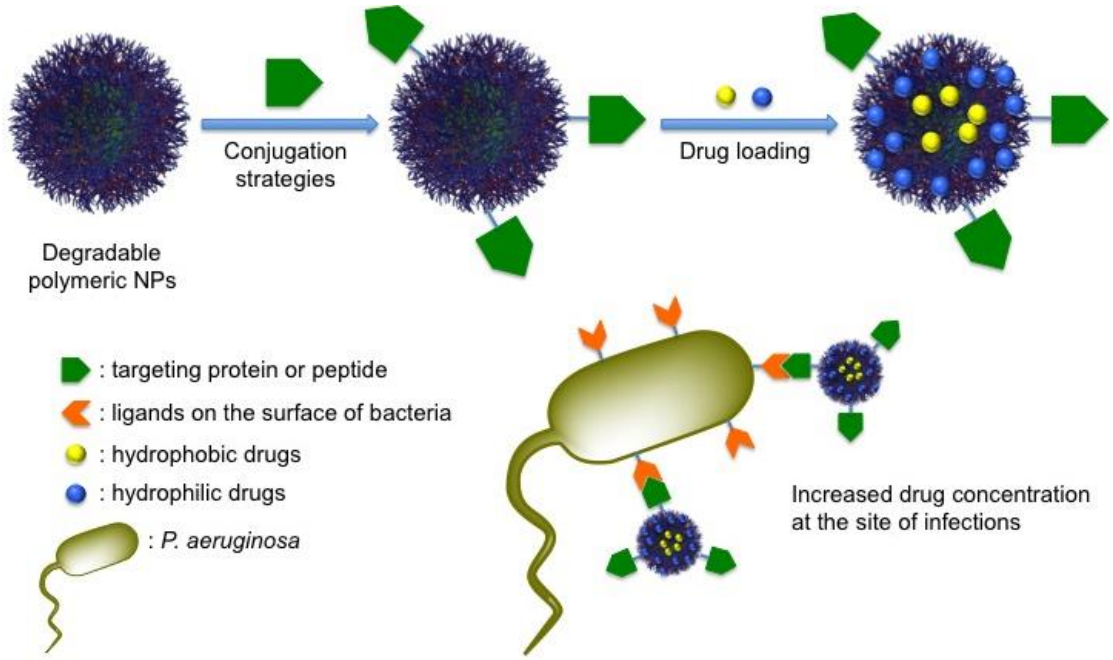

Figure A.1. Pathogen targeting, a novel strategy to target bacterial infections associated with Cystic Fibrosis.

For the preparation of CFTR-targeted SCKs, after introduction of thioester functionalities on the shell of SCKs which were prepared from anionic polyphosphester-*b*-poly(L-lactide) (aPPE-*b*-PLLA), native chemical ligation (NCL) with CFTR peptide provided the peptide-SCK conjugates (**Figure A.2.**). After CFTR conjugation, hydrodynamic diameters increased while zeta potentials changed little. SDS-PAGE with silver staining of crude reaction mixtures showed no free peptide in the sample. However,

small peptides have transfer issues during typical SDS-PAGE/Western blot process. Also, harsh conditions of SDS-PAGE could cause unpredicted problems with degradable SCKs. So, we used simple dot blots to bypass those problems and confirmed the existence of peptide in the sample.

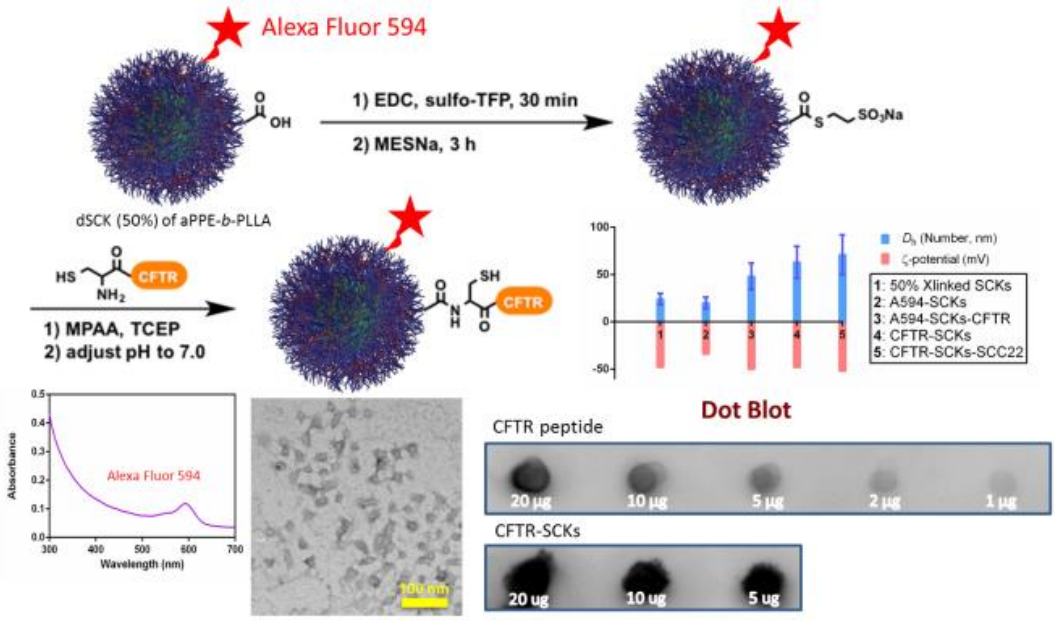

Figure A.2. Targeted degradable nanoparticles were prepared by native chemical ligation (NCL) between N-terminal cysteine of CFTR peptide and thioester functionalities of degradable nanoparticles.

Preliminary confocal studies using CFTR-conjugated SCKs with PA showed higher colocalization of targeted-SCKs than that of naked SCKs *in vitro*, which suggests that this approach offers a viable option for targeting the pathogen (Figure A.3). Overall, CFTR-conjugated dSCKs appear to have targeting capability and warrant further exploration as antimicrobial devices for *P. aeruginosa* lung infection.

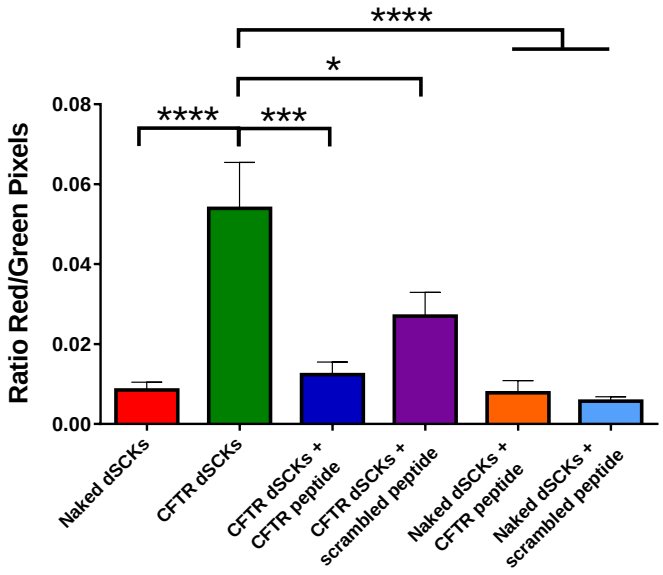

Figure A.3. Comparison of the binding affinity of naked SCKs and CFTR peptide-conjugated SCKs, with or without 100 μg/mL CFTR peptide or scrambled peptide, as determined by the ratio of red pixels (SCKs) to green pixels (PAO1-GFP). Pixels counted in ImageJ after segmentation using Renyi entropy. Significance determined with One-Way ANOVA with Geisser-Greenhouse correction. * $P < 0.05$, *** $P < 0.001$, **** $P < 0.0001$.

REFERENCES OF APPENDIX A

(1) Mulholland, E.; Smith, L.; Carneiro, I.; Becher, H.; Lehmann, D. *Bulletin of the World Health Organization* **2008**, *86*, 399.

(2) Lönnroth, K.; Raviglione, M. *Semin Respir Crit Care Med* **2008**, *29*, 481.

(3) LoBue, P.; Sizemore, C.; Castro, K. G. *MMWR Recomm Rep* **2009**, *58*, 1.

APPENDIX B

DEVELOPMENT OF FULLY DEGRADABLE CYLINDRICAL MICELLES VIA CRYSTALLIZATION-DRIVEN SELF-ASSEMBLY

In Chapter II, we studied to improve amidation-based conjugation conditions between $FimH_A$ and shell crosslinked polymeric nanostructures. However, resulting conjugates did not exhibit better behaviors *in vitro*. One of potential approaches to enhance cell binding and internalization efficiency is utilization of larger and/or longer nanostructures. UPEC internalizes into bladder epithelial cells *via* polyvalent interactions between $FimH_A$ at the tip of Type 1 pili and mannose moieties at interval of *ca*. 16 nm on the surface of bladder epithelial cells. However, sizes of our spherical SCKs measured by TEM are less than 20 nm, which would allow only monovalent interaction. Therefore, it is critical to make a comparative study of the effects of nanoparticle shape on binding one or multiple receptors on bladder epithelial cells and the effects on the cell internalization.

Since 2011, research groups of Andrew Dove and Rachel O'Reilly have developed and optimized crystallization-driven self-assembly (CDSA) of amphiphilic block copolymers, PAA-*b*-PLA. Semi-crystalline PLA segment allows for the growth of cylindrical nanostructures *via* crystallization of PLA which is induced by heating above glass transition temperature of PLA block. Using CDSA, we have attempted to prepare cylindrical nanoparticles. The advantage of this method is both spheres and cylinders could be prepared from the same amphiphilic block copolymer precursor, as well as potential capability to control the length of cylindrical micelles.

We first tried to synthesize fully degradable cylindrical micelles using PPE-*b*-PLLA *via* CDSA. Both anionic and cationic PPE-*b*-PLLAs were tested (Figure B.1). Although cylinders were produced from cationic polymers, those nanostructures precipitated out during CDSA process, which is relatively harsh conditions for readily degradable PPE segment. Therefore, we needed to search other hydrophilic blocks, which are stable under CDSA conditions, while still retaining degradability. As we discussed earlier in this dissertation, aliphatic polycarbonates are excellent candidates due to their biocompatibility, biodegradability, as well as low *in vivo* toxicity. In addition, polycarbonate backbone is known to be stable at 90 ˚C for 24 h at least.

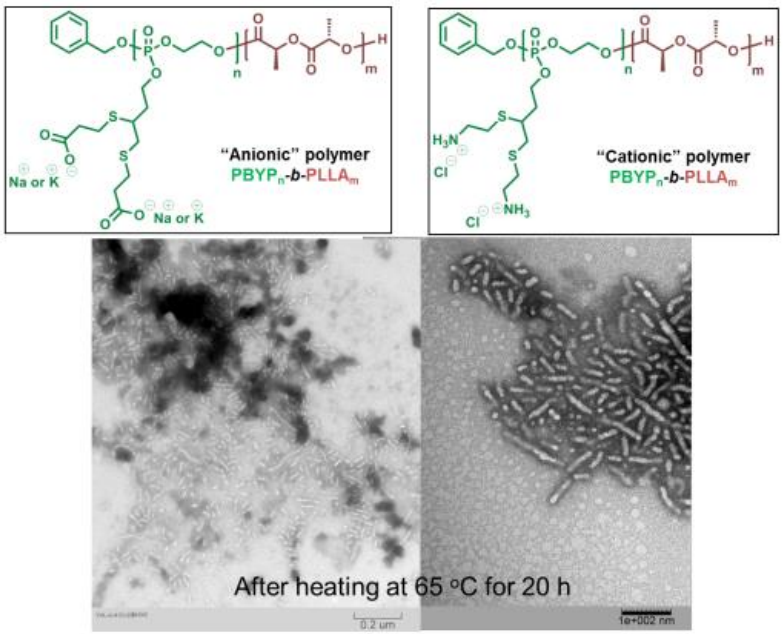

Figure B.1. Anionic and cationic PPE-*b*-PLLAs and TEM images of cylindrical micelles prepared from the cationic polymer *via* CDSA.

We synthesized PMHPAC-*b*-PLLA (Scheme B.1). Unexpectedly, $PMHPAC_{70}$-*b*-$PLLA_{20}$ formed cylindrical micelles after direct dissolution in water without CDSA. However, CDSA of short cylinders allowed the existing cylinders to be elongated. Hydrodynamic diameter increased and longer cylinders were observed by TEM (Figure B.2). Conditions for cylinder formation using PMHPAC-*b*-PLLA need to be optimized for further applications. In addition, other functional hydrophilic polycarbonates could be employed such as analogs to anionic and cationic PPE-*b*-PLLAs in Figure B.1.

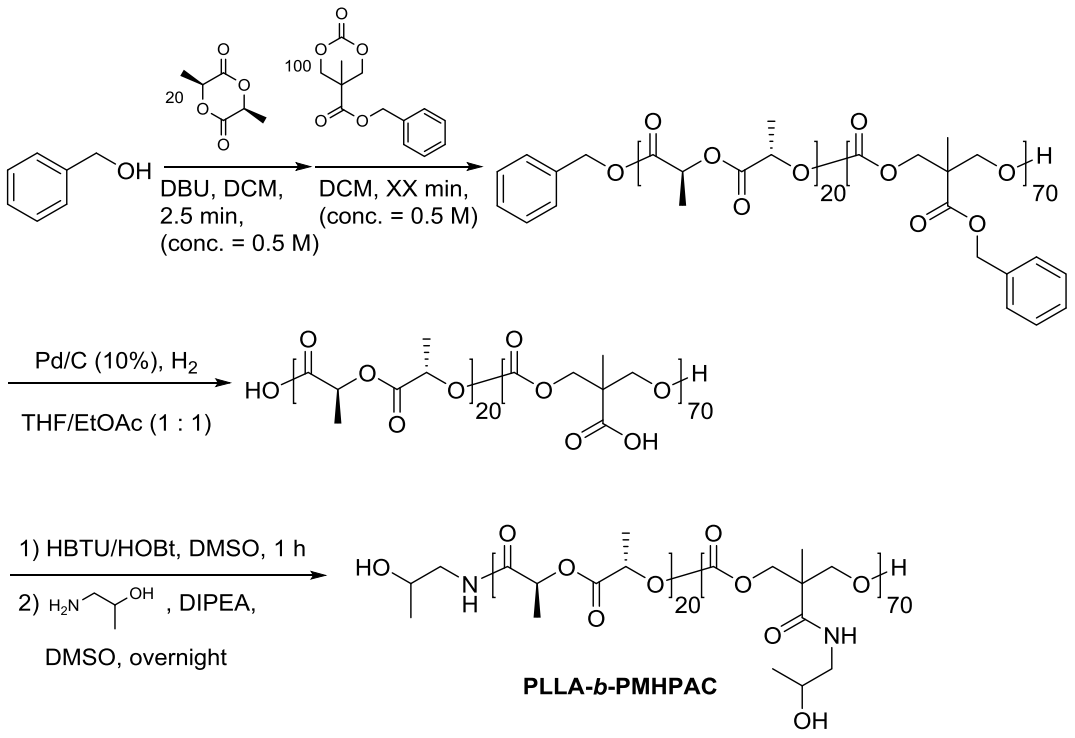

Scheme B.1. Synthesis of PMHPAC-*b*-PLLA.

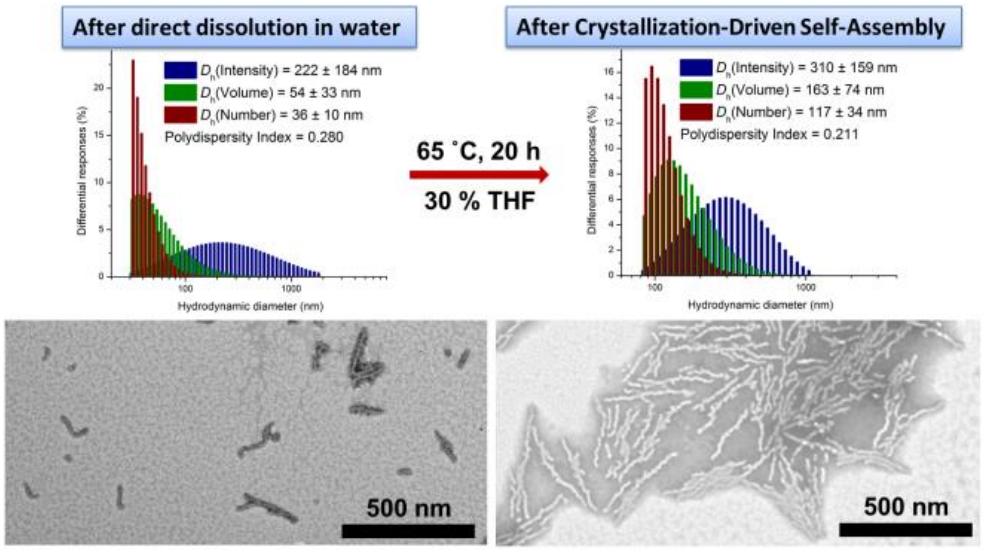

Figure B.2. Cylindrical micelles produced from PMHPAC-*b*-PLLA by direct dissolution (left) and their elongated cylinders *via* CDSA (right)